Characterizing the Role of the *Epsilon* Subunit in Regulation of the *Escherichia coli* ATP Synthase

By

Naman B. Shah

A dissertation in the Department of Biochemistry and Molecular Biology

Submitted in partial fulfillment of the requirements for the degree of Doctor of Philosophy

In the College of Graduate Studies of State University of New York, Upstate Medical University

Approved: _____

(Sponsor's signature)

Date: _____

Acknowledgements

My relatively short journey through Doctor of Philosophy has been enjoyable and enlightening in equal measures. When I look back at it, I realize that many people played pivotal roles in making this journey possible. I would like to grab this opportunity to express my appreciation for their amazing support without which this endeavor wouldn't have reached fruition.

I would like to begin by thanking my advisor, Dr. Thomas M. Duncan for showing immense faith in me and for his superlative guidance. Tom has been a great source of inspiration owing to his deep knowledge of the field combined with his down-to-earth attitude and a willingness to listen. I am grateful to him for allowing me to advance the projects in my desired direction. My life-long desire was to work with *Mycobacterium tuberculosis* and, it reflects Tom's magnanimity that he agreed to divert the lab's research focus towards pathogenic bacteria including tuberculosis. Here was a PI, a true Biochemist, willing to move away from his strengths and embrace a different field just to accommodate his student's wishes. I do not think there can be a better example of mentoring and I will forever remain indebted to him for this. I believe the *epsilon* truncation project has repaid his faith and will facilitate a smooth transition from pure protein Biochemistry to Biochemistry in pathogenic bacteria. Thank you Tom for being the most amazing mentor a student can hope for and thank you for helping me sail smoothly through the rough waters of PhD studies.

Next, I would like to thank Dr. Richard L. Cross, Dr. Patricia Kane and Dr. Stephan Wilkens for serving on my thesis advisory committee members. I consider myself extremely fortunate to have three professors, in addition to my PI, who have such in-depth

knowledge in the field of ATPases. I am very lucky to have the chance to work with Rich whose contributions to the field of ATP synthase need no introduction. I am also thankful to him for editing my thesis. Patty is the Wonder Woman of Upstate as she can handle tasks like running a successful lab, deftly handling the duties of the department chair, serving on a vast number of students' committees, amassing the best-rounded knowledge in so many different fields and then devote time to her family; Patty can do everything. Stephan is equally awe-inspiring. The sheer number of structural biology techniques that he has command on is mind-boggling. I would also like to thank Dr. Steven Vik, Dr. David Mitchell and Dr. Steven Youngentob for agreeing to serve on my committee. Steve Vik's work on *epsilon* subunit has no parallels and David is an expert in flagellar ATPase. Steven Youngentob was the first scientist at Upstate to host me for dinner. From our debates on religion to arm-wrestling in Dinosaur BBQ, I have enjoyed his company. The individual expertise of all three of them will contribute immensely to the discussion during my defense.

I have had the good fortune of working with some special people in the lab as well as the Biochemistry department during my Ph.D. course work. I would like to thank Mr. Marcus Hutcheon for being a supportive co-worker in the Duncan lab; Ms. Nancy Walker-Kopp for being an absolute delight to work with, greeting me every morning with a smile and providing a pleasant environment in the lab; Dr. Brian K. Haarer for teaching me many Molecular Biology techniques in a short span of time, for always having time to share new ideas about my research, and for taking time to edit my thesis; Dr. Yakov (Yanick) Milgrom for training me to use all the departmental centrifuges as well as autoclave, and

for going easy on me when I made mistakes; and Ms. Mariam Bhatti for bringing a breath of fresh air by her cheerful nature.

The Biochemistry and Molecular Biology department at Upstate is a closely knit community that welcomes one and all with open arms and I am very fortunate to have been a part of this department. I am especially grateful to Dr. Rebecca Oot for warmly hosting me during the Upstate Recruitment drive that tilted my decision in favor of accepting the admission offer and for lending her editing skills that helped in improving my thesis. A big thank you to Ms. Maureen Tarsio and Dr. Anne Smardon from the Kane lab for sharing their scientific experience and chemical stocks when I was in a hurry; Ms. Elena Milgrom for allowing me to share the autoclave with her on numerous occasions; Ms. Penny McPhilmy and Ms. Sandra Jarvis for ensuring a very smooth functioning of the department as well as taking care of my paperwork. All the other members of the department have been a delight to work with and I wish them the very best for their respective careers.

The Scottish evangelist and writer Henry Drummond once said, "Wherever we are, it is our friends that make our world." Indeed it were my friends who provided constant support and encouragement that enabled me to keep going when things got tough. My high school friends Mr. Harsh Parikh and Mr. Rikin Shah have been the best friends one can hope for. We do not get a chance to meet often owing to geographical restraints but whenever we have met, it has been nothing but pure enjoyment. Ms. Shivangi Shah has helped me in not missing India by cooking Gujarati dishes with an expertise of a chef. My lengthy but enjoyable video gaming sessions with Mr. Gourav Choudhary helped me unwind after a hard day of work in the lab. Ms. Mansi Babbar was always kind to me and has fed me many delicious north Indian delicacies. All of my classmates from the batch of

the year 2010 have been very cooperative and friendly and I couldn't have hoped for better. Ms. Julie Gilbert has been a guide and a mentor of sorts, helping me learn the nuances of American society and also improve as a human being. Many of my documents have benefited from her linguistic and editorial skills. Ms. Thuy La started as an amiable lunch buddy and went on to become a close friend. Another close friend is Ms. Bhumika Upadhyay whose thinking is very similar to mine and has always been available when I needed advice or support.

I met Ms. Vaidehi Patel some ten years back and we hit it off right away. She has been a friend, a philosopher and a reliable partner all these years. She is the sole reason behind my arrival to the US and has played the most pivotal role in shaping my career. Thank you for standing with me in my thick and thin. I love you and am proud to have you in my life! Last but not the least I could not have become the person I am without my loving and caring family. My grandparents are not with us physically but have always been there in spirit. I miss you! My father has taught me many valuable lessons that help me navigate through difficult situations. My brother is four years younger than me. So he is not only my first best friend but also like my kid. We have fought numerous times but in the face of any adversity, we always had each other's back. The bacterial ATP synthase is regulated by autoinhibition through its ε subunit. My mother has played the biggest role in building my ethics and character. She has helped me maintain my sanity when I was struggling and I am utterly grateful to have her in my life. In the end, I thank The United States of America for generously providing the funding and facilities to a non-citizen like me, which helped in undertaking such high level of education. God bless America!

Abstract

The F-type ATP synthase is a rotary nanomotor central to cellular energy metabolism in almost all living organisms. In bacteria, the enzyme also plays a role in nutrient uptake and pH regulation underlining its importance. All ATP synthases can be inhibited by ADP, whereas in bacteria, the enzyme is also autoinhibited by its ε subunit. The inhibition involves a drastic conformational change of the C-terminal domain of the ε subunit (εCTD) that blocks catalytic turnover. This regulation by ε is believed to play an important role in maintaining viability of the cell. Recent development in the field of antibiotics has validated ATP synthase as a drug target against pathogenic bacteria. Thus, there is a renewed interest in studying the role of the ε subunit in regulation of the enzyme and exploiting it to develop antimicrobials that can kill pathogenic bacteria. The present work describes advances in our understanding of the regulatory interactions of εCTD in *E. coli* ATP synthase. In the first approach, we used an optical binding assay to understand the transitions of εCTD between its active and inhibitory conformations. Using different ligands we revealed the relationship between ADP inhibition and ε inhibition. In the second novel approach, the terminal five amino acids of εCTD were deleted to observe the effects on *in vivo* and *in vitro* functions of ATP synthase. The results obtained from these studies advance our understanding of ε inhibition in bacteria and also provide a novel target within bacterial ATP synthase to obtain antibacterial drugs.

Table of Contents

I. List of Figures

Chapter 1

Chapter 2

Supplementary Figures

Chapter 3

Chapter 4

a. Hyperlink connects to http://www.jove.com/video/51383/bio-layer-interferometry-for-measuring-kinetics-protein-protein?access=dweg2wcs

Chapter 6

II. List of Tables

Chapter 1

Chapter 2

Supplementary Table

Chapter 3

III. List of Abbreviations

Å	Angstrom unit (unit; distance)
A_0	F_1-ATPase activity without ε
ADP	Adenosine diphosphate
A_e	F_1-ATPase activity with ε
Ala101	Alanine residue at 101st position
Ala117	Alanine residue at 117th position
Ala124	Alanine residue at 124th position
Ala94	Alanine residue at 94th position
Ala97	Alanine residue at 97th position
AMPPNP	Adenylyl-imidodiphosphate
Asp61	Aspartate at 61st position
ATP	Adenosine triphosphate
Bap	Biotin acceptor peptide
BLI	BioLayer Interferometry
BSA	Bovine serum albumin
CTD	C-terminal domain
DCCD	Dicyclohexylcarbodiimide
DNA	Deoxynucleic acid
DTNB	5, 5'-Dithio-bis-(2-nitrobenzoic acid)
DTT	Dithiothreitol
EDC	1-ethyl-3-[3-(dimethylamino)propyl]carbodiimide
EDTA	Ethylenediaminetetraacetic acid

ETC	Electron transport chain
F_OF_1	F-type ATP synthase
GTP	Guanosine triphosphate
HCl	Hydrochloric acid
His_{10}	Histidine tag
IF_1	ATPase inhibitory factor 1
K_D	Dissociation constant
kDa	Kilo dalton
K_I	Inhibition constant
K_M	Michaelis constant
LDAO	Lauryldimethylamine oxide
Leu	Leucine
M^{-1}	Molar inverse
MBP	Maltose-binding protein
MF_1	Mitochondrial F_1 domain
Mg	Magnesium
mg	Milligram (unit; weight)
min	Minute (unit; time)
ml	Milliliter (unit; volume)
mM	Milli molar (unit; concentration)
MTK-8	MOPS-Tris potassium buffer, pH 8
NaCl	Sodium chloride
NADH	Nicotinamide adenine dinucleotide (reduced)
Ni-NTA	Nickel-nitrilotriacetic acid tag

nm	Nano meter (unit; distance)
nM	Nano molar (unit; concentration)
NMR	Nuclear magnetic resonance
NTD	N-terminal domain
NTP	Nucleotide triphosphate
OD	Optical density
OSCP	Oligomycin sensitivity-conferring protein
PDB	Protein data bank
Pi	Inorganic phosphate
PMF	Proton Motive Force
RMSD	Root-mean-square deviation
RPM	Rotations per minute
S.E./SEM	Standard error/ standard error of mean
s^{-1}	Second inverse
SDS-PAGE	Sodium dodecyl sulfate Polyacrylamide gel electrophoresis
SM	Single molecule
v/v	Volume per volume
w/v	Weight per volume
WT	Wild type
β_{DP}	Catalytic site with ADP bound
β_{E}	Empty catalytic site
β_{FLAG}	β subunit with a FLAG-tag composed of amino acids DYKDDDDK
βME	β-mercapto ethanol

β_{TP}	Catalytic site with ATP bound
ΔpH	Proton gradient
$\Delta\psi$	Transmembrane potential difference
ε_C	Compact conformation of εCTD
ε_X	Extended conformation of εCTD
$\varepsilon\Delta5$	ε with last five amino acids deleted from C-terminal domain
µg	Microgram (unit; weight)
µm	Micrometer (unit; distance)
µmol	Micromole

Chapter One

General Introduction

1.1 Introduction

Adenosine triphosphate (ATP) is the universal currency of energy in living organisms. As a result, the enzyme that metabolizes ATP, F_OF_1 ATP synthase, assumes a very important role in cellular metabolism. Almost all of cellular ATP is generated from Adenosine diphosphate (ADP) and inorganic phosphate (Pi) by ATP synthase via oxidative or photophosphorylation. Both phosphorylation processes involve the transfer of electrons from a high energy molecule to a low energy molecule through redox reactions. The transfer of electrons is coupled with pumping of protons across a semi-permeable membrane which results in a proton gradient (ΔpH) and a membrane potential ($\Delta\psi$), collectively known as Proton Motive Force (PMF). The ATP synthase utilizes this PMF to generate ATP from ADP and Pi.

The F-type ATP synthase (F_OF_1) is a rotary nanomotor that is functionally conserved to a large extent in eukaryotes and eubacteria [1, 2]. It is located in the plasma membrane in eubacteria, inner mitochondrial membrane in eukaryotes and within the thylakoid membranes in plant chloroplasts. Structurally, F_OF_1 is made up of a membrane embedded F_O domain (Oligomycin sensitive) that is involved in proton translocation, and an external F_1 domain (Factor 1) that contains the catalytic sites (Fig. 1.1). Catalysis by the F_1 domain is coupled with proton transport by F_O. During respiratory growth, the products of glycolysis and Kreb's cycle feed into the electron transport chain (ETC) which is in the same vicinity as the ATP synthase. The ETC transports the electrons to the terminal electron acceptor, oxygen, coupled with pumping of a large number of protons across the membrane. This proton imbalance provides a high amount of potential energy that is converted into chemical energy by the coupled processes of proton transport by F_O and

ATP synthesis by F_1. When the PMF drops below the level required to drive ATP synthesis, the enzyme works in reverse, thereby hydrolyzing ATP and pumping protons in the opposite direction [3, 4]. Bacteria use this process for uptake of nutrients [5] as well as to maintain cytosolic pH [6, 7]. Mitochondria inhibit this process by a separate inhibitory protein IF_1 [8, 9] as otherwise the enzyme would burn through ATP stocks. IF_1 is specific for mitochondrial enzyme and does not inhibit the bacterial enzyme [10, 11] despite strong structural and functional similarity between mitochondrial and bacterial enzymes [1, 2].

My thesis work has primarily focused on *E. coli* ATP synthase. For the sake of simplicity, I will talk about the *E. coli* ATP synthase from here on. Wherever enzymes from other organisms will be described, the name of the source organism will be provided.

Figure 1.1

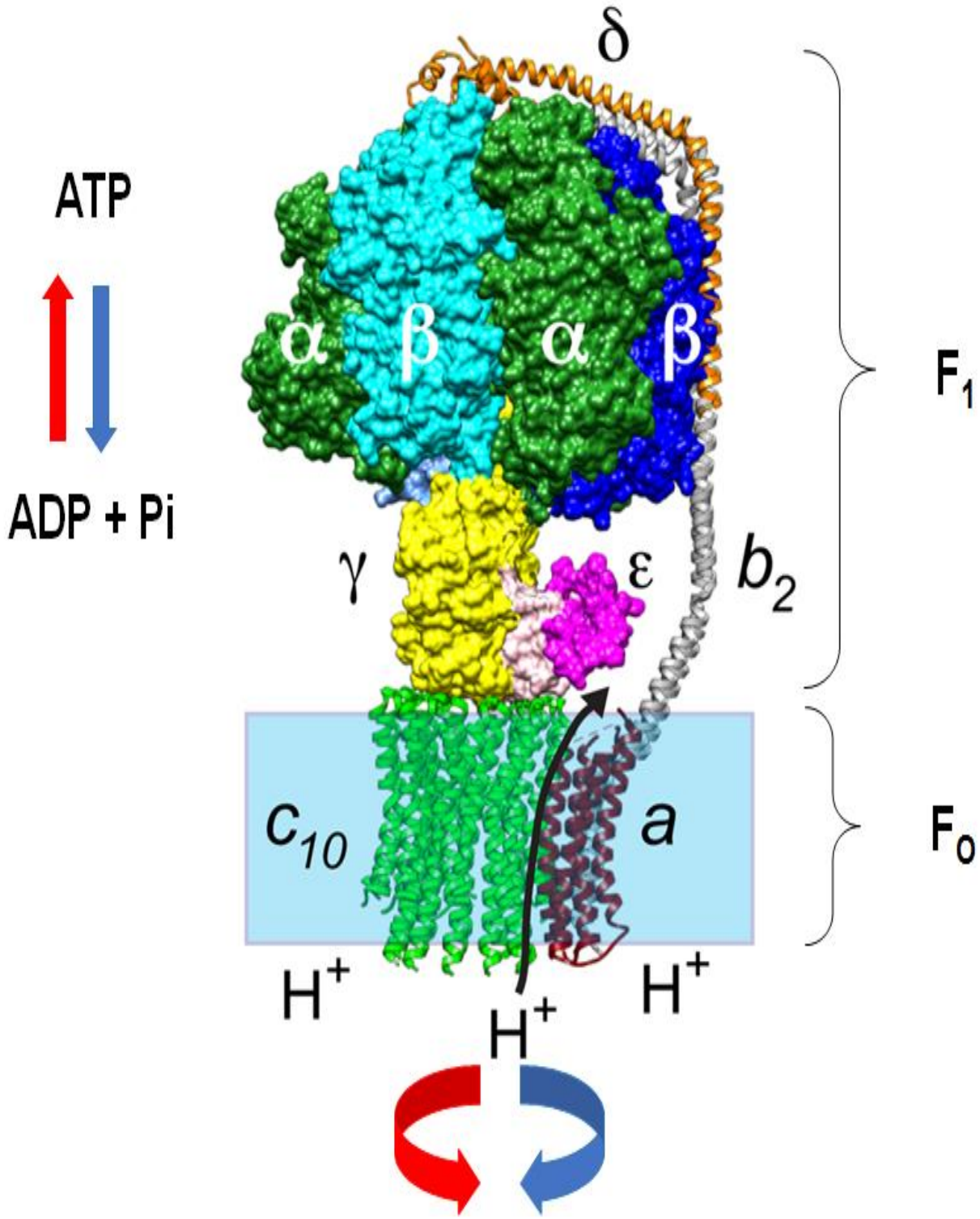

Figure 1.1. The bacterial ATP synthase.

E. coli ATP synthase is shown with F_O domain embedded in the cell membrane and a peripheral F_1 domain. All F_O subunits (**c_{10}** (green), **a** (red), **b_2** (grey)) and δ subunit (orange) from F_1 (shown in ribbons) are obtained by homology-modeling [13]. The surface-rendered F_1 domain (three α (green), three β (blue), γ (yellow), εNTD (light pink), εCTD (magenta)) is from determined structures where ε (PDB ID 1BSN) is docked to F_1-δ (PDB ID 3OAA). Step-wise rotation of the **c**-ring rotates transports protons in the direction shown. When PMF is high, the rotor turns in the red direction leading to ATP synthesis. When PMF is low, the rotor turns in the blue direction, leading to ATP hydrolysis-driven proton pumping. This figure is modified from ref. 109.

1.2 Structure of F_OF_1 ATP Synthase

F_OF_1 ATP synthase is a multisubunit complex that is made of up 20 or more polypeptide chains (Fig. 1.1). Structurally, the enzyme can be classified into two domains: **(1)** A membrane-embedded F_O domain and **(2)** An external F_1 domain. The F_O domain is made up of subunit **a**, dimer $\mathbf{b_2}$ and a circular ring made up of **c** subunits with the stoichiometry of $a_1b_2c_{8\text{-}15}$. The F_1 domain consists of subunits $\alpha_3\beta_3\gamma_1\delta_1\varepsilon_1$ [14, 15]. Overall $\alpha_3\beta_3\gamma_1\delta_1\varepsilon_1a_1b_2c_{8\text{-}15}$ is the shared stoichiometry observed in F-type ATP synthases and the architecture is similar across different kingdoms. The bacterial ATP synthase is the simplest of all the ATP synthases. The mitochondrial ATP synthase contains several extra subunits and function of some of these subunits are known. Subunit **d** makes contacts with subunits of the peripheral stalk such as subunit **b**, $\mathbf{h/F_6}$ and OSCP and is shown to be essential for enzyme function in yeast mitochondrial ATP synthase [16]. The subunit **h** (yeast) or $\mathbf{F_6}$ (mammal) is a water soluble protein that is shown to be important for assembly and/or catalysis in yeast ATP synthase [17]. The subunit **f** plays an important role in stable assembly of subunits **a** and **c** in mitochondrial ATP synthase [18]. The differences in subunit stoichiometry have been described before [2] as well as listed in Table 1.1.

The F_O domain: Based on function as a rotary motor, the subunits of ATP synthase can be classified into a rotor complex and a stator complex. In the F_O domain, the **c** subunit (~8 kDa) is the major part of the rotor complex. In bacterial enzymes, 10 to 15 **c** subunits are arranged in a ring. In mitochondrial enzymes, the ring is formed of 8 or 10 **c** subunits. Each **c** subunit is made up of two α-helices that span the entire membrane with a hydrophilic loop acting as a connector to F_1. This loop forms contacts

Table 1.1

Mitochondria	**Chloroplast**	**Bacteria**	**Stoichiometry**
α	α	α	3
β	β	β	3
γ	γ	γ	1
OSCP	δ	δ	1
δ	ε	ε	1
ε	-	-	1
a, subunit 6	a, subunit IV	a	1
b, subunit 4	b and b', subunit I and II	b	1 or 2
c, subunit 9	C, subunit III	c	8 to 15
d	-	-	1
e	-	-	1 or 2
f	-	-	1
g	-	-	1
h or F_6	-	-	1
A6L, subunit 8	-	-	1
IF_1	-	-	1
F_B, Factor B	-	-	1

Table 1.1. Subunit composition of ATP synthase [2, 18]. Subunits of ATP synthases from mitochondria, chloroplast and bacteria are listed. Subunits α, β, γ, δ, ε, a, b, c are common in all three types. In mitochondria, the homolog of bacterial δ is called OSCP (Oligomycin Sensitivity-Conferral Protein) and the homolog of bacterial ε is called δ. The mitochondrial enzyme contains one b subunit whereas the bacterial and chloroplast enzymes contain two. The c subunit stoichiometry ranges from eight to ten subunits in mitochondria, to fifteen in bacteria. Two copies of the subunit e has been found to be present in rat mitochondria.

with subunits γ and ε of the F_1 domain which form the rest of the rotor complex [19]. Adjacent to the **c**-ring is the hydrophobic and the largest subunit of F_O, subunit **a** (~30 kDa) [20]. It is also found to be in contact with the dimer $\mathbf{b_2}$ [21-23]. Subunit **a** and $\mathbf{b_2}$ form the "stator" complex of the F_O domain. Subunit **a** is made up of five α-helices that traverse the membrane, accessing cytoplasmic and periplasmic spaces [24-26]. The N-terminus is in the periplasm while the C-terminus is in the cytoplasm. Mutagenic studies have implicated both **c** and **a** subunits to be involved in proton translocation (discussed in [27]). The mechanism of proton transport is discussed below.

Proton translocation: Cox et al. gave the first model of proton transport via F_O that involved rotation of **a** and **c** subunits relative to each other. [28]. According to this model, the protons would travel through the "proton channels" in the **a** subunit. Polar residues from one or more of the α-helices of the **a** subunit form the aqueous half-channels and provide access to the center of the membrane from the cytoplasmic and periplasmic spaces [29, 30]. Mutagenic studies first showed that Arg210 was essential for proton transport [31], with later studies showing Glu219 and His245 [32] are also important for proton transport [33-35] and are part of water-accessible proton "half channels" (Fig. 1.2) [32]. The amino acids Arg210 and Glu219 reside on the fourth α-helix and His245 resides on the fifth α-helix of subunit **a** [31, 34]. On the **c** subunit, Asp61, residing on the second α-helix, is crucial for proton transport [36, 37]. The structural arrangement of the **a** and **c** subunits brings these amino acids in close proximity at different stages of proton transport. Different groups have presented similar models to explain the transport of protons through the assembly of **a** and **c** subunits [24, 38-42] (Fig. 1.2). It can be summarized in the following way: during ATP synthesis, an electrochemical proton gradient is generated by

the electron transport chain, with higher concentration of protons in the periplasmic space. At any given time, two **c** subunits interface with subunit **a**. The **c**Asp61 in the α-helices of both these **c** subunits have a pKa of 7.1 and are deprotonated whereas, the **a**Arg210 has a higher pKa that ensures protonation from the periplasmic space [42, 43]. The **a**Arg210 interacts with the deprotonated **c**Asp61 leading to protonation of that **c**Asp61 with protons from the periplasmic space. The protonation leads to an electrostatic rotation of the **c**-ring by one **c** subunit as the **a**Arg210 will now be strongly attracted to the remaining deprotonated **c**Asp61. This ensures a unidirectional rotation of the **c**-ring vs $\mathbf{ab_2}$. The movement facilitates the protonated **c** subunit to access the second half-channel with **a**Glu196 near the end. The pKa of the protonated **c**Asp61 gets lowered on exposure to the hydrophilic cytoplasmic half-channel, leading to the release of proton to the cytoplasm via the half-channel. This deprotonated **c**Asp61 starts its interaction with **a**Arg210 to continue the cycle.

Recently, Meier's group proposed a microscopic model that is reversible and can explain proton transport when it is driven by ATP hydrolysis [175]. X-ray crystal structures of the **c**-ring in low and high pH conditions and in presence of DCCD were presented to support the model. The model proposes that when the carboxylic group of the **c** subunit faces a hydrophobic dehydrated environment, it assumes a proton-locked state and coordinates the proton tightly. This state is thermodynamically stabilized by the lipid membrane environment. During ATP synthesis, when the carboxylic group of a **c** subunit enters the interface with subunit **a**, it encounters a locally hydrated environment, which promotes proton transport to the cytoplasmic side via the aqueous half-channel of subunit **a**. A proton can enter the second half-channel from the periplasmic side and can reprotonate

the now deprotonated **c** subunit. The reprotonated **c** subunit can now adopt the proton-locked state and can interface with the hydrophobic lipid membrane to carry on the cycle. The stochastic alternating of the **c**-ring between these environments is what drives the rotation. It is the proton gradient across the membrane which determines the direction of the rotation of the **c**-ring.

Subunit **b** (~17 kDa) forms the peripheral, stator stalk connecting the membrane-embedded F_O with subunit δ of F_1 [44]. Connection of dimer $\mathbf{b_2}$ with δ is important for functional assembly of the enzyme [45, 46] as well as for stabilizing the enzyme against the torque generated by the rotating **c**-ring, γ and ε subunits [47]. Suggestions have been made regarding the role of the peripheral stalk as an elastic structure that can deform with stepwise movement of protons through F_O [48]. On the other hand, using spin label studies it has been proposed that subunit **b** can affect the conformation of catalytic sites and play a role in coupling of the enzyme [49].

Figure 1.2

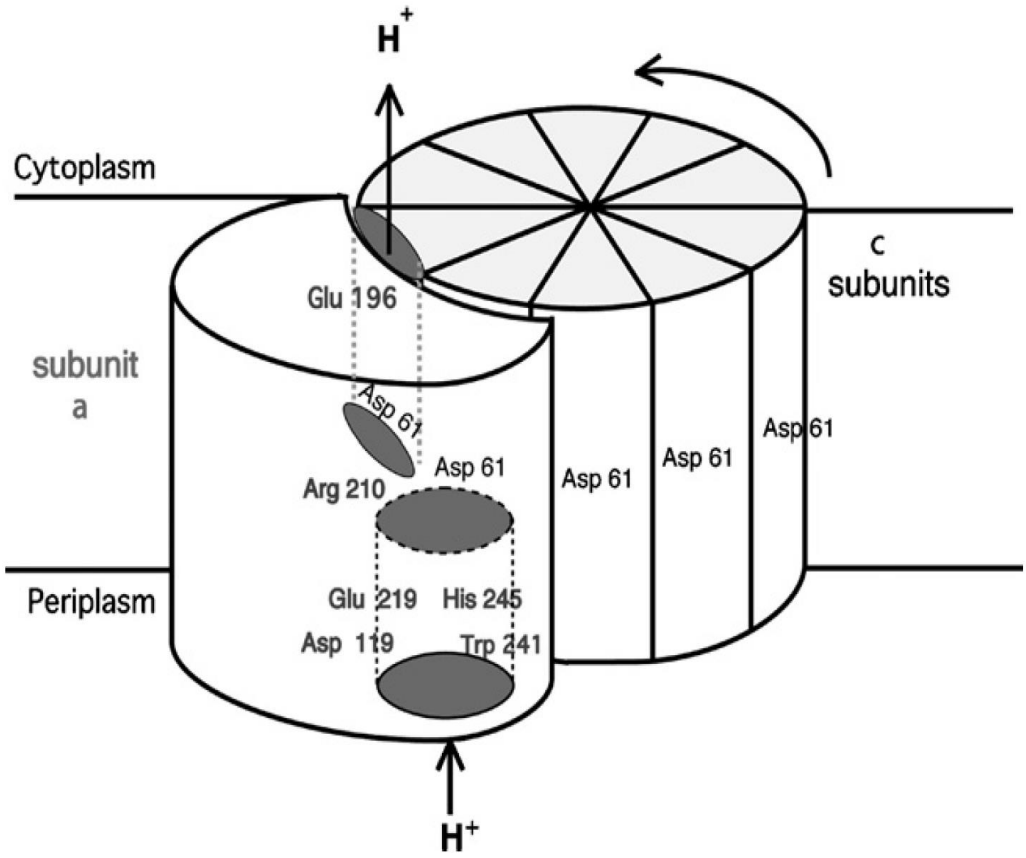
H+
Cytoplasm
c
subunits
Glu 196
subunit
a
Asp 61
Asp 61
Arg 210
Asp 61
Asp 61
Asp 61
Periplasm
Glu 219
His 245
Asp 119
Trp 241
H+

Figure 1.2. Assembly of the a and c subunits for proton transport [24].

Ten **c** subunits are shown to form a ring spanning the membrane. Asp61 residues are located at the center of the **c** subunit. The **a** subunit forms an interface with two subunits of the **c**-ring. The two half-channels are indicated with dotted lines along with important residues that form the channels. The half-channel with access to the periplasmic space is contained within the **a** subunit whereas the half-channel with access to cytoplasm is shown at the interface of **a** and **c** subunit. Movement of protons is from the periplasm to the cytoplasm during net ATP synthesis. This figure has been used with permission from Springer International Publishing AG, license # 3544831260545.

The F_1 domain: The external F_1 domain contains the catalytic sites and is responsible for catalysis in ATP synthesis or hydrolysis direction when coupled with F_O. In bacterial ATP synthase, it can be dissociated from the F_O domain *in vitro* and can function as an ATP hydrolase (ATPase) on its own [50].

The α-β hexamer: In the F_1 domain, three α (~55 kDa) and three β (~50 kDa) subunits are arranged like alternating "segments of an orange" and form a hexamer with a diameter of 100 Å [51, 52]. This hexamer is a part of the stator complex. Both the α and β subunits have high amount of sequence homology and have likely originated by gene duplication [53, 54]. Hence, both the α and β subunits have similar architecture where there are three distinct domains: **(1)** The N-terminus forms a domain that is made up of a β-barrel. The six N-terminal domain β-barrels interact and form a 24-stranded β-barrel "crown" at the top of the α-β hexamer that is thought to play a stabilizing role [55], **(2)** There are a total of six nucleotide binding sites in the central region [55-58], one on each subunit. These binding sites are located at the interface of α and β subunits. They contain an α-helix/β-sheet sandwich motif, which is similar to many nucleotide-binding proteins. Only the sites located predominantly on β subunits participate in catalysis (catalytic sites), whereas the sites on α subunits do not exchange nucleotide during catalysis (non-catalytic sites), **(3)** The bottom region is made up of the C-terminal domain formed by a bundle of six or seven α-helices. In the C-terminal domain of β, an acidic cluster sequence known as DELSEED motif moves with the γ subunit when a nucleotide occupies the catalytic site [59]. This DELSEED motif is thought to play an important role in coupling between rotation of the γ subunit and catalysis.

The γ subunit: At the center of the F_1 domain is a 90 Å long γ subunit (~32 kDa) that connects the F_1 domain to the F_O. The N and C-terminal helices of the asymmetrical γ subunit reside in part within the central cavity of the α-β hexamer. The lower part of γ is in contact with the **c**-ring and the N-terminal domain of the ε subunit. The γ subunit is the major rotor component within the F_1 domain. A full 360° rotation by γ involves hydrolysis of 3 ATP molecules, so hydrolysis of 1 ATP molecule involves 120° rotation of γ [60]. Rotation of the γ subunit within the hexameric cavity leads to interactions with the α-β hexamer at three specific sites labeled as the "catch" sites [61]. These interactions co-ordinate conformational changes in the catalytic sites on the β subunits. The conformational changes are important for binding of substrates, catalysis and release of products in agreement with the "binding change mechanism" proposed by Boyer [62].

The δ and ε subunits: Subunit δ is part of the stator complex and forms the peripheral stalk connecting F_O with F_1. The δ subunit is required for assembly of F_1 with F_O [63]. Its homolog within the mitochondrial ATP synthase is denoted as OSCP [18]. The δ/OSCP subunit plays a structural role and is important for binding and functional coupling of the F_O domain with the F_1 domain.

The ε subunit (~15 kDa) contacts the base of γ as well as the **c**-ring via its N-terminal domain (εNTD). The εNTD is a β barrel made up of ten β sheets and is required for functional assembly of the enzyme. The C-terminal domain (εCTD) is formed by two α-helices that can transition between different conformations and play a major role in regulation of bacterial ATP synthase [12] (more details are in the later part of introduction).

1.3 Binding-change Mechanism

Historically, Mitchell's theory of chemiosmotic coupling proposed that electron transport through the electron transport chain could create a proton motive force and it could drive synthesis of ATP [64, 65]. As a result, many theories were proposed to explain the relationship between proton movement and ATP synthesis. The most widely accepted model was originally proposed by Boyer and was based on oxygen exchange reactions; this later became known as the "binding-change mechanism" [66]. The transport of protons across the membrane lead to conformational changes at the catalytic sites in F-type ATP synthase. These conformational changes cause changes in affinity for reactants and ultimately lead to the formation and release of products. The binding change mechanism encompasses three main postulates: **(1)** during ATP synthesis, energy from PMF is used for binding of ADP and Pi to and release of tightly bound ATP from the catalytic sites and formation of ATP involves a very small free energy change. **(2)** Catalysis is carried out by multiple catalytic sites that are strongly cooperative and function in a sequential cycle. The binding of ADP and Pi to one catalytic site is necessary for release of ATP from the adjacent catalytic site and this is consistent for all three catalytic sites [62]. **(3)** The sequential, cyclical conformational changes in catalytic sites that are necessary for binding and release of reactants are coordinated by rotation of one or more subunits relative to these sites [67]. Experimental data from various groups supported the first two postulates in intact enzyme [68, 69] and isolated F_1 [70-75] of different organisms. Data from other groups supporting these postulates have been discussed in detail [62]. Using cross-linking studies, Duncan et al. were able to demonstrate the third postulate by showing that γ rotates within the central cavity [76]. Further proof was provided through microscopic studies that

involved direct visualization of rotation of an actin filament attached to the γ subunit [77]. It was also proposed that proton transport by F_O involves rotation of subunits [28, 78], which also proved to be true as studies have shown rotation of the **c**-ring [79-81].

The binding-change mechanism entails cooperativity between catalytic sites that are alternating between three different conformational states. These states vary in terms of their affinity, occupancy and/or the type of nucleotide interacting with them [51]. The asymmetry of the γ subunit ensures that no two β subunits adopt the same conformation at any given time. For example, the conformational difference between β subunits in *E. coli* and mitochondrial F_1 has been observed in X-ray crystal structures [12, 51]. The conformational differences cause the catalytic sites to cycle between "tight" "loose" and "open" states with each of the three sites occupying one of the three states at any given time (Fig. 1.3). The tight site has tightly bound nucleotide and is catalytically active whereas the loose and open sites are catalytically inactive and contain loosely bound nucleotide and no nucleotide, respectively. To describe the presence/absence of ATP or ADP on specific β subunits, they have been referred to as β_{TP} (ATP bound, tight), β_{DP} (ADP bound, loose) and β_E (empty, open) (Fig 1.3). A recent X-ray crystal structure with bovine heart mitochondrial F_1-ATPase showed that in the ground state, both β_{TP} and β_{DP} have ATP bound and are loose and tight sites respectively [82].

Figure 1.3

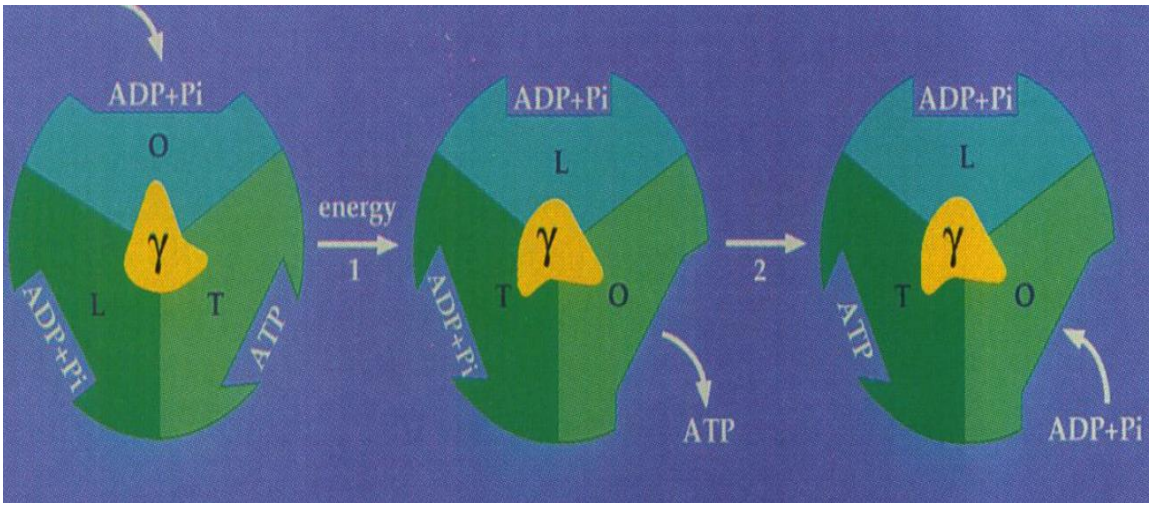
ADP+Pi
O
γ
L
T
ADP+Pi
ATP
energy
1
ADP+Pi
L
γ
T
O
ADP+Pi
2
ATP
ADP+Pi
L
γ
T
O
ATP
ADP+Pi

Figure 1.3. The binding change mechanism of ATP synthase [76]. The three catalytic sites of ATP synthase located mainly on the β subunits are shown in blue/green color. The letters T, L and O denote "tight", "loose" and "open" (empty) conformational states of the catalytic sites. Subunit γ is shown in yellow and rotates with respect to stationary β subunits. In the left panel, ATP and ADP + Pi occupy the T and L sites respectively. The empty O site is shown to bind ADP + Pi. In the first step, the γ subunit rotates 120° and induces changes in the conformational states. As a result, the L site now binds ADP + Pi tightly and becomes T site, the O site now binds ADP + Pi loosely and becomes L site, and the T site releases ATP and becomes empty or O site. In step 2, ATP is formed spontaneously from ADP + Pi bound at the T site. The empty O site now prepares to bind ADP and Pi. This sequence is repeated on all three sites with each 120° rotation of the γ subunit. This figure has been used with permission from Proceedings of the National Academy of Sciences of the United States of America. The figure is subject to copyright protection.

1.4 Rotary Catalysis

The rotational model of ATP synthase involves rotation of the rotor complex to transport protons as well as carry out catalysis. In the F_O domain, the **c**-ring rotates relative to subunits **a** and dimer $\mathbf{b_2}$. Each **c** subunit contains a conserved residue with a carboxyl group (*asp61* in *E. coli*) that gets protonated and transports the proton to the **a** subunit in a step-wise rotating manner. The proton travels through the half-channels of the **a** subunit. The asymmetric γ subunit is in contact with the **c**-ring and the rotation of the **c**-ring leads to rotation of γ relative to α and β subunits within the central cavity. The asymmetry of γ is accommodated in the central cavity through conformational changes in the α and β subunits. These conformational changes are necessary for binding and dissociation of reactants. This model has been used to explain the binding-change mechanism and there are biochemical and spectroscopic data that confirm this as seen below.

Most of the biochemical studies showing rotation involved cross linking subunits within F_1 or F_O or between F_1 and F_O. Duncan et al. [76] successfully showed rotation of γ within *E. coli* F_1 by creating a disulfide bond between β and γ subunits. The idea was that if the γ subunit rotates with respect to α and β, cross-linking γ with β would stop the rotation. If enzyme catalysis required rotation of γ, blocking the rotation would inhibit the enzyme. The crystal structure of bovine F_1 had shown that a homolog of *E. coli* γC87 was positioned close to the ^{380}DELSEED^{386} [59, 83, 84] sequence of β subunit. To take advantage of this positioning, β380D was mutated to βD380C. When disulfide bond was formed between the cysteine residues on γ and β by oxidation the enzyme was inactivated, whereas reduction restored the activity. As an extension of the experiment, the cross-linked enzyme was dissociated into individual subunits. Radio-labeled β subunits were then

introduced at the non-cross-linked positions and the enzyme was reassembled as shown here [85]. Now, oxidation-reduction of the enzyme was carried out again under conditions of catalysis and no catalysis. When oxidation was carried out under no enzymatic turnover, γ was found to be bound to the non-radio-labeled β. However, oxidation post turnover showed γ bound to the radio-labeled β. From this study, it was evident that in isolated F_1, γ rotated relative to the β subunits. Later, cross-linking studies in F_OF_1 linked γ rotation to proton translocation and enzymatic turnover during ATP hydrolysis [86] and ATP synthesis [87]. In both studies, isolated F_1 subunits with βD380C mutation were bound to F_1-depleted membranes. Under oxidizing conditions, one of the three β subunits cross-linked with γ. The remaining two non-cross-linked β subunits were replaced with epitope-tagged βD380C (β_{FLAG}) subunits by dissociation-reassembly [85]. When subjected to reducing conditions to remove β-γ cross-link, the intact enzyme regained coupled membrane activity. In the first study [86], when the enzyme was reduced, exposed to ATP hydrolysis conditions and then oxidized, γ was found to cross-link with β_{FLAG}. Repeating the same events but with no ATP hydrolysis resulted in little or no β_{FLAG} cross-linked with γ. In the second study [87], the enzyme was exposed to ATP synthesis conditions with the same experimental setup. Again, ATP synthesis conditions led to γ cross-linking with β_{FLAG} and preventing ATP synthesis led to little or no β_{FLAG} cross-linked with γ. This showed that γ rotation was necessary for enzymatic turnover in F_OF_1. In addition, in both studies, membranes were treated with DCCD (dicyclohexylcarbodiimide). DCCD is a covalent modifier of Asp61 of **c** subunit and treatment of F_O with DCCD blocks proton transport [88]. When DCCD treated membranes were reduced and subjected to either ATP synthesis

or hydrolysis conditions, β_{FLAG}-γ cross-linking was considerably reduced. This showed that blocking proton transport by **c**-ring in F_O leads to blocking of γ rotation in F_1.

Rotation of other subunits was also investigated by cross-linking studies. Cross-linking ε and γ had no effect on hydrolysis activity, suggesting that ε and γ rotate together [89]. Further, hydrolysis and synthesis activity was inhibited by cross-linking of ε, γ and β, and fully restored when cross-linking was removed, indicating that ε and γ rotate relative to β [90]. Subunit δ was shown to be part of the stator as α-δ cross-linking did not affect ATPase activity of the enzyme [91]. Whereas rotation of the **c**-ring was demonstrated via γ-ε-**c** [92] and **c**-$\mathbf{b_2}$ cross-linking [93]. The cross-linking of **c**-ring with rotor subunits γ and ε did not affect ATP hydrolysis, synthesis or proton pumping indicating that the **c**-ring was a part of the rotor complex. With these studies, subunits α, β, δ, **a** and $\mathbf{b_2}$ appear to be part of the stator complex whereas γ, ε and the **c**-ring make up the rotor complex.

A more direct demonstration of rotation was achieved by attaching fluorophores to one of the subunits and then observing the movement via microscopy. The first study to show rotation of γ within F_1 used a fluorescent actin filament to observe rotation in F_1-ATPase of thermophilic *Bacillus PS3* [77]. Isolated F_1 domain was immobilized in a top-down orientation on a Ni^{+2}-nitrilotriacetic acid (Ni-NTA)-coated coverslip via a His_{10} tag added to the N-terminus of β subunits. On the γ subunit, γS107 was mutated to obtain γS107C, which was then labeled with biotin maleimide. A biotinylated actin filament (≤ 3 μm) that was fluorescently labeled, was attached to the biotin maleimide via streptavidin (Fig. 1.4A). This facilitated visual observation of γ subunit rotation in the epifluorescence microscope. Actin filaments were observed to be rotating in the presence of ATP, but not in the absence of ATP or in the presence of ATP plus sodium azide (inhibitor of catalysis

by F_1). This linked rotation of γ with net hydrolysis by the enzyme. When viewed from the top, the direction of γ's rotation was observed to be counterclockwise relative to the α-β hexamer. A similar approach was used for observing γ rotation in *E. coli* [94] and chloroplast F_1 [95] and ε rotation in thermophilic *Bacillus PS3*, where actin was attached to ε [96]. The rotation of actin filaments took place in three 120° steps. Observation of actin filament rotation was a novel approach to prove subunit rotation in the enzyme; however problems related to steric effects and viscosity due to actin filament's size impacted determination of the true rate of rotation and torque. Other problems included binding of one filament to multiple complexes that were close to each other and collision between closely spaced actin filaments.

Figure 1.4

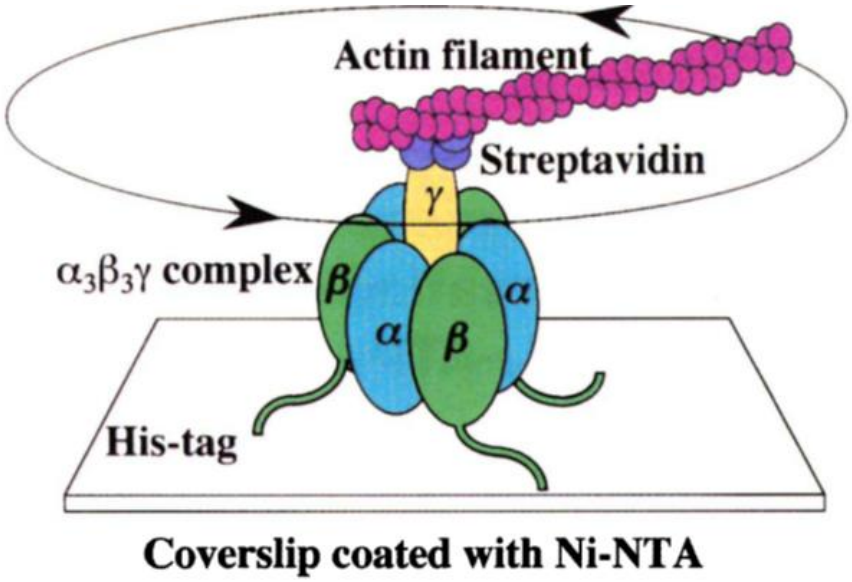
Actin filament
Streptavidin
γ
α3β3γ complex
β
α
α
β
His-tag
Coverslip coated with Ni-NTA

A

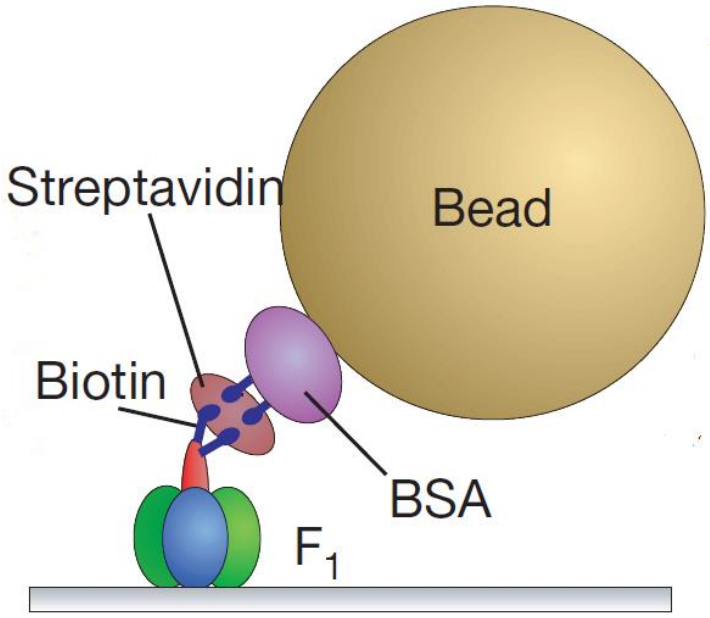
Streptavidin
Bead
Biotin
BSA
F1

B

Figure 1.4. Direct observation of rotation of the γ subunit. A. Schematic shows overall experimental setup with isolated F_1 [77]. The subunits are not to scale. Three β subunits with His_{10} tags at the N-terminus were immobilized on Ni-NTA coated cover slip. Subunit δ was removed. An introduced cysteine near the "foot" of γ was labeled with biotin-maleimide. Biotinylated fluorescent actin filament was bound to the biotin-maleimide tag via streptavidin. Rotation of actin filament was measured by epifluorescence. **B.** Modified setup shows F_1 immobilized on a coverslip through β His_{10}-Ni-NTA binding [97]. Biotinylated Gold bead of 40 nm was attached at an angle to the γ subunit using streptavidin and bovine serum albumin (BSA). Rotation was observed by laser dark-field microscopy. Figures in panel A and B have been used with permission from Nature Publishing Group. License # 3544840407249 and 3544840587661.

The experimental conditions were modified later to attach a fluorescent bead instead of actin filament and spacing F_1 complexes at fixed distances such that the beads would neither bind to more than one complex nor collide with other beads [98]. However, the size of the fluorescent bead was still large (diameter = 1 μm) and the rotational rate and torque measured in this study was lower than what other groups have reported. Critical advancement was made in the field with replacement of fluorescent beads with gold beads of 40 nm diameter (Fig. 1.4B) [97]. The smaller size reduced the viscous drag on rotation of γ and the 120° steps of γ were observed with saturating concentrations of MgATP. With ATP concentration below K_M, the 120° steps were found to occur in substeps of 90° and 30°. These substeps were later corrected to be of 80° and 40° rotation [99]. The 120° rotation of γ was proposed to follow this scheme: binding of ATP to β_E drives an 80° rotation of γ. At this position, the enzyme halts for a brief period of time which is called the catalytic dwell. The ATP is hydrolyzed at β_{TP} during the catalytic dwell followed by Pi release from β_{DP}. Further 40° rotation releases ADP from β_{DP} which completes the 120° rotation of γ [100, 101]. These assays showed that γ rotation is involved in ATP hydrolysis. Proving it for ATP synthesis was tricky as ATP synthesis requires both F_O and F_1 assembled and coupled. Immobilizing the entire enzyme on the cover slip has proven to be tough. A way around this was worked out by attaching magnetic beads to γ [102, 103]. Magnetic tweezers were then used to force the rotation of γ in the synthesis direction with ADP and Pi present. Rotation of γ in the synthesis direction showed synthesis of ATP from ADP and Pi. When the magnetic field was turned off, γ rotated in the hydrolysis direction at a rate that was proportional to the concentration of ATP present. This was used to calculate the efficiency

of ATP synthase in synthesizing ATP to be ~80%. This proved that γ rotation is important for ATP hydrolysis and synthesis.

The rotational model serves best to explain the binding-change mechanism by which ATP synthase functions. Taken together, the complete process follows this series of events: Electron transport chain transports electrons coupled with pumping of protons across a semi-permeable membrane, leading to the establishment of proton motive force. The potential energy of the PMF is used by the enzyme to drive rotation of the **c**-ring relative to subunits **a** and $\mathbf{b_2}$ in F_O. Each **c** subunit carries one proton that is transported to the partial channels of subunit **a** and then to the cytoplasm. Rotation of the **c**-ring is coupled with rotation of γ via direct physical connection. The rotation of an asymmetric γ subunit within the hexameric cavity occurs coordinately with conformational changes in α and β subunits. These conformational changes change the affinities of the catalytic sites towards substrates and products and facilitate binding/dissociation of reactants. Thus, the potential energy of PMF is used to drive synthesis of ATP by the enzyme.

ATP synthase plays a pivotal role in energy metabolism. However, under certain conditions the cell has to inhibit the enzyme. As is the case with many other enzymes, there is more than one way to inhibit ATP synthase. While mitochondrial ATP synthase is inhibited by a separate protein IF_1 [104], bacterial [105, 106] and chloroplast [107] enzymes are inhibited by the native epsilon subunit. In addition, ADP can inhibit the enzyme [108] and has been shown to compete with ε inhibition [109]. Sodium azide is another catalytic site inhibitor [108] that can inhibit the enzyme by stabilizing the ADP-inhibited state. Other inhibitors include oligomycin, dicyclohexylcarbodiimide, venturicidin, tentoxin, efrapeptin and fluoro-aluminate [110]. In the following section, I

will talk about the *epsilon* subunit, which is the natural inhibitor of bacterial and chloroplast ATP synthases. The work described in this document has focused on understanding the regulatory role of the ε subunit in the *E. coli* ATP synthase.

1.5 The *Epsilon* subunit

The ATP synthase is ubiquitous in eubacteria and in many pathogenic species, it plays a role that is not restricted to cellular energy metabolism. For example, the anaerobic pathogen *Streptococcus pneumoniae* uses the enzyme as an ATP-driven proton pump to maintain pH homeostasis [111]. The pathogen causes pneumonia, meningitis and otitis media and deaths of three million children per year [112]. Studies showed that when the expression of the enzyme was prevented by genetic disruption, it led to loss of viability in the bacteria, indicating that the enzyme is essential [113]. In *Streptococcus mutans* that cause dental caries, ATP synthase again functions as a proton pump and provides acid-tolerance at pH values that otherwise would prove lethal [6]. Similarly, *Listeria monocytogenes*, a food-borne, gram positive, facultative anaerobic bacteria that causes deadly infection of the central nervous system [114], requires ATP synthase for acid-tolerance as evidenced from the increased sensitivity of the bacteria to low pH following DCCD treatment [7]. In addition, ATP synthase appears to be important in gastrointestinal gram negative pathogens like *Salmonella enterica* [115], *Helicobacter pylori* [116] and Enterohemorrhagic *E. coli* [117]. All these studies demonstrate a crucial role for ATP synthase in bacterial pathogens. Recent FDA approval of a drug targeting the ATP synthase of *M. tuberculosis* has shown that the enzyme can be an attractive target [118]. This has generated a lot of interest in finding compounds and ways to inhibit the enzyme in order to develop antimicrobials.

The ε subunit is the smallest subunit in the F_1 domain and plays an inhibitory role in chloroplast and bacterial enzymes. Its inhibitory properties were first seen in chloroplast enzyme [119]. In the bacterial ATP synthase, ε was shown to be inhibitory first in *E. coli* [105, 120, 121]. Its inhibitory role was confirmed in *E. coli* [122, 123] as well as

thermophillic *Bacillus PS3* [124]. In contrast, the homolog of ε in mitochondria, δ, is not inhibitory [174]. In addition to regulating the enzyme, ε or its homolog is required for proper assembly of the bacterial [122, 125, 126] and mitochondrial enzyme [127]. While not required for assembly of the chloroplast enzyme, absence of ε leads to loss of coupling between proton transport and catalysis [128, 129]. In one study, bacterial enzyme that contained ε subunit without the entire C-terminal domain, showed increased uncoupled ATP hydrolysis and decreased proton pumping. This led to a proposal of an additional role of ε in energy coupling [130]. It was speculated that the primary role for ε is to prevent uncoupled ATP hydrolysis and not to regulate the coupled activity.

With ε playing such an important role in regulation and function of the enzyme in bacteria but no known inhibitory role in mitochondria, it is only natural to search for ways that allow targeting it in pathogens to inhibit growth or viability. The goal would be to either increase the ε-mediated inhibition to reduce the enzymatic activity or to decrease the inhibition to interfere with the regulation of enzyme function. Any compound that either improves or reduces ε's inhibitory ability may be of interest. Thus, targeting ε provides fair amount of flexibility. The following section contains a detailed account of the ε subunit of *E. coli* ATP synthase in order to set up a proper background for the remaining chapters of the thesis.

Structure of epsilon: *E. coli* ε subunit is a 138 amino acid long protein of approximately 15 kDa. It is located at the "foot" of the γ stalk, interacting with γ and the **c**-ring. The structure of isolated ε subunit was determined first by NMR spectroscopy [131] and later by X-ray crystallography [132] (Fig. 1.5). Both of these structures showed that ε is formed by two domains: an N-terminal domain (εNTD) (residues 1-87) and C-terminal

domain (residues 88-138). The NTD consists of two antiparallel β-sheets, each made up of five β-strands, arranged in two layers and making up a flattened β-barrel (Fig. 1.5). Except for β1 and β9 strands, all other β strands are arranged anti-parallel to each other. Hydrophobic amino acids are arranged such that they point towards the interior of the β barrel. One of the two sheets contains a hydrophobic patch spanning all five β strands, which plays an important role in binding with the γ subunit.

The CTD is formed by two antiparallel α-helices connected by a loop [131]. The contact surface between the helices is hydrophobic and involves five highly conserved alanine residues that are arranged like a "zipper" such that Ala94, Ala97 and Ala101 on one α-helix interact with Ala117 and Ala124 on the adjoining α-helix. The CTD had been observed to adopt two distinct conformations based on trypsin digestion studies with *E. coli* F_1 as well as intact F_OF_1 [133, 134]. In the presence of MgADP and Pi, ε was resistant to trypsin but in presence of ATP without Mg^{2+}, trypsin treatment showed extensive cleaving. So the conformations depended on the state of the enzyme with the "active" state of the enzyme allowing trypsin digestion and the "inactive" state preventing it. But the exact details of those conformations were not known. High resolution crystal structures of *E. coli* F_1 revealed that the conformational change involves changes in the CTD α-helices whereupon the α helices can stay in a coiled coil close to each other (termed as compact conformation, ε_C) or the second helix can extend and insert in the central cavity of the α-β hexamer (termed as extended conformation, ε_X) [12].

Figure 1.5

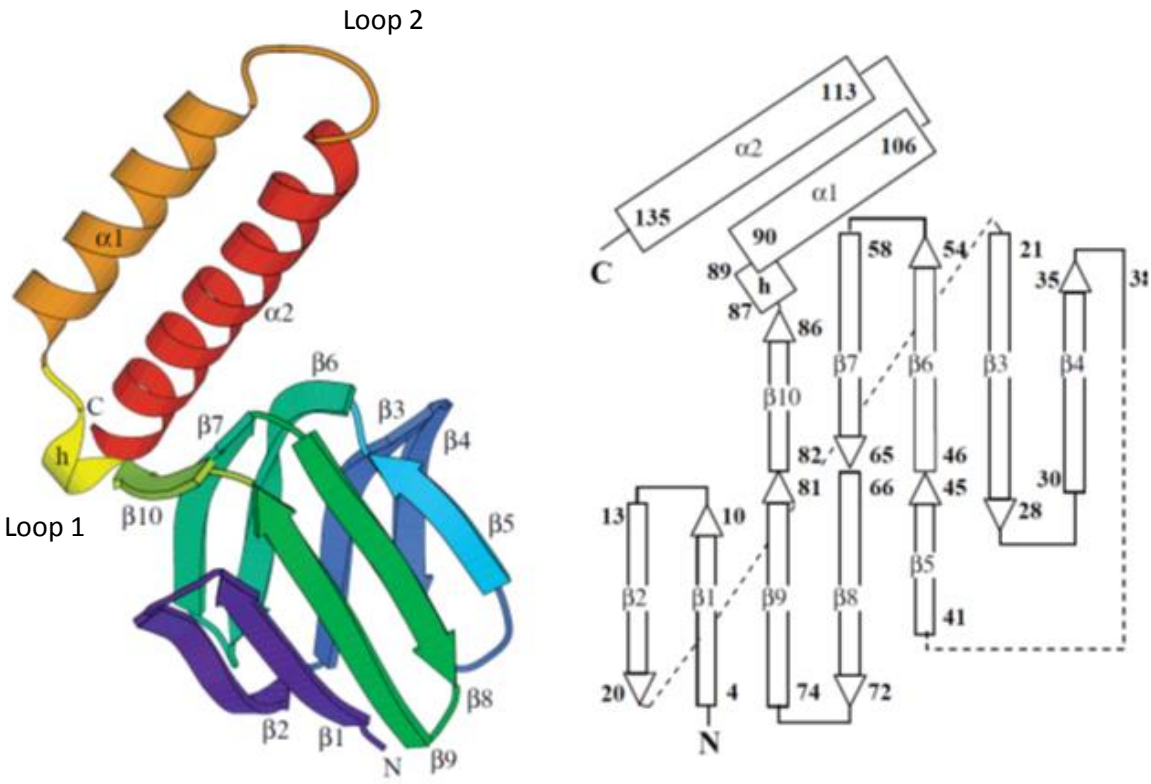
Loop 2
α1
α2
C
h
β7
β6
β3
β4
β10
Loop 1
β5
β8
β2
β1
N
β9
113
α2
106
α1
135
90
C
89
h
87
86
58
54
21
35
β7
β6
β3
β4
β10
82
65
46
81
66
45
30
13
10
28
β5
β2
β1
β9
β8
41
20
4
74
72
N

(A) **(B)**

Figure 1.5. The structure of *E. coli* ε subunit [132]. Panel (A) shows the 3-dimentional structure of the *E. coli* ε subunit (PDB ID 1aqt). Ten β sheets of the NTD form a flattened barrel and are depicted in shades of green and blue. The CTD α-helices form a coiled-coil close to the NTD and are depicted in yellow (loop1), orange (helix1 and loop2) and red (helix2). Panel (B) shows the arrangement of the β sheets with respect to each other in a 2-dimentional form. Figures in panel A and B have been used with permission from Elsevier Limited. License # 3544841066015.

Interaction of epsilon with other subunits: The localization of ε with respect to other subunits was not clear from the initial crystal structure of mitochondrial F_1 [51]. In electron microscopy studies of F_1, γ was found to form the central stalk and ε was positioned with it [135]. Cross-linking studies involving cross-linking of ε with other subunits gave hints regarding the location of ε [136, 137]. They also revealed that ε establishes numerous contacts with subunits of both F_O [138] and F_1 [137] domains. In addition, information regarding the specific amino acids involved in when ε interacts with other subunits, and the possible conformational change of the ε subunit was also obtained. The regulatory function of the ε subunit in bacterial and chloroplast ATP synthase was known but the mechanism by which it regulated the enzyme was not yet clear. Hence, to understand the function of ε its interactions with other subunits of the enzyme under different conditions were investigated.

εNTD interactions: Initial studies in *E. coli* revealed that ε interacts with the γ subunit [139]. Later, it was shown that ε binds to the γ subunit with high affinity (K_D = 3 nM) [140]. Other studies have shown ε10 cross-linking with γ228 [136], ε38 with γ205 [89] and ε43 to γ between γ202 and γ286 [141]. Originally, a genetic study showed that a mutation in the ε subunit at residue 31 recoupled ATP hydrolysis and proton pumping in *E. coli* ATP synthase that was uncoupled due to Q42E substitution in the **c** subunit [142]. This suggested that there was some functional interaction between the ε and **c** subunits. Using cross-linking studies, it was shown that εNTD interacts with the **c**-ring of the F_O domain at multiple positions [142]. These interactions of ε with γ and **c**-ring were consistent with the location of ε in intact enzyme seen by electron microscopy [135, 143]. The conformation of ε was similar to that of the isolated ε observed in NMR and crystal

structures [131, 132]. In this conformation, the NTD and CTD were in close proximity of each other and would be positioned under the α-β hexamer. However, Lotscher et al. showed direct interaction of β and ε by cross-linking through a water-soluble carbodiimide that only cross-links sites in very close proximity [144]. This cross-linking would only be possible if ε exists in a conformation that is different from the one seen in the structures.

εCTD interactions: The structure of isolated ε showed the εCTD α-helices close to each other [131]. In addition, the α-helices contact the εNTD with a buried surface area of 910 Å^2 [132]. This region is closely packed, hydrophobic in nature and inaccessible to solvent. When ε was shown to cross-link with γ or **c** subunit, it adopted the same conformation as the isolated ε [145]. In other studies εS108 in the loop between α-helices was found to interact with β380 [76] and β381 (Fig. 1.7, [146]) residues as well as with α411 [147]. Hence, the cross-linking of ε to α and β gave further indication of conformational change in ε. Moreover, the interactions were shown to be dependent on the type of nucleotide present, indicating an interplay between ε and nucleotides [147]. Cingolani and Duncan resolved a X-ray crystal structure of *E. coli* F_1 at a resolution of 3.26 Å that showed ε in a markedly different conformation than previously available crystal and solution structures (Fig. 1.6 and 1.7) [12]. In this state, the α-helices had undocked from the coiled coil (compact conformation, ε_C) and partly inserted in the central cavity of α-β hexamer. This state was called the "extended" conformation (ε_X). In this conformation, εCTD contacts five subunits in total and buries ~2900 Å^2 of surface area [12]. As shown in Fig. 1.6, in the εCTD, the helix1 and loop1 contact the γ subunit with helix1 binding to the Rossmann fold of γ. The last β strand of the εNTD changes folding when εCTD transitions between the compact and extended conformations. With εCTD in the ε_C state,

the β strand is folded and is part of εNTD; whereas in the ε_X state, the strand gets unfolded into a loop1 and becomes part of εCTD (Fig. 1.6). In the ε_X state, helix2 establishes contacts with β1, β3, α1, α2 subunits within the central cavity. These interactions of helix2 appear important for stabilizing the ε_X conformation. The antiparallel coiled coil between helix2 and γ is accompanied with hydrogen bonds and electrostatic contacts making a very stable interaction. On the other hand, helix2 is further stabilized by interactions with α1 and α2. Post insertion, rotation of γ is thought to position helix2 directly between γ and β1 and leads to blocking of the interaction between β1 and γ. The "hook" region of εCTD appears to have few if any specific bonds with other subunits but shows a large amount of buried surface area with β3.

Figure 1.6

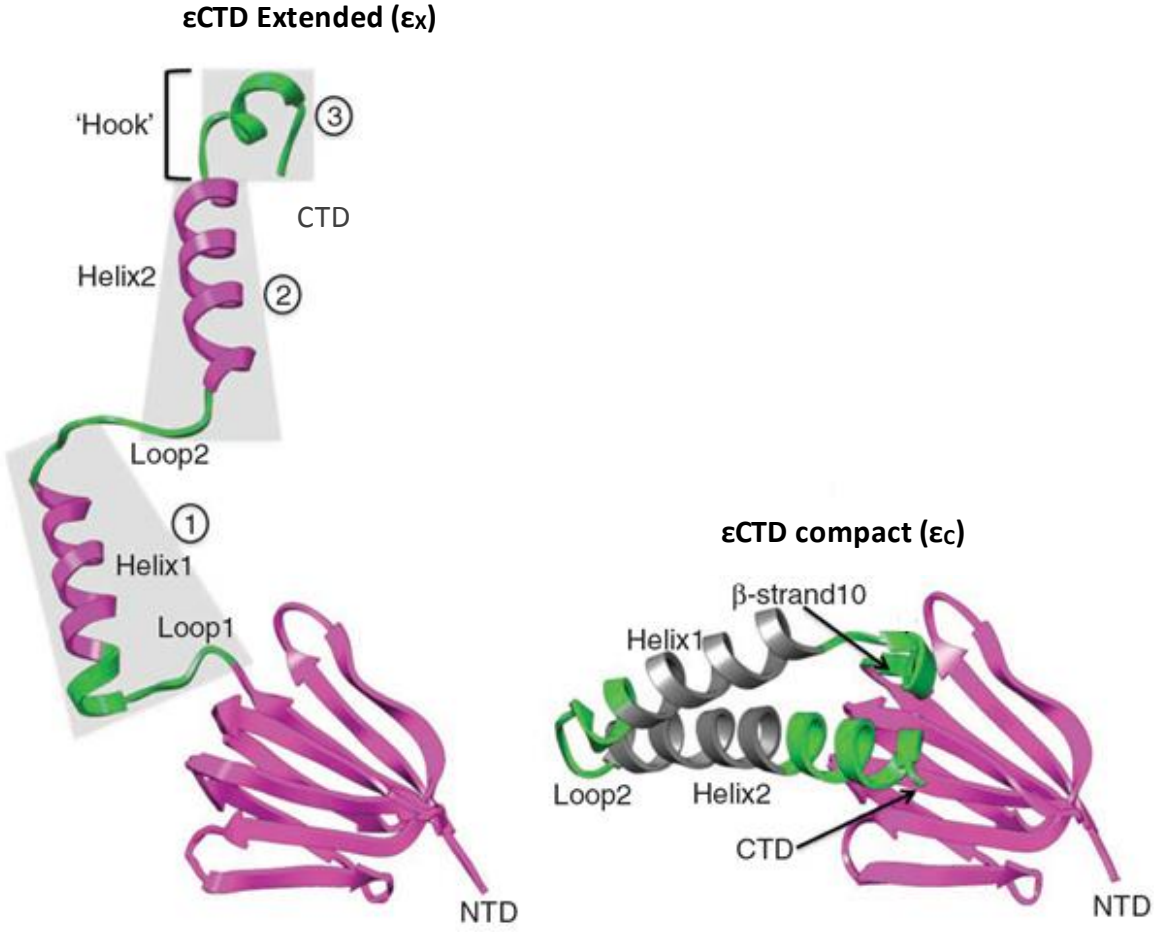
εCTD Extended (εX)
'Hook'
③
CTD
Helix2
②
Loop2
①
Helix1
Loop1
NTD
εCTD compact (εC)
β-strand10
Helix1
Loop2
Helix2
CTD
NTD

Figure 1.6. Conformational changes in the εCTD of *E. coli* ATP synthase [12]. The panels show alternative conformations adopted by the C-terminal domain of ε. On the right is the compact conformation (ε_C) where the CTD α-helices (grey and green) are in a coiled coil, close to the N-terminal domain (magenta) and β-strand 10 is folded. The CTD contains helix1, loop2 and helix2. On the left is the extended conformation (ε_X) in which the three regions of the CTD that interact with other subunits are numbered. Region 1 contains loop1 which, in the ε_X state, is formed by unfolding of tenth β strand of NTD and part of helix1. Region 2 contains loop2, which is longer in ε_X than in ε_C, and helix2 which becomes two α-helices punctuated by a "hook" region (Region 3) in ε_X. This figure has been used with permission from Nature Publishing Group. License # 3544830888375.

Figure 1.7

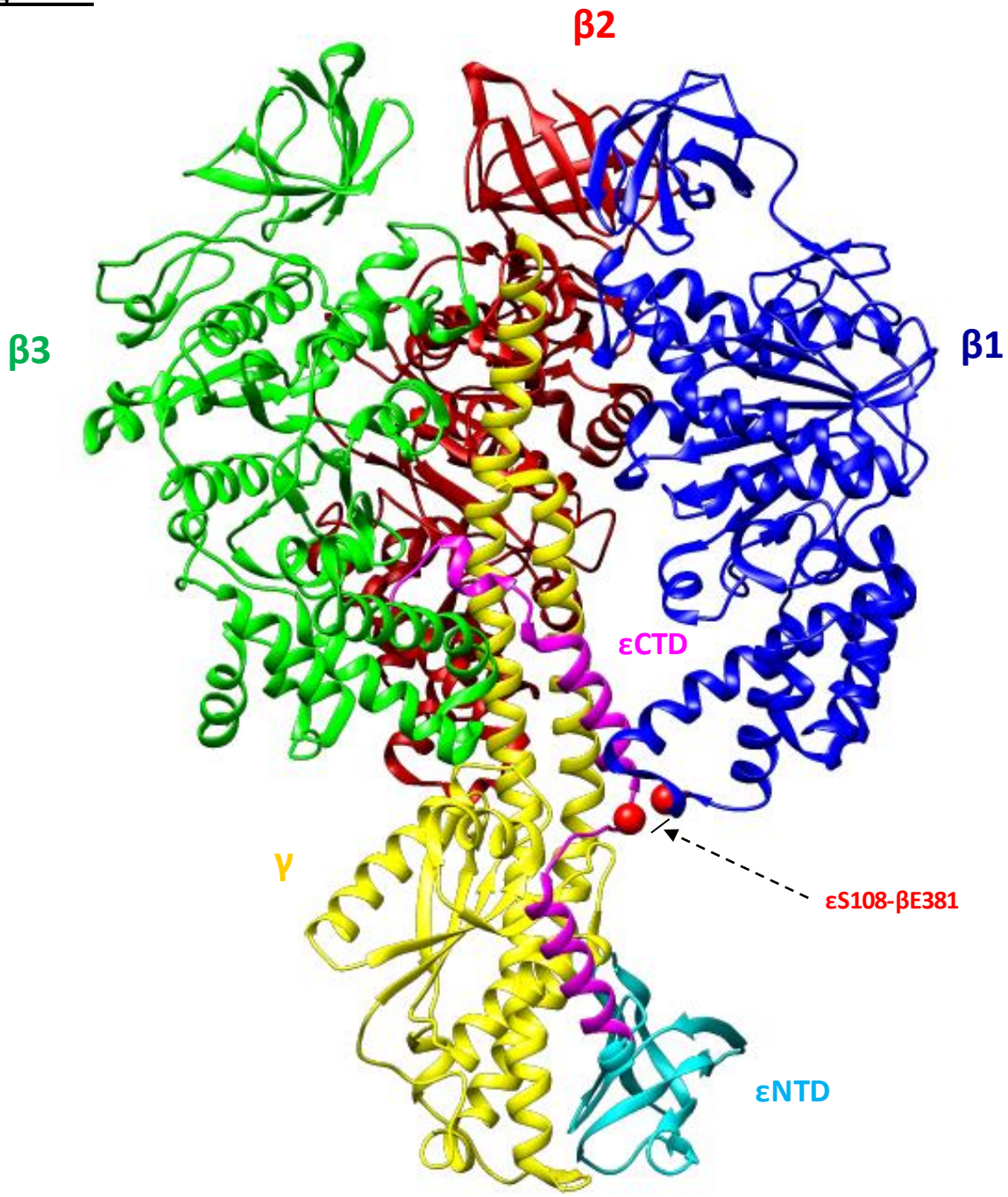

Figure 1.7. *E. coli* F_1 domain with the εCTD in extended conformation. F_1 X-ray crystal structure is shown in a similar manner as [12] (PDB ID 3OAA). The three β subunits are depicted in red, green and blue and the three α subunits are omitted to allow better visualization. The γ (yellow) and the εCTD (magenta) are shown to insert in the central cavity. The εNTD (cyan) is near the foot of γ. The residues εS108 and βE381 are shown by space filling atoms.

Functional role of epsilon: In bacterial ATP synthase, ε assumes a critical role for ensuring proper assembly and function [122]. Since ATP synthase is at the center of energy metabolism, it is safe to say that ε's role in the bacterial cell is very important. The primary role of εCTD was found to be in inhibiting ATP hydrolysis by bacterial [120, 124, 148] and chloroplast enzymes [107]. The first documentation of ε's inhibitory property was in the chloroplast F_1 where it was identified as a cold stable, hydrophobic inhibitor specific for chloroplast and having no effect on mitochondrial F_1 [119]. Later on, Smith et al. [120] were able to partially purify ε from *E. coli* F_1 and show inhibition of ATP hydrolysis by ε for the first time. The same group further characterized *E. coli* ε's inhibitory property and showed that ε can be dissociated from F_1 by dilution [105, 121]. It had become evident that ε can strongly (~90%) inhibit the ATPase activity of isolated F_1. Treatment with the detergent lauryldimethylamine oxide (LDAO) increased ATPase activity, revealing that ATP hydrolysis of isolated F_1 was inhibited by about 5-6 fold by ε [149]. Studies using reagents like LDAO, ethylene glycol and octyl glucoside, that alleviated the inhibition, shed light on the mechanism of inhibition by ε [149-151]. LDAO was found to cause dissociation of δ from F_1 [151] but the ε subunit was able to inhibit the F_1ATPase in absence of δ [105]. Cross-linking of ε and β by a water-soluble, zero length carbodiimide was reduced in the presence of both ethylene glycol and LDAO, suggesting that ε interacted physically with the β subunits to inhibit the enzyme. In addition, the inhibition was alleviated by heat (in chloroplast enzyme) [105, 119], alcohol (in chloroplast enzyme [152] and in bacteria [153]) and trypsin treatment [134, 154]. The exact mechanisms by which of many of the above mentioned factors alleviate the inhibition are not completely understood. The data suggested that ethylene glycol and LDAO perturbed ε's interactions

with β without dissociation of ε, alcohol caused dissociation of ε and treatment with trypsin cleaved the C-terminal domain. Thus, reduction of inhibition thus appeared to work by interfering with the normal interactions of ε within the enzyme. This further confirmed the inhibitory role of ε in bacteria and chloroplasts.

Since ε contains two distinct domains, the question arose about which domain is predominant in exerting the inhibitory effect. To investigate this, ε was truncated to different lengths and the effects of these truncations were observed on the enzyme's function. Masamitsu Futai's group showed that deleting 60 amino acids (78-138) in *E. coli* ε prevented inhibition of ATPase activity [123]. This result was the first indication that the C-terminal domain is primarily involved in inhibition and dispensable for growth. In another study, different residues of εCTD were substituted with alanine [155]. The membrane ATPase activity of the enzyme with the truncated ε was less inhibited than the wild-type. This study again gave strong evidence for ε's role in inhibition of the ATPase activity. With the high resolution crystal structure revealing the conformational changes as well as extensive contacts between εCTD and other subunits, it became clear that the εCTD inhibited the enzyme by jamming the gears of the rotor complex [12]. The interactions of helix1, helix2, loop1 and loop2 of εCTD with F_1 were suggested to be facilitating the inhibition of γε rotation within the cavity. The inhibition by εCTD in bacteria is non-competitive with ATP except in the case of *Bacillus PS3* where ε physically binds ATP and competes [156]. Further evidence that the εCTD is dispensable for growth is seen in *E. coli* mutants that lack the entire εCTD, yet show nearly normal activity and growth [123, 130]. Further, wild-type anaerobic organisms like those from the *Bifidobacterium* genera

contain ATP synthases whose ε is devoid of both εCTD α helices [157]. In these bacteria, ATP synthase primarily acts as an ATPase-driven proton pump.

There were doubts regarding ε's role in inhibition of synthesis [148, 158] as most of the studies showed ε inhibition of ATP hydrolysis and were carried out with isolated F_1. As measurement of ATP synthesis required working with intact F_OF_1 in membranes and removal of ε led to dissociation of F_1 from F_O [122], it was tough to document inhibition by ε on membranes. Moreover, the inhibition of ATP hydrolysis on membranes by ε was markedly lower than that of isolated F_1. This led many to believe that ε-inhibition was limited to ATP hydrolysis only in isolated F_1 and inhibition was actually relieved when ε-inhibited F_1 bound to F_O on the membrane [158, 159]. As a result, many groups concluded that ε's inhibition was limited to ATP hydrolysis and only in isolated F_1.

This conclusion however proved to be untrue. Past studies had shown that protease digestion of isolated F_1 cleaved the ε subunit [154], which led to an increase in enzymatic activity [160]. When intact *E. coli* F_OF_1 within cell membrane was treated with trypsin, it also increased the hydrolytic activity at a rate similar to that obtained with ε digestion [133]. This indicated that ε may inhibit enzymatic activity in whole F_OF_1, too. Moreover, treatment with LDAO had shown that ε was able to inhibit ATP hydrolysis of membranes by 3-fold [149]. Taken together, these results were supportive of ε's inhibitory role in the intact ATP synthase. It also opened up the possibility that ε may have an inhibitory role in the ATP synthesis direction. The studies that showed that ε inhibits ATP hydrolysis and synthesis by intact *E. coli* [161] and *Bacillus PS3* [124, 162] confirmed ε's inhibitory role in ATP synthesis.

Many studies had shown that ε is necessary for binding of the F_O domain to the F_1 domain in *E. coli* and *Bacillus PS3* [125, 126], though one study demonstrated that deletion of first 15 residues still results in proper assembly and a functional enzyme [163]. In addition, most of the binding energy for ε's binding to F_1 is provided by the εNTD [109]. The facts that the enzyme could not assemble without ε [122, 123, 148], and that *E. coli* mutants with deletion of residues 73-138 (εNTD contains residues 1 to 88; so part of εNTD is deleted) failed to grow aerobically, proved that the NTD was necessary for assembly and indispensable for growth. The mutants with deletions of 1-16 residues in εNTD show defective coupling between F_O and F_1, further demonstrating a role for εNTD in enzyme assembly [163]. Alanine-scanning mutagenesis of *E. coli* ε residues 10-93 (mainly the N-terminal domain) resulted in mutants that had either increased ATPase inhibition and decreased DCCD sensitivity or increased ATPase activity and lower membrane bound F_1 [164]. The results hinted at the role of εNTD in binding to the γ subunit and in assembly of F_O and F_1. Mutations that probably interfered with the binding led to lower inhibition of the enzyme and dissociation of F_1 from the membrane, which again pointed at its importance for assembly of the enzyme.

Apart from inhibition, ε has been found to have a role in coupling of catalysis with proton pumping. *E. coli* mutants lacking the entire CTD of ε (ε88stop) and fusion of 20 kDa Flavodoxin on NTD showed higher ATP hydrolysis that was uncoupled from proton pumping [130]. Moreover, ε88stop mutants without the NTD fusion showed decreased ATPase-driven proton pumping compared to wild-type membranes. With partial deletion of εCTD, mutants showed reduced proton pumping without any effect on ATPase activity.

In *E. coli*, ε is required for conformational changes in γ which, in turn, may be required for coupling of proton pumping with catalysis [165, 166].

The ε subunit plays an important role in ATP synthesis. In chloroplasts, intact F_OF_1 has markedly lower ATP synthesis rates if ε is absent [128, 129, 167]. In isolated F_1-ATPase when γ is forced to rotate in the direction of ATP synthesis, ε is required to achieve respectable ATP synthesis efficiency [103]. In the absence of ε, the forced rotation led to a production of ~0.5 ATPs per 1 rotation of γ, while in the presence of ε, ~2.3 ATPs were produced (an efficiency of 77%). The exact role of ε in ATP synthesis is unclear but speculations range from stabilizing part of γ, which experiences the mechanical torque, to facilitating a switch to ATP synthesis mode by undergoing structural changes.

Effects of ligands/chemicals on ε's conformation: As mentioned earlier, the C-terminal domain of ε can adopt different conformations that play important roles in enzyme regulation. The C-terminal α-helices can adopt a compact conformation (ε_C) with both helices close together in a coiled-coil or an extended conformation (ε_X) with both helices extended and making multiple contacts with other subunits of F_1 [12]. The conformational change is related to the ligand interacting with the catalytic sites of the enzyme at any given time. The interactions of ligands with non-catalytic sites are not crucial for conformational change [168]. In this section, effects of different ligands on εCTD's conformational changes will be discussed.

As discussed earlier, the *E. coli* ε subunit can be digested by trypsin treatment of F_1 and F_OF_1. As a result, trypsin treatment experiments have led to important information about the conformational changes in εCTD as they relate to F_OF_1 function. The CTD of ε can transition between an extended (ε_X) conformation and a compact ε_C conformation. Intact ATP synthase and isolated F_1 were trypsin treated in the presence of various nucleotides to elucidate changes in the conformational states of εCTD [133, 134]. The main cleavage site where trypsin acts is in εhelix2 [133, 169]. The cleavage by trypsin is slow in isolated ε (ε_C) or in *E. coli* F_OF_1 in the presence of post turnover conditions (Mg-ADP-Pi or Mg-ATP to obtain Mg-ADP-Pi) that favor the ε_X state. This is because εhelix2 is inaccessible to trypsin as it is packed between εNTD and εhelix1. Whereas, pre-hydrolysis conditions of AMPPNP alone (non-hydrolysable structural analog of ATP), ATP/EDTA, ADP alone or Mg-ADP but no Pi lead to fast εCTD cleavage. The explanation to this is that although these conditions disfavor the ε_X state, εCTD is thought to adopt an intermediate conformation between ε_C and ε_X such that εhelix2 is available to trypsin [12].

The post turnover nucleotides appear to either increase the rate of transition from ε_C to ε_X or decrease the rate of transition from ε_X to ε_C. Inorganic phosphate (Pi) appears to play an important role in maintaining the ε_X conformation. On the other hand, the presence of ATP + EDTA, AMPPNP, Mg-ADP, ADP alone predispose ε to the trypsin accessible conformation either by preventing transition to the ε_X conformation or by pushing ε out of the ε_X conformation. It is likely that they prevent the transition to ε_X conformation as otherwise pushing ε out of the ε_X state would mean that the ligands are competitive with ε. These changes were also studied in cross-linking studies with 1-ethyl-3-[3-(dimethylamino)propyl]carbodiimide (EDC) which allowed cross-linking of ε with β only when ε is in the ε_X conformation. The presence of Mg-ADP-Pi or Mg-ATP allowed cross-linking of ε with β which indicated that ε adopted the ε_X conformation. Low amount of cross-linking was observed when ATP + EDTA or Mg-ADP were present, indicating that ε was in the ε_C conformation. Similar trends were also observed in thermophillic *Bacillus PS3* [168, 170]. In addition, sodium azide, which inhibits the enzyme by stabilizing the ADP inhibited state, and aluminum fluoride also lead to the ε_C conformation in *Bacillus PS3*. In addition to ligands, the conformation of ε has been found to be modulated by exposure to light in chloroplast ATP synthase [171, 172]. This is important evidence that PMF can drive conformational change of εCTD to activate the enzyme for ATP synthesis.

Detergents have also been shown to have effects on ε inhibition. LDAO and ethylene glycol have an alleviating effect on ε inhibition of isolated F_1 or intact F_OF_1 in bacteria [149]. Since ε can only inhibit in the ε_X conformation, LDAO treatment probably results in an ε population that has predominantly adopted the ε_C conformation. It is not known how exactly this is achieved. In addition to its effects on ε, LDAO has been found

to affect β's conformation. Short-chain alkyl-beta-D-glucopyranoside (alkylglucosides) detergents have been shown to activate chloroplast ATPase by removal of ε [173].

Many antimicrobial agents that successfully inhibit the growth of pathogens, do so by interfering with the function of enzymes that are vital for their survival. In bacteria, the ATP synthase is one of the most critical enzymes that plays important role in energy metabolism, nutrient uptake and pH regulation. These are important physiological processes and interference with any of these can result in reduced growth or reduced viability. As a result, molecules that interfere with the normal functioning of this enzyme within pathogenic bacteria can be potential leads for antimicrobial agents. As discussed in the introduction, the εCTD plays a regulatory role in the bacterial ATP synthase. The mechanism of inhibition by εCTD is now known. However, intricate details regarding the functional interplay between ε and the enzyme are still not completely clear. During active enzyme turnover, there are multiple factors that affect the conformational changes in ε. It is necessary to understand how these factors come into play so as to use the inhibitory function of ε to target pathogenic bacteria. The research work described in the following chapters will help in developing better understanding about the sequence of events in enzymatic turnover, place of ε in that sequence and the regulatory function of the ε subunit.

1.6 Dissertation Overview

The goal of this dissertation is to offer more details about the regulatory role of the ε subunit in bacterial F-type ATP synthase. We first attempt to understand the biochemistry and kinetics related to ε C-terminal domain's conformational changes. Our studies offer further confirmation of regulatory role for the εCTD. At the same time, we show effects of different ligands on the changes in conformation of the εCTD and tie these conformational changes within the sequence of rotational steps of the γ subunit. Next, we demonstrate the importance of the terminal segment of the εCTD for optimal enzyme function and the subsequent impact on growth of bacteria with the hope that this new understanding will aid in the development of better antimicrobials in the future.

Chapter 2 describes the use of two *E. coli* mutants that have constraints in the native function of their ε subunit. We apply the constraints through manipulation of the C-terminal domain either by deletion or by cross-linking of its two α-helices. Previous studies have showed that the εCTD is responsible for enzyme inhibition and the εNTD is primarily responsible for binding to the γ subunit. However, the relationship between εCTD's conformational change and γ rotation is not understood well. By using the two mutants and an innovative binding assay, we attempt to address these questions here.

Chapter 3 presents compelling data that shows the importance of ε's C-terminal domain for optimal bacterial ATP synthase function. We show that perturbing ε's native interactions with the enzyme can lead to drastic reduction in respiratory growth of *E. coli*. When ATP synthase switches from synthesis of ATP to hydrolysis, the direction of the γ

subunit rotation reverses. This chapter shows that even though both reactions involve mere reversal of γ subunit rotation, the regulation by ε may not be that simple and may involve distinct interactions with the enzyme in either direction.

Chapter 4 presents an innovative binding assay that can be used as an alternative to Surface Plasmon Resonance. BioLayer Interferometry can offer binding kinetics of two molecules with a small amount of sample. We describe BioLayer Interferometry in the form of a methods paper and list out the technical requirements as well as precautions necessary to successfully use this technique.

1.7 References

1. Blair A, Ngo L, Park J, Paulsen IT, Saier MH, Jr.: Phylogenetic analyses of the homologous transmembrane channel-forming proteins of the F_OF_1-ATPases of bacteria, chloroplasts and mitochondria. *Microbiology* 1996, 142(1):17-32.
2. Walker JE, Fearnley IM, Lutter R, Todd RJ, Runswick MJ: Structural aspects of proton-pumping ATPases. *Philos Trans R Soc Lond [Biol]* 1990, 326:367-378.
3. Noji H, Okuno D, Ikeda T: Mechanochemistry of F_1 motor protein. *Chemical Science* 2011, 2(11):2086-2093.
4. Oster G, Wang H: Reverse engineering a protein: The mechanochemistry of ATP Synthase. *Biochimica et Biophysica Acta* 2000, 1458:482-510.
5. Maloney PC: Coupling to an energized membrane: Role of ion-motive gradients in the transduction of metabolic energy. In: *Escherichia coli and Salmonella typhimurium: Cellular and Molecular Biology*. *Volume 1*, 1st edition.
6. Sheng J, Marquis RE: Enhanced acid resistance of oral streptococci at lethal pH values associated with acid-tolerant catabolism and with ATP synthase activity. *FEMS Microbiol Lett* 2006, 262(1):93-98.
7. Cotter PD, Gahan CG, Hill C: Analysis of the role of the Listeria monocytogenes F_OF_1-AtPase operon in the acid tolerance response. *Int J Food Microbiol* 2000, 60(2-3):137-146.
8. Harris DA, Das AM: Control of mitochondrial ATP synthesis in the heart. *Biochem J* 1991, 280:561-573.
9. Walker JE: The regulation of catalysis in ATP synthase. [Review]. *Current Opinion in Structural Biology* 1994, 4(6):912-918.

10. Gledhill JR, Walker JE: Inhibition sites in F_1-ATPase from bovine heart mitochondria. *Biochem J* 2005, 386(Pt 3):591-598.

11. Green DW, Grover GJ: The IF(1) inhibitor protein of the mitochondrial F(1)F(0)-ATPase. *Biochim Biophys Acta* 2000, 1458(2-3):343-355.

12. Cingolani G, Duncan TM: Structure of the ATP synthase catalytic complex (F(1)) from Escherichia coli in an autoinhibited conformation. *Nat Struct Mol Biol* 2011, 18(6):701-707.

13. Sielaff H, Rennekamp H, Engelbrecht S, Junge W: Functional halt positions of rotary F_OF_1-ATPase correlated with crystal structures. *Biophys J* 2008, 95(10):4979-4987.

14. Foster DL, Fillingame RH: Stoichiometry of subunits in the H+-ATPase complex of Escherichia coli. *J Biol Chem* 1982, 257:2009-2015.

15. Bragg PD, Hou C: Purification of a factor for both aerobic-driven and ATP-driven energy-dependent transhydrogenases of Escherichia coli. *FEBS Letters* 1972, 28(3):309-312.

16. Norais N, Promé D, Velours J: ATP synthase of yeast mitochondria. Characterization of subunit d and sequence analysis of the structural gene ATP7. *Journal of Biological Chemistry* 1991, 266(25):16541-16549.

17. Velours J, Arselin G, Paul M-F, Galante M, Durrens P, Aigle M, Guerin B: The yeast ATP synthase subunit 4: structure and function. *Biochimie* 1989, 71(8):903-915.

18. Devenish RJ, Prescott M, Rodgers AJW: The structure and function of mitochondrial F_1F_O-ATP synthases. *International Review of Cell & Molecular Biology* 2008, 267:1-58.

19. Stock D, Leslie AG, Walker JE: Molecular architecture of the rotary motor in ATP synthase. *Science* 1999, 286(5445):1700-1705.

20. Walker JE, Saraste M, Gay NJ: The unc operon. Nucleotide sequence, regulation and structure of ATP-synthase. *Biochim Biophys Acta* 1984, 768:164-200.

21. Long JC, DeLeon-Rangel J, Vik SB: Characterization of the first cytoplasmic loop of subunit a of the Escherichia coli ATP synthase by surface labeling, cross-linking, and mutagenesis. *J Biol Chem* 2002, 277(30):27288-27293.

22. Aris JP, Simoni RD: Cross-linking and labeling of the Escherichia coli F_1F_O-ATP synthase reveal a compact hydrophilic portion of F_O close to an F_1 catalytic subunit. *J Biol Chem* 1983, 258:14599-14609.

23. Hermolin J, Gallant J, Fillingame RH: Topology, organization, and function of the psi subunit in the F_O sector of the H+-ATPase of Escherichia coli. *J Biol Chem* 1983, 258:14550-14555.

24. Vik SB, Ishmukhametov RR: Structure and function of subunit a of the ATP synthase of Escherichia coli. *J Bioenerg Biomembr* 2005, 37(6):445-449.

25. Long JC, Wang S, Vik SB: Membrane topology of subunit a of the F_1F_O ATP synthase as determined by labeling of unique cysteine residues. *J Biol Chem* 1998, 273(26):16235-16240.

26. Wada T, Long JC, Zhang D, Vik SB: A novel labeling approach supports the five-transmembrane model of subunit a of the Escherichia coli ATP synthase. *J Biol Chem* 1999, 274(24):17353-17357.

27. Cox GB, Devenish RJ, Gibson F, Howitt SM, Nagley P: The structure and assembly of ATP synthase. In: *Molecular Mechanisms in Bioenergetics*.

28. Cox GB, Fimmel AL, Gibson F, Hatch L: The mechanism of ATP synthase: a reassessment of the functions of the b and a subunits. *Biochim Biophys Acta* 1986, 849:62-69.

29. Angevine CM, Fillingame RH: Aqueous access channels in subunit a of rotary ATP synthase. *J Biol Chem* 2003, 278(8):6066-6074.

30. Angevine CM, Herold KA, Fillingame RH: Aqueous access pathways in subunit a of rotary ATP synthase extend to both sides of the membrane. *Proc Natl Acad Sci USA* 2003, 100(23):13179-13183.

31. Cain BD, Simoni RD: Proton translocation by the F_1F_0 ATPase of *Escherichia coli*. Mutagenic analysis of the a subunit. *J Biol Chem* 1989, 264:3292-3300.

32. Vik SB, Antonio BJ: A mechanism of proton translocation by F_1F_O ATP synthases suggested by double mutants of the a subunit. *Journal of Biological Chemistry* 1994, 269(48):30364-30369.

33. Ballmoos CV, Wiedenmann, A., Dimroth, P.: Essentials for ATP Synthesis by F_1F_O ATP Synthases. *Annual Review of Biochemistry* 2009, 78:649-672.

34. Cain BD: Mutagenic Analysis of the F0 Stator Subunits. *Journal of Bioenergetics and Biomembranes* 2000, 32(4):365-371.

35. Fillingame RH, Angevine, C. M., Dmitriev, O. Y.: Coupling proton movements to c-ring rotation in F_1F_O ATP synthase: aqueous access channels and helix rotations at the a–c interface. *Biochimica et Biophysica Acta (BBA) - Bioenergetics* 2002, 1555(1–3):29-36.

36. Dmitriev OY, Altendorf K, Fillingame RH: Reconstitution of the F_O complex of *Escherichia coli* ATP synthase from isolated subunits. Varying the number of essential carboxylates by co-incorporation of wild-type and mutant subunit c after purification in organic solvent. *European Journal of Biochemistry* 1995, 233(2):478-483.

37. Groth G, Walker JE: Model of the c-subunit oligomer in the membrane domain of F-ATPases. *FEBS Letters* 1997, 410(2-3):117-123.

38. Junge W, Lill H, Engelbrecht S: ATP synthase: an electrochemical transducer with rotatory mechanics. *Trends in Biochemical Sciences* 1997, 22(11):420-423.

39. Aksimentiev A, Balabin IA, Fillingame RH, Schulten K: Insights into the molecular mechanism of rotation in the Fo sector of ATP synthase. *Biophys J* 2004, 86(3):1332-1344.

40. Vik SB, Long JC, Wada T, Zhang D: A model for the structure of subunit a of the Escherichia coli ATP synthase and its role in proton translocation. *Biochim Biophys Acta* 2000, 1458(2-3):457-466.

41. Rastogi VK, Girvin ME: Structural changes linked to proton translocation by subunit c of the ATP synthase. *Nature* 1999, 402(6759):263-268.

42. Elston T, Wang H, Oster G: Energy transduction in ATP synthase. *Nature* 1998, 391(6666):510-513.

43. Assadi-Porter FM, Fillingame RH: Proton-translocating carboxyl of subunit c of F_1F_O H(+)-ATP synthase: the unique environment suggested by the pKa determined by 1H NMR. *Biochemistry* 1995, 34(49):16186-16193.

44. Rodgers AJ, Wilkens S, Aggeler R, Morris MB, Howitt SM, Capaldi RA: The subunit d-subunit b domain of the *Escherichia coli* F1F0 ATPase. The b subunits interact with F_1 as a dimer and through the d subunit. *Journal of Biological Chemistry* 1997, 272(49):31058-31064.

45. Dunn SD, Revington M, Cipriano DJ, Shilton BH: The b subunit of Escherichia coli ATP synthase. *J Bioenerg Biomembr* 2000, 32(4):347-355.

46. Dunn SD, McLachlin DT, Revington M: The second stalk of Escherichia coli ATP synthase. *Biochim Biophys Acta* 2000, 1458(2-3):356-363.

47. Dickson VK, Silvester JA, Fearnley IM, Leslie AG, Walker JE: On the structure of the stator of the mitochondrial ATP synthase. *Embo J* 2006, 25(12):2911-2918.

48. Cherepanov DA, Mulkidjanian AY, Junge W: Transient accumulation of elastic energy in proton translocating ATP synthase. *FEBS Lett* 1999, 449(1):1-6.

49. Kersten MV, Dunn SD, Wise JG, Vogel PD: Site-directed spin-labeling of the catalytic sites yields insight into structural changes within the F_OF_1-ATP synthase of Escherichia coli. *Biochemistry* 2000, 39(13):3856-3860.

50. Pullman ME, Penefsky HS, Datta A, Racker E: Partial resolution of the enzymes catalysing oxidative phosphorylation. I. Purification and properties of soluble dinitrophenyl-stimulated adonosine triphophatase. *J Biol Chem* 1960, 235:3322-3329.

51. Abrahams JP, Leslie AG, Lutter R, Walker JE: Structure at 2.8 Å resolution of F_1-ATPase from bovine heart mitochondria. *Nature* 1994, 370(6491):621-628.

52. Gogol EP, Aggeler R, Sagermann M, Capaldi RA: Cryoelectron microscopy of Escherichia coli F_1 adenosinetriphosphatase decorated with monoclonal antibodies to individual subunits of the complex. *Biochemistry* 1989, 28:4717-4724.

53. Walker JE, Fearnley IM, Gay NJ, Gibson BW, Northrop FD, Powell SJ, Runswick MJ, Saraste M, Tybulewicz VL: Primary structure and subunit stoichiometry of F_1-ATPase from bovine mitochondria. *J Mol Biol* 1985, 184:677-701.

54. Gogarten JP, Kibak H, Dittrich P, Taiz L, Bowman EJ, Bowman BJ, Manolson MF, Poole RJ, Date T, Oshima T *et al*: Evolution of the vacuolar H+-ATPase: implications for the origin of eukaryotes. *Proceedings of the National Academy of Sciences of the United States of America* 1989, 86(17):6661-6665.

55. Menz RI, Walker JE, Leslie AG: Structure of bovine mitochondrial F_1-ATPase with nucleotide bound to all three catalytic sites: implications for the mechanism of rotary catalysis. *Cell* 2001, 106(3):331-341.

56. Garrett NE, Penefsky HS: Interaction of adenine nucleotides with multiple binding sites on beef heart mitochondrial adenosine triphosphatase. *Journal of Biological Chemistry* 1975, 250(17):6640-6647.

57. Harris DA, Rosing, J., Van de Stadt, R.J., Slater, E.C.: Tight binding of adenine nucleotides to beef-heart mitochondrial ATPase. *Biochimica Biophysica Acta* 1973, 314(2):149-153.

58. Lunardi J, Satre, M., Vignais, P.V.: Exploration of adenosine 5'-diphosphate-adenosine 5'-triphosphate binding sites of Escherichia coli adenosine 5'-

triphosphatase with arylazido adenine nucleotides. *Biochemistry* 1981, 20(3):473-480.

59. Mnatsakanyan N, Krishnakumar AM, Suzuki T, Weber J: The role of the βDELSEED-loop of ATP synthase. *The Journal of biological chemistry* 2009, 284(17):11336-11345.

60. Yasuda R, Noji H, Kinosita K, Jr., Yoshida M: F_1-ATPase is a highly efficient molecular motor that rotates with discrete 120 degree steps. *Cell* 1998, 93(7):1117-1124.

61. Duncan TM: The ATP Synthase: Parts and Properties of a Rotary Motor. In: *The Enzymes, vol XXIII: Energy Coupling and Molecular Motors*. *Volume 23*, 3rd edition

62. Boyer PD: The binding change mechanism for ATP synthase--some probabilities and possibilities. *Biochim Biophys Acta* 1993, 1140(3):215-250.

63. Futai M, Sternweis PC, Heppel LA: Purification and properties of reconstitutively active and inactive adenosinetriphosphatase from Escherichia coli. *Proceedings of the National Academy of Sciences of the United States of America* 1974, 71(7):2725-2729.

64. Mitchell P: Coupling of phosphorylation to electron and hydrogen transfer by a chemi-osmotic type of mechanism. *Nature* 1961, 191:144-148.

65. Mitchell P: Chemiosmotic coupling in oxidative and photosynthetic phosphorylation. *Biochimica et Biophysica Acta (BBA) - Bioenergetics* 2011, 1807(12):1507-1538.

66. Boyer PD, Cross RL, Momsen W: A new concept for energy coupling in oxidative phosphorylation based on a molecular explanation of the oxygen exchange reactions. *Proceedings of the National Academy of Sciences of the United States of America* 1973, 70(10):2837-2839.

67. Boyer PD, Kohlbrenner WE: The Present Status of the Binding-Change Mechanism and Its Relation to ATP Formation by Chloroplasts. In: *Energy Coupling in Photosynthesis*y.

68. Cross RL, Kohlbrenner WE: The mode of inhibition of oxidative phosphorylation by efrapeptin (A23871). Evidence for an alternating site mechanism for ATP synthesis. *Journal of Biological Chemistry* 1978, 253(14):4865-4873.

69. Rosen G, Gresser M, Vinkler C, Boyer PD: Assessment of total catalytic sites and the nature of bound nucleotide participation in photophosphorylation. *Journal of Biological Chemistry* 1979, 254(21):10654-10661.

70. Cross RL, Grubmeyer C, Penefsky HS: Mechanism of ATP hydrolysis by beef heart mitochondrial ATPase. Rate enhancements resulting from cooperative interactions between multiple catalytic sites. *J Biol Chem* 1982, 257:12101-12105.

71. Grubmeyer C, Cross RL, Penefsky HS: Mechanism of ATP hydrolysis by beef heart mitochondrial ATPase. Rate constants for elementary steps in catalysis at a single site. *J Biol Chem* 1982, 257:12092-12100.

72. Cunningham D, Cross RL: Catalytic site occupancy during ATP hydrolysis by MF_1-ATPase. Evidence for alternating high affinity sites during steady-state turnover. *J Biol Chem* 1988, 263:18850-18856.

73. Noumi T, Taniai M, Kanazawa H, Futai M: Replacement of arginine 246 by histidine in the beta subunit of Escherichia coli H+-ATPase resulted in loss of multi-site ATPase activity. *J Biol Chem* 1986, 261:9196-9201.

74. Rao R, Senior AE: The properties of hybrid F_1-ATPase enzymes suggest that a cyclical catalytic mechanism involving three catalytic sites occurs. *J Biol Chem* 1987, 262:17450-17454.

75. Cross RL, Nalin CM: Adenine nucleotide binding sites on beef heart F_1-ATPase. Evidence for three exchangeable sites that are distinct from three noncatalytic sites. *J Biol Chem* 1982, 257:2874-2881.

76. Duncan TM, Bulygin VV, Zhou Y, Hutcheon ML, Cross RL: Rotation of subunits during catalysis by *Escherichia coli* F_1-ATPase. *Proceedings of the National Academy of Sciences of the United States of America* 1995, 92(24):10964-10968.

77. Noji H, Yasuda R, Yoshida M, Kinosita K, Jr.: Direct observation of the rotation of F_1-ATPase. *Nature* 1997, 386(6622):299-302.

78. Cox GB, Jans DA, Fimmel AL, Gibson F, Hatch L: Hypothesis. The mechanism of ATP synthase. Conformational change by rotation of the *b*-subunit. *Biochim Biophys Acta* 1984, 768:201-208.

79. Sambongi Y, Iko Y, Tanabe M, Omote H, Iwamoto-Kihara A, Ueda I, Yanagida T, Wada Y, Futai M: Mechanical rotation of the c subunit oligomer in ATP synthase (F_OF_1): direct observation. *Science* 1999, 286(5445):1722-1724.

80. Tanabe M, Nishio K, Iko Y, Sambongi Y, Iwamoto-Kihara A, Wada Y, Futai M: Rotation of a complex of the gamma subunit and c ring of Escherichia coli ATP

synthase. The rotor and stator are interchangeable. *J Biol Chem* 2001, 276(18):15269-15274.

81. Panke O, Gumbiowski K, Junge W, Engelbrecht S: F-ATPase: specific observation of the rotating c subunit oligomer of EF(o)EF(1). *FEBS Letters* 2000, 472(1):34-38.

82. Bowler MW, Montgomery MG, Leslie AG, Walker JE: Ground state structure of F_1-ATPase from bovine heart mitochondria at 1.9 Å resolution. *J Biol Chem* 2007, 282(19):14238-14242.

83. Hara KY, Kato-Yamada Y, Kikuchi Y, Hisabori T, Yoshida M: The role of the betaDELSEED motif of F_1-ATPase: propagation of the inhibitory effect of the epsilon subunit. *Journal of Biological Chemistry* 2001, 276(26):23969-23973.

84. Tanigawara M, Tabata Kazuhito V, Ito Y, Ito J, Watanabe R, Ueno H, Ikeguchi M, Noji H: Role of the DELSEED Loop in Torque Transmission of $F(_1)$-ATPase. *Biophysical Journal* 2012, 103(5):970-978.

85. Vogel G, Steinhart R: ATPase from Escherichia coli: Purification, dissociation and reconstitution of the active complex from the isolated subunits. *Biochemistry* 1976, 15:208-216.

86. Zhou Y, Duncan TM, Bulygin VV, Hutcheon ML, Cross RL: ATP hydrolysis by membrane-bound Escherichia coli F_OF_1 causes rotation of the g subunit relative to the b subunits. *Biochimica et Biophysica Acta* 1996, 1275(1-2):96-100.

87. Zhou Y, Duncan TM, Cross RL: Subunit rotation in Escherichia coli F_OF_1-ATP synthase during oxidative phosphorylation. *Proc Natl Acad Sci U S A* 1997, 94(20):10583-10587.

88. Hermolin J, Fillingame RH: H^+-ATPase activity of *Escherichia coli* F_1F_0 is blocked after reaction of dicyclohexylcarbodiimide with a single proteolipid (subunit c) of the F_0 complex. *J Biol Chem* 1989, 264:3896-3903.

89. Watts SD, Tang C, Capaldi RA: The stalk region of the Escherichia coli ATP synthase. Tyrosine 205 of the gamma subunit is in the interface between the F_1 and F_O parts and can interact with both the epsilon and c oligomer. *J Biol Chem* 1996, 271(45):28341-28347.

90. Bulygin VV, Duncan TM, Cross RL: Rotation of the epsilon subunit during catalysis by *Escherichia coli* FOF1-ATP synthase. *J Biol Chem* 1998, 273(48):31765-31769.

91. Ogilvie I, Aggeler R, Capaldi RA: Cross-linking of the delta subunit to one of the three alpha subunits has no effect on functioning, as expected if delta is a part of the stator that links the F_1 and F_O parts of the Escherichia coli ATP synthase. *J Biol Chem* 1997, 272(26):16652-16656.

92. Tsunoda SP, Aggeler R, Yoshida M, Capaldi RA: Rotation of the c subunit oligomer in fully functional F1Fo ATP synthase. *Proceedings of the National Academy of Sciences of the United States of America* 2001, 98(3):898-902.

93. Jones PC, Hermolin J, Jiang W, Fillingame RH: Insights into the rotary catalytic mechanism of F0F1 ATP synthase from the cross-linking of subunits b and c in the escherichia coli enzyme. *Journal of Biological Chemistry* 2000, 275(40):31340-31346.

94. Noji H, Hasler K, Junge W, Kinosita K, Jr., Yoshida M, Engelbrecht S: Rotation of Escherichia coli F(1)-ATPase. *Biochem Biophys Res Commun* 1999, 260(3):597-599.

95. Hisabori T, Kondoh A, Yoshida M: The gamma subunit in chloroplast F(1)-ATPase can rotate in a unidirectional and counter-clockwise manner. *FEBS Lett* 1999, 463(1-2):35-38.

96. Kato-Yamada Y, Noji H, Yasuda R, Kinosita K, Jr., Yoshida M: Direct observation of the rotation of e subunit in F_1-ATPase. *J Biol Chem* 1998, 273(31):19375-19377.

97. Yasuda R, Noji H, Yoshida M, Kinosita K, Jr., Itoh H: Resolution of distinct rotational substeps by submillisecond kinetic analysis of F_1-ATPase. *Nature* 2001, 410(6831):898-904.

98. Montemagno C, Bachand G: Constructing nanomechanical devices powered by biomolecular motors. *Nanotechnology* 1999, 10:225-231.

99. Nishizaka T, Oiwa K, Noji H, Kimura S, Muneyuki E, Yoshida M, Kinosita K, Jr.: Chemomechanical coupling in F_1-ATPase revealed by simultaneous observation of nucleotide kinetics and rotation. *Nat Struct Mol Biol* 2004, 11(2):142-148.

100. Adachi K, Oiwa K, Nishizaka T, Furuike S, Noji H, Itoh H, Yoshida M, Kinosita K, Jr.: Coupling of rotation and catalysis in F($_1$)-ATPase revealed by single-molecule imaging and manipulation. *Cell* 2007, 130(2):309-321.

101. Shimo-Kon R, Muneyuki E, Sakai H, Adachi K, Yoshida M, Kinosita K, Jr.: Chemo-mechanical coupling in F(1)-ATPase revealed by catalytic site occupancy during catalysis. *Biophysical Journal* 2010, 98(7):1227-1236.

102. Itoh H, Takahashi A, Adachi K, Noji H, Yasuda R, Yoshida M, Kinosita K: Mechanically driven ATP synthesis by F_1-ATPase. *Nature* 2004, 427(6973):465-468.

103. Rondelez Y, Tresset G, Nakashima T, Kato-Yamada Y, Fujita H, Takeuchi S, Noji H: Highly coupled ATP synthesis by F_1-ATPase single molecules. *Nature* 2005, 433(7027):773-777.

104. Harris DA, von Tscharner, V., Radda, G.K.: The ATPase inhibitor protein in oxidative phosphorylation. The rate-limiting factor to phosphorylation in submitochondrial particles. *Biochimica Biophysica Acta* 1979, 548(1):72-84.

105. Smith JB, Sternweis PC: Purification of membrane attachment and inhibitory subunits of the proton translocating adenosine triphosphatase from Escherichia coli. *Biochemistry* 1977, 16:306-311.

106. Keis S, Stocker A, Dimroth P, Cook GM: Inhibition of ATP hydrolysis by thermoalkaliphilic F_1F_o-ATP synthase is controlled by the C terminus of the ε subunit. *J Bacteriol* 2006, 188(11):3796-3804.

107. Nowak KF, McCarty RE: Regulatory role of the C-terminus of the epsilon subunit from the chloroplast ATP synthase. *Biochemistry* 2004, 43(11):3273-3279.

108. Hanson RL, Kennedy EP: Energy-Transducing Adenosine Triphosphatase from Escherichia coli: Purification, Properties, and Inhibition by Antibody. *Journal of Bacteriology* 1973, 114(2):772-781.

109. Shah NB, Hutcheon ML, Haarer BK, Duncan TM: F1-ATPase of Escherichia coli: THE ϵ-INHIBITED STATE FORMS AFTER ATP HYDROLYSIS, IS DISTINCT FROM THE ADP-INHIBITED STATE, AND RESPONDS DYNAMICALLY TO

CATALYTIC SITE LIGANDS. *Journal of Biological Chemistry* 2013, 288(13):9383-9395.

110. Hong S, Pedersen PL: ATP Synthase and the Actions of Inhibitors Utilized To Study Its Roles in Human Health, Disease, and Other Scientific Areas. *Microbiology and Molecular Biology Reviews : MMBR* 2008, 72(4):590-641.

111. Martin-Galiano AJ, Ferrandiz MJ, de la Campa AG: The promoter of the operon encoding the F_OF_1 ATPase of Streptococcus pneumoniae is inducible by pH. *Molecular Microbiology* 2001, 41(6):1327-1338.

112. Greenwood B: The epidemiology of pneumococcal infection in children in the developing world. *Philosophical Transactions of the Royal Society B: Biological Sciences* 1999, 354(1384):777-785.

113. Ferrandiz MJ, de la Campa AG: The membrane-associated F_OF_1 ATPase is essential for the viability of *Streptococcus pneumoniae*. *FEMS Microbiol Lett* 2002, 212(1):133-138.

114. Vázquez-Boland JA, Kuhn M, Berche P, Chakraborty T, Domínguez-Bernal G, Goebel W, González-Zorn B, Wehland J, Kreft J: Listeria Pathogenesis and Molecular Virulence Determinants. *Clinical Microbiology Reviews* 2001, 14(3):584-640.

115. Northen H, Paterson GK, Constantino-Casas F, Bryant CE, Clare S, Mastroeni P, Peters SE, Maskell DJ: Salmonella enterica serovar Typhimurium mutants completely lacking the $F(_O)F(_1)$ ATPase are novel live attenuated vaccine strains. *Vaccine* 2010, 28(4):940-949.

116. McGowan CC, Cover TL, Blaser MJ: Analysis of F_1F_O-ATPase from Helicobacter pylori. *Infect Immun* 1997, 65(7):2640-2647.

117. Jones SA, Chowdhury FZ, Fabich AJ, Anderson A, Schreiner DM, House AL, Autieri SM, Leatham MP, Lins JJ, Jorgensen M *et al*: Respiration of *Escherichia coli* in the mouse intestine. *Infect Immun* 2007, 75(10):4891-4899.

118. Mahajan R: Bedaquiline: First FDA-approved tuberculosis drug in 40 years. *International Journal of Applied and Basic Medical Research* 2013, 3(1):1-2.

119. Nelson N, Nelson H, Racker E: Partial Resolution of the Enzymes Catalyzing Photophosphorylation: XII. PURIFICATION AND PROPERTIES OF AN INHIBITOR ISOLATED FROM CHLOROPLAST COUPLING FACTOR 1. *Journal of Biological Chemistry* 1972, 247(23):7657-7662.

120. Smith JB, Sternweis PC, Heppel LA: Partial purification of active delta and epsilon subunits of the membrane ATPase from escherichia coli. *J Supramol Struct* 1975, 3(3):248-255.

121. Laget PP, Smith JB: Inhibitory propeties of endogenous subunit e in the Escherichia coli F1 ATPase. *Arch Biochem Biophys* 1979, 197:83-89.

122. Klionsky DJ, Brusilow WS, Simoni RD: In vivo evidence for the role of the epsilon subunit as an inhibitor of the proton-translocating ATPase of Escherichia coli. *J Bacteriol* 1984, 160:1055-1060.

123. Kuki M, Noumi T, Maeda M, Amemura A, Futai M: Functional domains of epsilon subunit of Escherichia coli H+-ATPase (F0F1). *J Biol Chem* 1988, 263:17437-17442.

124. Kato-Yamada Y, Bald D, Koike M, Motohashi K, Hisabori T, Yoshida M: Epsilon subunit, an endogenous inhibitor of bacterial F(1)-ATPase, also inhibits F(0)F(1)-ATPase. *Journal of Biological Chemistry* 1999, 274(48):33991-33994.

125. Sternweis PC: The epsilon subunit of Escherichia coli coupling factor 1 is required for its binding to the cytoplasmic membrane. *J Biol Chem* 1978, 253:3123-3128.

126. Yoshida M, Okamoto H, Sone N, Hirata H, Kagawa Y: Reconstitution of thermostable ATPase capable of energy coupling from its purified subunits. *Proc Natl Acad Sci U S A* 1977, 74(3):936-940.

127. Giraud MF, Velours J: The absence of the mitochondrial ATP synthase delta subunit promotes a slow growth phenotype of rho- yeast cells by a lack of assembly of the catalytic sector F_1. *European Journal of Biochemistry* 1997, 245(3):813-818.

128. Patrie WJ, McCarty RE: Specific binding of coupling factor 1 lacking the delta and epsilon subunits to thylakoids. *J Biol Chem* 1984, 259(17):11121-11128.

129. Richter ML, Patrie WJ, McCarty RE: Preparation of the epsilon subunit and epsilon subunit-deficient chloroplast coupling factor 1 in reconsitutively active forms. *J Biol Chem* 1984, 259:7371-7373.

130. Cipriano DJ, Dunn SD: The role of the epsilon subunit in the Escherichia coli ATP synthase. The C-terminal domain is required for efficient energy coupling. *J Biol Chem* 2006, 281(1):501-507.

131. Wilkens S, Dahlquist FW, McIntosh LP, Donaldson LW, Capaldi RA: Structural features of the epsilon subunit of the Escherichia coli ATP synthase determined by NMR spectroscopy. *Nat Struct Biol* 1995, 2(11):961-967.

132. Uhlin U, Cox GB, Guss JM: Crystal structure of the epsilon subunit of the proton-translocating ATP synthase from Escherichia coli. *Structure* 1997, 5(9):1219-1230.

133. Mendel-Hartvig J, Capaldi RA: Nucleotide-dependent and dicyclohexylcarbodiimide-sensitive conformational changes in the ε subunit of *Escherichia coli* ATP synthase. *Biochemistry* 1991, 30:10987-10991.

134. Mendel-Hartvig J, Capaldi RA: Catalytic site nucleotide and inorganic phosphate dependence of the conformation of the epsilon subunit in Escherichia coli adenosinetriphosphatase. *Biochemistry* 1991, 30:1278-1284.

135. Gogol EP, Lucken U, Capaldi RA: The stalk connecting the F_1 and F_O domains of ATP synthase visualized by electron microscopy of unstained specimens. *FEBS Lett* 1987, 219:274-278.

136. Aggeler R, Chicas Cruz K, Cai SX, Keana JF, Capaldi RA: Introduction of reactive cysteine residues in the epsilon subunit of Escherichia coli F_1 ATPase, modification of these sites with tetrafluorophenyl azide-maleimides, and examination of changes in the binding of the epsilon subunit when different nucleotides are in catalytic sites. *Biochemistry* 1992, 31:2956-2961.

137. Aggeler R, Haughton MA, Capaldi RA: Disulfide bond formation between the COOH-terminal domain of the b subunits and the g and e subunits of the *Escherichia coli* F_1-ATPase. Structural implications and functional consequences. *Journal of Biological Chemistry* 1995, 270(16):9185-9191.

138. Bulygin VV, Duncan TM, Cross RL: Rotor/Stator interactions of the epsilon subunit in Escherichia coli ATP synthase and implications for enzyme regulation. *J Biol Chem* 2004, 279(34):35616-35621.

139. Bragg PD, Hou C: A cross-linking study of the Ca2+, Mg2+-activated adenosine triphosphatase of Escherichia coli. *European Journal of Biochemistry* 1980, 106(2):495-503.

140. Dunn SD: The isolated g subunit of *Escherichia coli* F_1 ATPase binds the e subunit. *J Biol Chem* 1982, 257:7354-7359.

141. Tang C, Capaldi RA: Characterization of the interface between g and e subunits of *Escherichia coli* F_1-ATPase. *Journal of Biological Chemistry* 1996, 271(6):3018-3024.

142. Zhang Y, Fillingame RH: Subunits coupling H+ transport and ATP synthesis in the Escherichia coli ATP synthase. Cys-Cys cross-linking of F1 subunit epsilon to the polar loop of F_O subunit c. *J Biol Chem* 1995, 270(41):24609-24614.

143. Lucken U, Gogol EP, Capaldi RA: Structure of the ATP synthase complex (ECF_1F_O) of Escherichia coli from cryoelectron microscopy. *Biochemistry* 1990, 29(22):5339-5343.

144. Lotscher HR, deJong C, Capaldi RA: Inhibition of the adenosinetriphosphatase activity of Escherichia coli F_1 by the water-soluble carbodiimide 1-ethyl-3-[3-(dimethylamino)propyl]carbodiimide is due to modification of several carboxyls in the beta subunit. *Biochemistry* 1984, 23:4134-4140.

145. Tsunoda SP, Rodgers AJ, Aggeler R, Wilce MC, Yoshida M, Capaldi RA: Large conformational changes of the epsilon subunit in the bacterial F_1F_O ATP synthase provide a ratchet action to regulate this rotary motor enzyme. *Proceedings of the National Academy of Sciences of the United States of America* 2001, 98(12):6560-6564.

146. Dallmann HG, Flynn TG, Dunn SD: Determination of the 1-ethyl-3-[(3-dimethylamino)propyl]-carbodiimide-induced cross-link between the b and e subunits of *Escherichia coli* F_1-ATPase. *J Biol Chem* 1992, 267(26):18953-18960.

147. Aggeler R, Capaldi RA: Nucleotide-dependent movement of the ε subunit between α and β subunits in the *Escherichia coli* F_1F_O-type ATPase. *Journal of Biological Chemistry* 1996, 271(23):13888-13891.

148. Sternweis PC, Smith JB: Characterization of the inhibitory (epsilon) subunit of the proton-translocating adenosine triphosphatase from Escherichia coli. *Biochemistry* 1980, 19:526-531.

149. Lotscher HR, deJong C, Capaldi RA: Interconversion of high and low adenosinetriphosphatase activity forms of Escherichia coli F_1 by the detergent lauryldimethylamine oxide. *Biochemistry* 1984, 23:4140-4143.

150. Dunn SD, Tozer RG, Zadorozny VD: Activation of Escherichia coli F_1-ATPase by lauryldimethylamine oxide and ethylene glycol: relationship of ATPase activity to the interaction of the epsilon and beta subunits. *Biochemistry* 1990, 29:4335-4340.

151. Pick U, Bassilian S: Activation of magnesium ion specific adenosinetriphosphatase in chloroplast coupling factor 1 by octyl glucoside. *Biochemistry* 1982, 21:6144-6152.

152. Sakurai H, Shinohara K, Hisabori T: Enhancement of adenosine triphosphatase activity of purified chloroplast coupling factor 1 in aqueous organic solvent. *J Biochem* 1981, 90:95-102.

153. Yoshida M, Sone N, Hirata H, Kagawa Y: A highly stable adenosine triphosphatase from a thermophillie bacterium. Purification, properties, and reconstitution. *J Biol Chem* 1975, 250(19):7910-7916.

154. Gavilanes-Ruiz M, Tommasino M, Capaldi RA: Structure-function relationships of the Escherichia coli ATP synthase probed by trypsin digestion. *Biochemistry* 1988, 27(2):603-609.

155. Xiong H, Zhang D, Vik SB: Subunit epsilon of the Escherichia coli ATP synthase: novel insights into structure and function by analysis of thirteen mutant forms. *Biochemistry* 1998, 37(46):16423-16429.

156. Kato-Yamada Y: Isolated epsilon subunit of Bacillus subtilis F_1-ATPase binds ATP. *FEBS Lett* 2005, 579(30):6875-6878.

157. Feniouk BA, Suzuki T, Yoshida M: The role of subunit ε in the catalysis and regulation of F_OF_1-ATP synthase. *Biochimica et Biophysica Acta* 2006, 1757(5-6):326-338.

158. Ketchum CJ, Nakamoto RK: A mutation in the Escherichia coli F0F1-ATP synthase rotor, gammaE208K, perturbs conformational coupling between transport and catalysis. *J Biol Chem* 1998, 273(35):22292-22297.

159. Peskova YB, Nakamoto RK: Catalytic control and coupling efficiency of the Escherichia coli FoF1 ATP synthase: influence of the Fo sector and epsilon subunit on the catalytic transition state. *Biochemistry* 2000, 39(38):11830-11836.

160. Bragg PD, Hou C: Ligand-induced conformational changes in the Escherichia coli F_1 adenosine triphosphatase probed by trypsin digestion. *Biochim Biophys Acta* 1987, 894:127-137.

161. Iino R, Hasegawa R, Tabata KV, Noji H: Mechanism of inhibition by C-terminal alpha-helices of the epsilon subunit of Escherichia coli F_OF_1-ATP synthase. *J Biol Chem* 2009, 284(26):17457-17464.

162. Masaike T, Suzuki T, Tsunoda SP, Konno H, Yoshida M: Probing conformations of the beta subunit of F_OF_1-ATP synthase in catalysis. *Biochem Biophys Res Commun* 2006, 342(3):800-807.

163. Jounouchi M, Takeyama M, Noumi T, Moriyama Y, Maeda M, Futai M: Role of the amino terminal region of the epsilon subunit of Escherichia coli H(+)-ATPase (F_OF_1). *Arch Biochem Biophys* 1992, 292:87-94.

164. Xiong H, Vik SB: Alanine-scanning mutagenesis of the epsilon subunit of the F_1-F_O ATP synthase from Escherichia coli reveals two classes of mutants. *J Biol Chem* 1995, 270(40):23300-23304.

165. Aggeler R, Capaldi RA: ATP hydrolysis-linked structural changes in the N-terminal part of the gamma subunit of Escherichia coli F_1-ATPase examined by cross-linking studies. *Journal of Biological Chemistry* 1993, 268(20):14576-14578.

166. Turina P, Capaldi RA: ATP hydrolysis-driven structural changes in the gamma-subunit of Escherichia coli ATPase monitored by fluorescence from probes bound at introduced cysteine residues. *Journal of Biological Chemistry* 1994, 269(18):13465-13471.

167. Nowak KF, Tabidze V, McCarty RE: The C-terminal domain of the epsilon subunit of the chloroplast ATP synthase is not required for ATP synthesis. *Biochemistry* 2002, 41(51):15130-15134.

168. Iino R, Murakami T, Iizuka S, Kato-Yamada Y, Suzuki T, Yoshida M: Real-time monitoring of conformational dynamics of the epsilon subunit in F_1-ATPase. *J Biol Chem* 2005, 280(48):40130-40134.

169. Wilkens S, Capaldi RA: Solution structure of the ε subunit of the F_1-ATPase from *Escherichia coli* and interactions of this subunit with β subunits in the complex. *Journal of Biological Chemistry* 1998, 273(41):26645-26651.

170. Kato-Yamada Y, Yoshida M, Hisabori T: Movement of the helical domain of the epsilon subunit is required for the activation of thermophilic F_1-ATPase. *Journal of Biological Chemistry* 2000, 275(46):35746-35750.

171. Komatsu-Takaki M: Energy-dependent conformational changes in the epsilon subunit of the chloroplast ATP synthase (CF_OCF_1). *J Biol Chem* 1989, 264:17750-17753.

172. Johnson EA, McCarty RE: The carboxyl terminus of the epsilon subunit of the chloroplast ATP synthase is exposed during illumination. *Biochemistry* 2002, 41(7):2446-2451.

173. Yu F, McCarty RE: Detergent activation of the ATPase activity of chloroplast coupling factor 1. *Arch Biochem Biophys* 1985, 238:61-68.

174. Gibbons, C., Montgomery, M. G., Leslie, A. G., and Walker, J. E. (2000) The structure of the central stalk in bovine F_1-ATPase at 2.4 Å resolution. *Nat. Struct. Biol.* 7, 1055–1061

175. Pogoryelov D, Krah A, Langer JD, Yildiz ñ, Faraldo-Gomez JD, Meier T: Microscopic rotary mechanism of ion translocation in the Fo complex of ATP synthases. *Nat Chem Biol* 2010, 6(12):891-899.

Chapter Two

F_1-ATPase of *Escherichia coli:* The ε-inhibited state forms after ATP hydrolysis, is distinct from the ADP-inhibited state, and responds dynamically to catalytic site ligands

Naman B. Shah, Marcus L. Hutcheon, Brian K. Haarer and Thomas M. Duncan[1]

Department of Biochemistry and Molecular Biology, State University of New York Upstate Medical University, 750 East Adams Street, Syracuse, New York 13210

This research was originally published in Journal of Biological Chemistry. Naman B. Shah, Marcus L. Hutcheon, Brian K. Haarer, and Thomas M. Duncan. **F_1-ATPase of *Escherichia coli:* THE ε-INHIBITED STATE FORMS AFTER ATP HYDROLYSIS, IS DISTINCT FROM THE ADP-INHIBITED STATE, AND RESPONDS DYNAMICALLY TO CATALYTIC SITE LIGANDS.** *Journal of Biological Chemistry*. 2013; **288**:9383-9395.

2.1 Abstract

F_1-ATPase is the catalytic complex of rotary nanomotor ATP synthases. Bacterial ATP synthases can be autoinhibited by the C-terminal domain of subunit ε, which partially inserts into the enzyme's central rotor cavity to block functional subunit rotation. Using a kinetic, optical assay of F_1·ε binding and dissociation, we show that formation of the extended, inhibitory conformation of ε (ε_X) initiates after ATP hydrolysis at the catalytic dwell step. Prehydrolysis conditions prevent formation of the ε_X state, and post-hydrolysis conditions stabilize it. We also show that ε inhibition and ADP inhibition are distinct, competing processes that can follow the catalytic dwell. We show that the N-terminal domain of ε is responsible for initial binding to F_1 and provides most of the binding energy. Without the C-terminal domain, partial inhibition by the ε N-terminal domain is due to enhanced ADP inhibition. The rapid effects of catalytic site ligands on conformational changes of F_1-bound ε suggest dynamic conformational and rotational mobility in F_1 that is paused near the catalytic dwell position.

2.2 Introduction

ATP synthases play a key role in energy metabolism in most living organisms and achieve energy coupling as dual engine rotary nanomotors [1–3]. The F-type ATP synthase of *Escherichia coli* (Fig. 2.1), a bacterial prototype, is composed of core subunits that all have homologs in the ATP synthases of mitochondria and chloroplasts [4]. The membrane-embedded F_O complex (**ab_2c_{10}**) acts like a turbine to transport protons across the membrane, and the external F_1 complex ($\alpha_3\beta_3\gamma\delta\varepsilon$) contains three cooperative catalytic sites for ATP synthesis or hydrolysis. The ring of *c*-subunits, with the critical proton transport sites, is the rotor complex of F_O and connects to the central rotor stalk of F_1, composed of γ and the N-terminal domain $(NTD)^2$ of ε. The three catalytic β subunits alternate with three α subunits to surround the upper half of the asymmetric rotor stalk of γ, and the δ-**b_2** connection forms a peripheral stator stalk anchoring $\alpha_3\beta_3$ to the other stator subunit of F_O, *a*. *In vitro*, F_1 from eukaryotes and bacteria can be dissociated from F_O as a soluble, rotary motor ATPase, and these F_1-ATPases have been useful for both mechanistic studies and the determination of high resolution structures.

Despite general conservation between bacterial and mitochondrial ATP synthases, it has been demonstrated that bacterial ATP synthase can be an effective target for antibacterial treatment. It is the target of a novel class of compounds that are bactericidal for actively replicating and dormant mycobacteria [5, 6] and that show promising effects against multidrug-resistant tuberculosis in phase II clinical trials [7]. However, the lead compound is only effective against a narrow spectrum of mycobacteria, and, because it targets the H^+-transporting sites of F_O, adapting this scaffold to target other pathogenic bacteria introduces a significant risk of cross-reaction with mitochondrial ATP synthase.

Figure 2.1

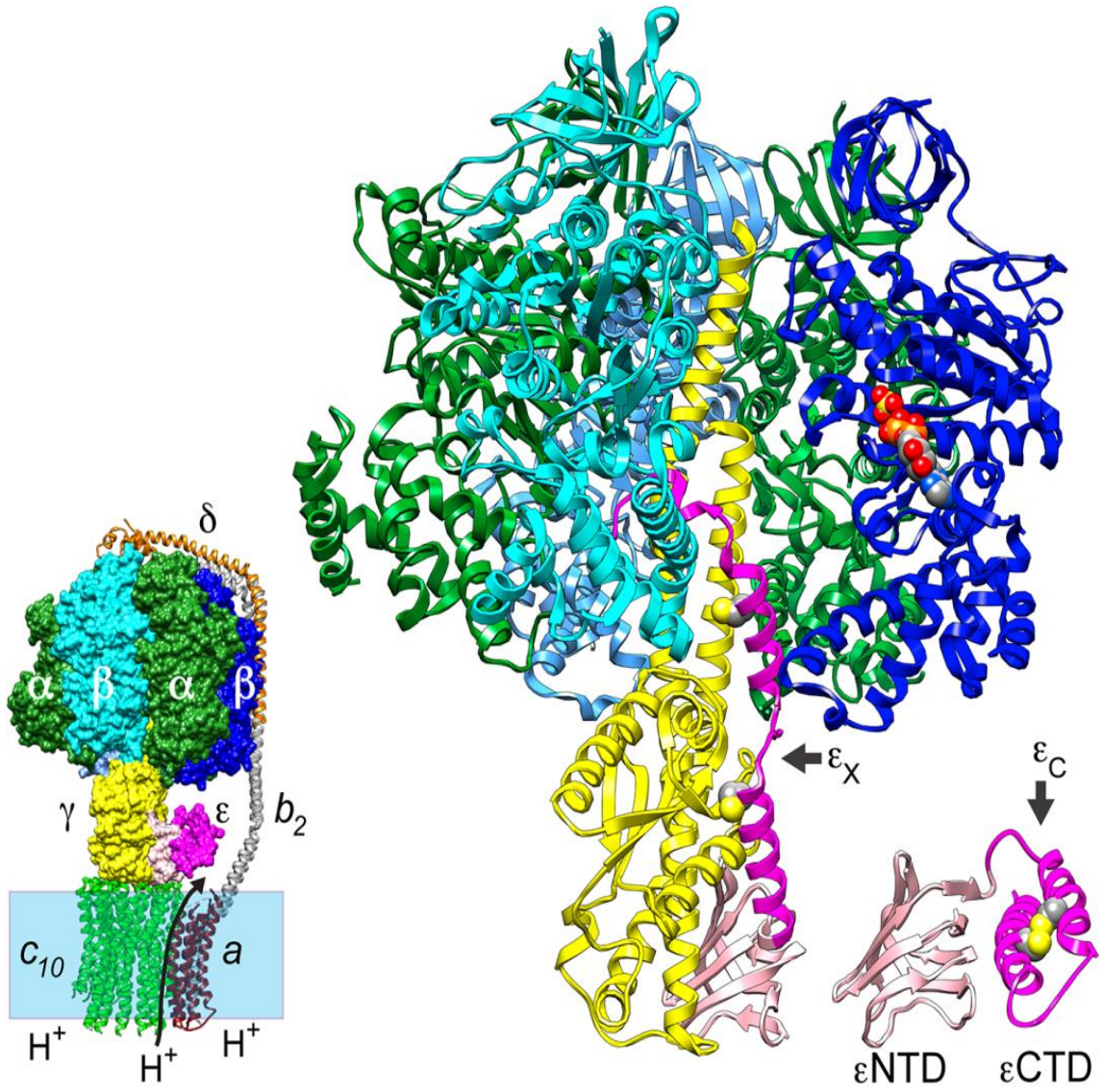

Figure 2.1. Architecture of bacterial ATP synthase, and alternate conformations of subunit ε. The smaller image (*bottom left*) depicts the *E. coli* ATP synthase, with F_O subunits spanning the membrane bilayer (*shaded box*); the *arrow across* the bilayer indicates the direction of proton (H^+) transport during net ATP synthesis. F_O subunits (*ribbons*, **a** (*dark red*), $\mathbf{b_2}$ (*gray*), $\mathbf{c_{10}}$ (*green*)) and F_1 subunit δ (*orange ribbon*) are from a homology-modeled assembly [13]]. All other F_1 subunits are from determined structures and are surface-rendered in the F_OF_1 model but displayed as ribbons in the magnified view of *E. coli* F_1 (3 α (*green*); 3 β (*shades of blue*); γ (*yellow)*; εNTD (1-87) (*light pink*), εCTD (88-138) (*dark pink*)). The F_OF_1 model shows ε in the ε_C or compact conformation (Protein Data Bank entry 1BSN), docked to γ of EF_1-δ (Protein Data Bank entry 3OAA). The *magnified ribbon diagram* shows the ε-inhibited F_1-δ structure (Protein Data Bank entry 3OAA) and omits the foremost α subunit to reveal the extended conformation of ε (ε_X); for comparison, a ribbon model of the ε_C state is shown offset to the right. The ribbon diagram of each ε conformation shows space-filling side-chain atoms (*colored* by element) predicted *in silico* for mutations εA101C/L121C. Space-filling atoms are also shown for ADP and SO_4^{2-} on the one occupied catalytic β subunit (chain D). The molecular graphics were prepared with Chimera [81].

Recently, our group determined the first crystal structure of a bacterial F_1-ATPase that is in an autoinhibited state mediated by the C-terminal domain (CTD) of its ε subunit [8]. Inhibition by ε may serve regulatory roles in ATP synthases of bacteria [2, 9] and chloroplasts [10] but does not occur in mitochondrial ATP synthase, which has a distinct inhibitor protein [11]. Recent studies confirmed that the bacterial εCTD inhibits ATP synthesis as well as hydrolysis [12, 13], indicating that ε inhibition may provide a new target for future development of antimicrobial drugs selective for bacteria. With that in mind, the current study focuses on improving our biochemical understanding of how the catalytic F_1 complex of *E. coli* ATP synthase is inhibited by ε.

As shown in Fig. 2.1, the ε subunit has two domains. The εNTD, essential for the F_1 rotor connection to the **c**-ring in F_O [2, 9], is a β-sandwich fold and exhibits a similar conformation and association with γ in several structures of bacterial F_1 [8, 14] and mitochondrial F_1 (MF_1) [15, 16]; essentially the same εNTD structure is also seen for isolated bacterial ε [17–19]. However, the α-helical εCTD has been observed in dramatically different conformations (Fig. 2.1). A compact conformation (the ε_C state) has a coiled-coil between its two α-helices, and the second helix packs against the εNTD. The ε_C state has been observed for isolated bacterial ε [17–19] and in one bacterial F_1 structure [14]. In structures of MF_1 [15] and MF_1·**c**-ring [20], the homolog of ε appears to be locked in the ε_C state by a mitochondria-specific subunit. *E. coli* ATP synthase can synthesize and hydrolyze ATP when ε is restricted to the ε_C state [21], in which the εCTD does not contact any F_1 subunits (Fig. 2.1, *left*). In contrast, in the recently determined structure of *E. coli* F_1 (Fig. 2.1) [8], an extended conformation of the εCTD (ε_X state) contacts five other subunits, and its terminal half is inserted into the central cavity of F_1. The position and subunit contacts of the εCTD within the *E. coli* F_1 structure correlate well with many

biochemical studies of ε inhibition and interaction with other F_1 subunits (reviewed in Refs. 2 and 9). The extensive buried surface of the εCTD within the F_1 structure and its interactions with two catalytic β subunits suggest that this form of the enzyme represents an inactive state. This correlates with results of "single-molecule" (SM) studies of F_1 from *E. coli* [22] and other bacteria [23–26], showing that ε can induce or extend long "pauses" (seconds) during which γ does not rotate in the presence of substrate MgATP. Some SM studies concluded that ε inhibits by stabilizing or extending an ADP-induced inhibitory pause that occurs at the catalytic dwell [22, 24, 27], whereas another recently concluded that ADP- and ε-induced inhibitions are separate processes for cyanobacterial F_1 [25]. Some studies also concluded that ε inhibition includes or is dominated by changes to one or more intrinsic kinetic steps along the catalytic pathway [12, 22, 28, 29]. In the current study, we adapt an optical assay to directly measure the kinetics of binding and dissociation for *E. coli* F_1·ε and correlate these with inhibitory effects for wild type (WT) and mutant forms of ε. Our biochemical evidence confirms that inhibition by the CTD of ε initiates at the catalytic dwell but also shows that ε inhibition competes with formation of the ADP-inhibited state. Further, whereas ε inhibition initiates at the catalytic dwell, we also show that the balance between active and ε-inhibited states responds dynamically to changing nucleotide conditions.

2.3 Results

Inhibition of E. coli F_1 by ε with and without the εCTD

Upon *in vitro* dissociation of *E. coli* F_1 from the membrane, ε becomes more inhibitory but can dissociate upon dilution of F_1, relieving inhibition of F_1-ATPase activity [2]. For most experiments in this study, we used F_1 that was depleted of δ and ε subunits, or $F_1(-\delta\varepsilon)$. The stator subunit δ does not significantly affect F_1-ATPase activity [42] but was removed because its dissociation from F_1 could interfere with assays below for $F_1{\cdot}\varepsilon$ binding and dissociation. Fig. 2.2 compares inhibition of $F_1(-\delta\varepsilon)$ by WT and mutant forms of H6-ε, and Table 2.1 summarizes the inhibition parameters from regression curves of Fig. 2.2 and an additional data set. As noted before [30], the N-terminal His6 tag on WT ε did not significantly alter inhibition compared with WT ε that had the tag removed (Table 2.1). Also, inhibition was not altered by the N-terminal Bap tag added to ε (WT and mutants) for kinetic assays of $F_1{\cdot}\varepsilon$ binding and dissociation (not shown).

For WT ε, values for the inhibitory constant K_I and residual activity of ε-saturated F_1 agree with earlier estimates [29, 43]. We obtained nearly the same parameters for ε inhibition in assays with ATP < K_M (not shown), consistent with noncompetitive inhibition by ε *versus* ATP [29, 44]. We also show that the >90% inhibition by saturating WT ε was unaffected by excess Mg^{2+} (Fig. 2.2*A*), although $F_1(-\delta\varepsilon)$ alone was inhibited >50% by 1 mM excess Mg^{2+} (Table 2.1).

To test for inhibition by ε lacking its CTD, we used ε88stop, one of the largest C-terminal deletions that still allows assembly of F_OF_1 that is functionally coupled, both *in vivo* and *in vitro* [31]. In Fig. 2.1, both conformations of ε are *colored magenta* for the C-

Figure 2.2

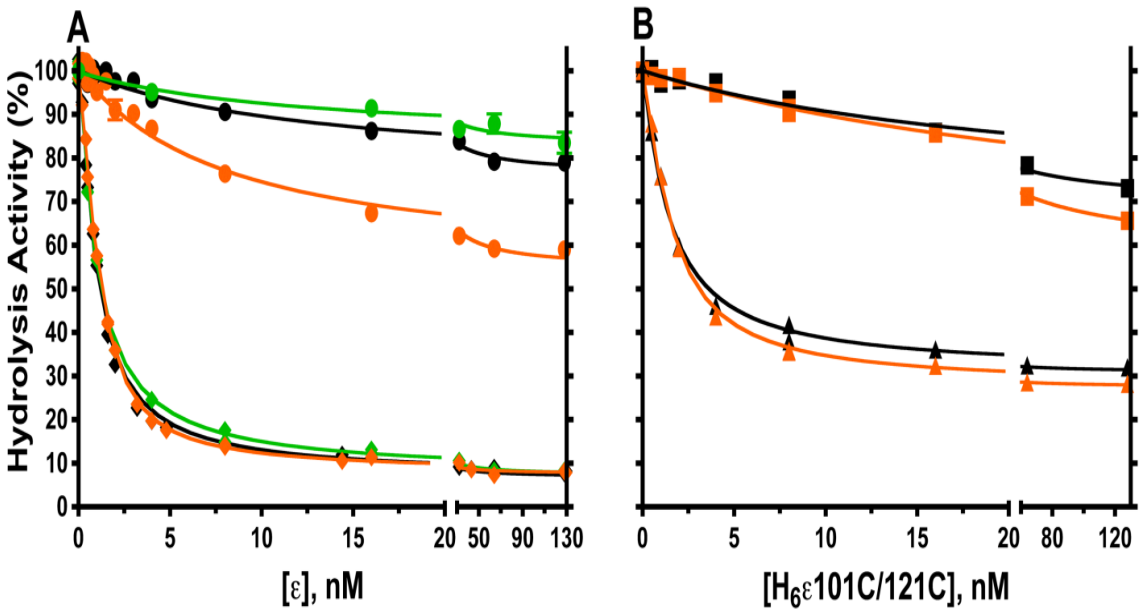
A
B
Hydrolysis Activity (%)
100
90
80
70
60
50
40
30
20
10
0
0
5
10
15
20
50
90
130
[ε], nM
0
5
10
15
20
80
120
[H6ε101C/121C], nM

Figure 2.2. Effects of truncating or crosslinking the εCTD on inhibition of F_1(-δε). *A*: F_1(-δε) was pre-incubated for 10 min with 0.1 mM EDTA and ATP (*black* and *orange* symbols) or GTP (*green* symbols) and the indicated concentrations of wild-type H_6-ε (◆) or H_6-ε88stop (●). Hydrolysis was initiated by adding Mg acetate. Final concentrations of added ligands were as follows: 2:1ATP:Mg^{2+} (*black*); 1:2 ATP:Mg^{2+} (*orange*); 1:2 GTP:Mg^{2+} (*green*). *B*: ATPase assays as for panel A, but H_6-ε101C/121C was used with 1 mM DTT present (▲) or with an ε101C-121C disulfide bond (■). See "Experimental Procedures" for assay details and regression analysis. With H_6-ε88stop, data points are averages from three (ATP) or two (GTP) experiments, and standard *error bars* are included but are smaller than the *symbols* for most points. Results of regression analyses for these and for a dataset with untagged WT ε are summarized in Table 2.1.

Table 2.1: Inhibition of $F_1(-\delta\varepsilon)$ by variants of subunit ε

ε	NTP/Mg^{2+} ratio *mM*	Activity of $F_1(-\delta\varepsilon)$ (A_0) [a] *μmol min^{-1} mg^{-1}*	Activity of ε-saturated F_1 (A_e/A_0)[b] (±S.E.[c]) *%*	K_I ±S.E.[c] *nM*
Wild-type	ATP 2:1	78	7.9 ±0.6	0.49 ±0.02
Wild-type H_6-ε	ATP 2:1	78	6.8 ±0.8	0.67 ±0.04
	ATP 1:2	37	7.9 ±0.5	0.46 ±0.02
	GTP 1:2	94	7.3 ±0.7	0.87 ±0.04
H_6-ε88stop	ATP 2:1	73	76.3 ±1.2	12.4 ±1.9
	ATP 1:2	36	54.6 ±1.4	7.2 ±0.8
	GTP 1:2	95	84 ±2.0	13 ±7
H_6-ε101C/121C, + 1 mM DTT	ATP 2:1	80	31 ±1	1.2 ±0.1
	ATP 1:2	41	27 ±1	0.98 ±0.06
H_6-ε101C/121C, disulfide bonded	ATP 2:1	80	69 ±2	23 ±3.7
	ATP 1:2	38	58 ±1	31 ±2

Table 2.1. Results of nonlinear regression for data shown in Fig. 2.2 and a data set with untagged WT ε. Equation 1 was used (see "Experimental Procedures").

[a] Hydrolysis activity units are $\mu mol \cdot min^{-1} \cdot mg^{-1}$ $F_1(-\delta\varepsilon)$.

[b] Activity of ε-saturated $F_1(-\delta\varepsilon)$, A_e, is listed as a percentage of A_0, the measured activity of $F_1(-\delta\varepsilon)$ alone.

[c] S.E., standard error from nonlinear regression.

terminal region that is absent in ε88stop. As shown in Fig. 2.2*A*, H_6-ε88stop caused much less inhibition than WT H_6-ε and had a >15-fold larger K_I, confirming that the εCTD is responsible for the majority of inhibition. However, unlike WT H_6-ε, the maximal extent of inhibition by H_6-ε88stop almost doubled to ~45% in the presence of excess free Mg^{2+}. Inhibitory effects of free Mg^{2+} are linked to inhibitory MgADP bound at a catalytic site on F_1 from *E. coli* (45, 46), from other bacteria [47], from mitochondria [48, 49] and chloroplasts [50, 51], and hydrolysis of GTP is less sensitive to this type of inhibition [45, 48, 52]. For example, with 1 mM excess Mg^{2+}, GTPase turnover by F_1(-δε) is ~2.5-fold faster than ATPase (Table 2.1). We show that WT H_6-ε exhibits similar high affinity inhibition for GTPase and ATPase (Fig. 2.2*A* and Table 2.1). However, H_6-ε88stop inhibited GTPase much less, ~16% maximal, both with excess free Mg^{2+} present (Fig. 2.2*A*) and without it (not shown). Thus, observed partial inhibition of ATPase by the εNTD is largely due to increased MgADP inhibition in the absence of the εCTD. This can also explain why ε truncated after ε94 (with only about half of the first helix remaining) inhibited *E. coli* F_1 ~50% because the assays contained 2 mM excess free Mg^{2+} [53]. The effects of the εNTD are distinct from the >90% inhibition caused by the εCTD of intact WT ε, which is not sensitive to the effects of excess Mg^{2+}.

As an alternative to removing the εCTD, we also used the εA101C/L121C mutant [21].[3] This cysteine pair can form a disulfide bond in nearly 100% yield (Fig. 2.3) that cross-links the two α-helices of the εCTD in the ε_C conformation, preventing ε from switching to the ε_X conformation (see Fig. 2.1). As shown in Fig. 2.2*B*, this disulfide linkage prevented high affinity inhibition of F_1(-δε) as effectively as removing the εCTD. However, the partial inhibition observed was less sensitive to excess free Mg^{2+} than with

H_6-ε88stop; this suggests that εCTD/εNTD interactions in the ε_C state can influence interactions of εNTD with γ that alter catalytic behavior. With DTT present to prevent the disulfide bond, H_6-εA101C/L121C could access the ε_X state and showed high affinity inhibition ($K_I \sim 1$ nM), similar to that with WT H_6-ε ($K_I \sim 0.5$ nM). However, the activity of F_1 saturated with reduced H_6-εA101C/L121C was 4-fold greater than with WT H_6-ε. In the structure of ε-inhibited F_1 [8], εLeu-121 is in a coiled-coil interface with the γ N-terminal helix, and the εL121C mutation probably perturbs this interface, favoring more F_1 complexes in the active state on average. This supports the concept that, with ε-saturated F_1, the residual ATPase activity (7–8% with WTε) is due to the time-averaged fraction of F_1 complexes in which ε is not in the inhibitory ε_X conformation.

Figure 2.3

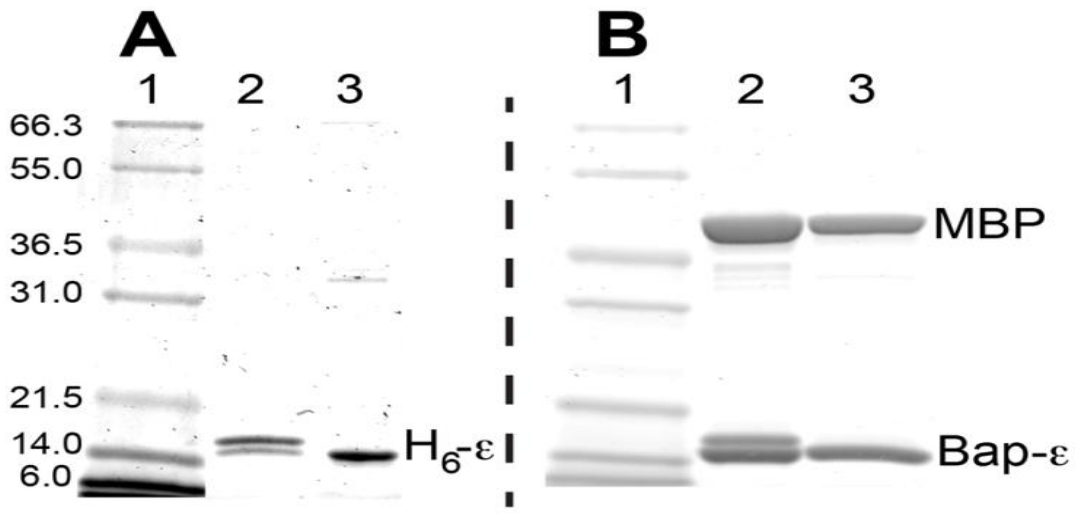

Figure 2.3. SDS-PAGE analysis of disulfide bond formation with εA101C/L121C. Samples were applied to 12% SDS-PAGE under non-reducing conditions. *Lane* 1 of each gel: molecular weight markers (approximate kDa noted for gel A). *Gel A*: samples of H_6εA101C/L121C (1 μg/lane) were taken (*lane 2*) immediately after DTT was removed from the sample by centrifuge column or (*lane 3*) after 2 min of reaction with 50 μM DTNB. *Gel B*: samples of (MBP cleaved)-Bap-ε (5 μg/lane) were taken (*lane 2*) after removing DTT as above or (*lane 3*) after reaction with 50 μM DTNB for 15 min. With 2-mercaptoethanol in the gel sample buffer (not shown), each εA101C/L121C migrated only at the upper band position (above 14 kDa standard), confirming that the lower band seen here was a faster migrating band due to the internal εA101C-L121C disulfide bond.

Kinetics of F_1·ε Binding and Dissociation, Assayed by BLI

In preliminary assays, H_6-ε was loaded on BLI sensors coated with Ni^{2+}-nitrilotriacetic acid, but slow dissociation of WT H_6-ε from the sensors prevented accurate measures of the slow dissociation rate of F_1 from WT H_6-ε. To achieve more stable and specific attachment of ε to the sensor surface, ε was engineered with an N-terminal Bap tag, so that a specific lysine could be

biotinylated *in vivo* [32]. Biotinylated Bap-ε could be stably bound to streptavidin-coated sensors (supplemental Fig. S1), and BLI was then used to measure binding and dissociation kinetics of F_1(-δε). For each Bap-ε variant, 4–7 sensors were used in parallel, with F_1(-δε) concentrations varied 10-fold in the association samples, and association/dissociation kinetics were fit globally to determine the rate constants (Table 2.2). K_D values derived from the rate constants correlate well with inhibitory K_I values (Table 2.1) for WT ε, ε88stop, and disulfide bonded εA101C/L121C. Representative kinetics for binding/dissociation of F_1(-δε) with sensors containing WT ε or ε88stop are shown in Fig. 2.4. The εCTD did not significantly alter the association rate, indicating that only εNTD/γ interactions are involved in initial F_1·ε binding. In contrast, removing the εCTD (Fig. 2.4) or preventing it from adopting the ε_X state (disulfide-bonded εA101C/L121C) increased the dissociation rate by 80-fold (Table 2.2). For sensors loaded with biotinylated WT BapH_6-ε, only a small fraction of bound F_1(-δε) could be observed to dissociate in buffer only (Fig. 2.4), but results presented below show that essentially all F_1(-δε) on the sensor is reversibly bound. Additional assays (not shown) included excess, non-biotinylated WT H_6-ε in the dissociation phase and confirmed that the observed, slow dissociation rate was not due to rebinding of F_1(-δε) to the sensor. Thus, the much slower dissociation of F_1(-

δε)/WT-ε is probably due to strong bias of bound WT ε to reside in the ε_X state, with the εCTD buried within F_1. However, from the K_D values (Table 2.2), note that the εCTD contributes only ~20% to the net free energy for F_1·ε binding ($\Delta\Delta G$, -10 or -12 kJ/mol for WT ε *versus* ε88stop or disulfide-bonded εA101C–L121C, respectively). This does not mean the ε_X state of εCTD has only weak interactions with other F_1 subunits; rather, the small contribution to net binding energy is probably due to the loss of favorable interactions between ε and $\alpha_3\beta_3$ that are blocked by insertion of the εCTD.

Figure 2.4

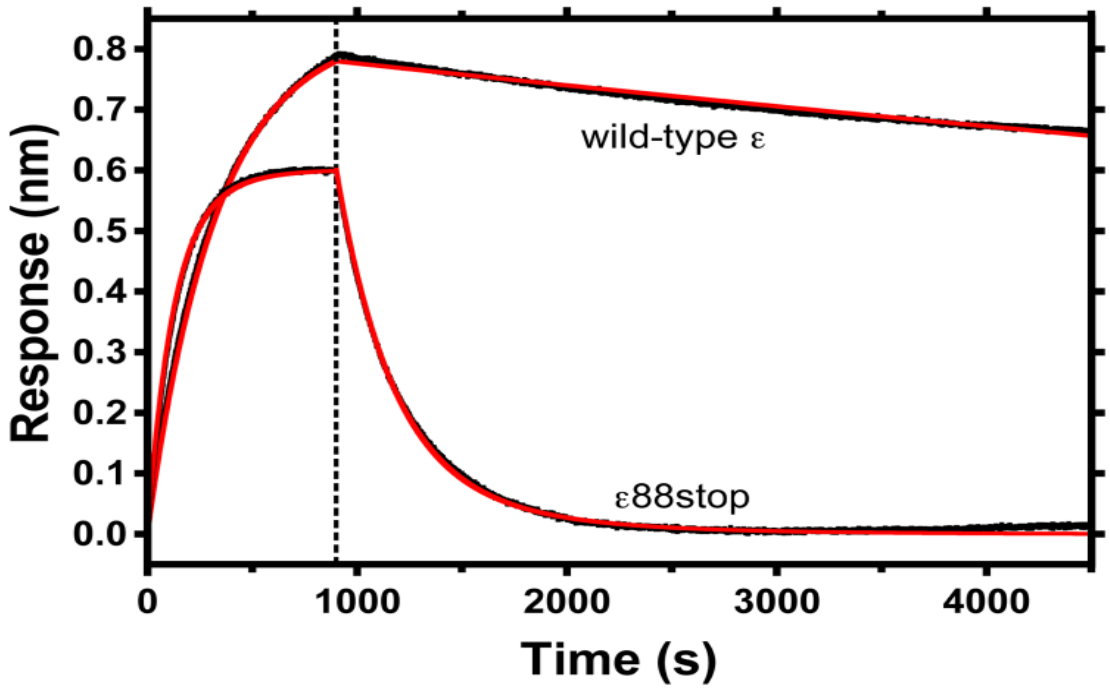
Response (nm)
0.0
0.1
0.2
0.3
0.4
0.5
0.6
0.7
0.8
0
1000
2000
3000
4000
Time (s)
wild-type ε
ε88stop

Figure 2.4. Binding and Dissociation Kinetics for $F_1(-\delta\varepsilon)$ and sensor-bound biotinylated $\varepsilon, \pm\varepsilon$CTD. Biotinylated Bap-ε (wild-type or ε88stop, as noted) was loaded on streptavidin biosensors. At time 0, each sensor was transferred from buffer alone to a sample containing 15 nM $F_1(-\delta\varepsilon)$. After 900 s (*vertical dashed line*), each sensor was moved into buffer without $F_1(-\delta\varepsilon)$. *Black lines*, experimental data; *red lines*, the kinetic fits for each ε, from global regression of kinetic data at varied concentrations of $F_1(-\delta\varepsilon)$. Kinetic parameters and K_D values derived from the fittings are summarized in Table 2.2.

Table 2.2 Binding/dissociation rates and K_D values for F_1(-δε) with variants of subunit ε

Biotinylated ε	**k_a, ±SE[a]** **$M^{-1}s^{-1}$**	**k_d ±SE[a]** **s^{-1}**	***K_D*** **nM**
Wild-type	$2.0x10^5$ ±0.1%	$4.8x10^{-5}$ ±0.1%	0.24
Wild-type, +1 mM EDTA/ATP	$2.3x10^5$ ±0.1%	$4.1x10^{-3}$ ±0.1%	17
ε88stop	$3.1x10^5$ ±0.6%	$3.8x10^{-3}$ ±0.4%	12.2
ε101C/121C, disulfide bonded	$2.1x10^5$ ±0.3%	$6.6x10^{-3}$ ±0.2%	32

Table 2.2. Binding/dissociation rates and K_D values for F_1(-δε) with variants of subunit ε

[a]S.E., standard error from global fitting analysis (presented as a percentage of the parameter's value).

Effects of F_1 Ligands (Mg^{2+}, Nucleotides, Pi) on Conformational Bias of Bound, Full-length ε

From the crystal structure of ε-inhibited F_1 [8], the extensive surface area of εCTD that is buried within the central cavity of F_1 suggests that the ε_X state of ε does not directly dissociate from F_1; the slow dissociation observed in Fig. 2.4 probably occurs due to dynamic transition of ε between ε_X and conformations like ε_C in which the εCTD is outside of the central rotor cavity. Thus, factors that influence the fraction of F_1 complexes with ε in the ε_X state should alter the kinetics of F_1·ε dissociation. To show that the conformation of ε on *E. coli* F_1 and F_OF_1 can be influenced by nucleotides and other ligands that interact with catalytic sites, early studies used static assays, such as the capacity to form a β-ε cross-link; crosslinking of β-ε was minimized by non-hydrolysis conditions, such as ATP/EDTA or MgAMPPNP but maximized by post hydrolysis conditions (MgADP/Pi) [54, 55]. The β-ε cross-linking residues [56] are within hydrogen-bonding distance in the structure of ε-inhibited F_1 but should be at least 35 Å apart with ε in the ε_C state [8]. Here, we use the BLI assay for F_1·ε binding/dissociation for more dynamic analyses of how different ligands may shift the conformation of F_1-bound ε between the ε_X state and other conformations of the εCTD that allow faster F_1·ε dissociation. In control assays (not shown), the various ligands tested did not alter the rate at which F_1(-δε) dissociated from biotinylated ε88stop, confirming that the ligand effects are specific to the εCTD of WT ε. F_1(-δε) was bound in parallel to multiple sensors with biotinylated WT ε, and Fig. 2.5 shows dissociation of F_1(-δε) when sensors were exposed to different ligands. For Fig. 2.5*A*, F_1(-δε) was bound to all sensors in MTK8 buffer + BSA, and dissociation in this buffer was slow (Fig. 2.5*A*, *curve 4*,~$5.4x10^{-5}$ s^{-1} ± 0.2%).

Figure 2.5

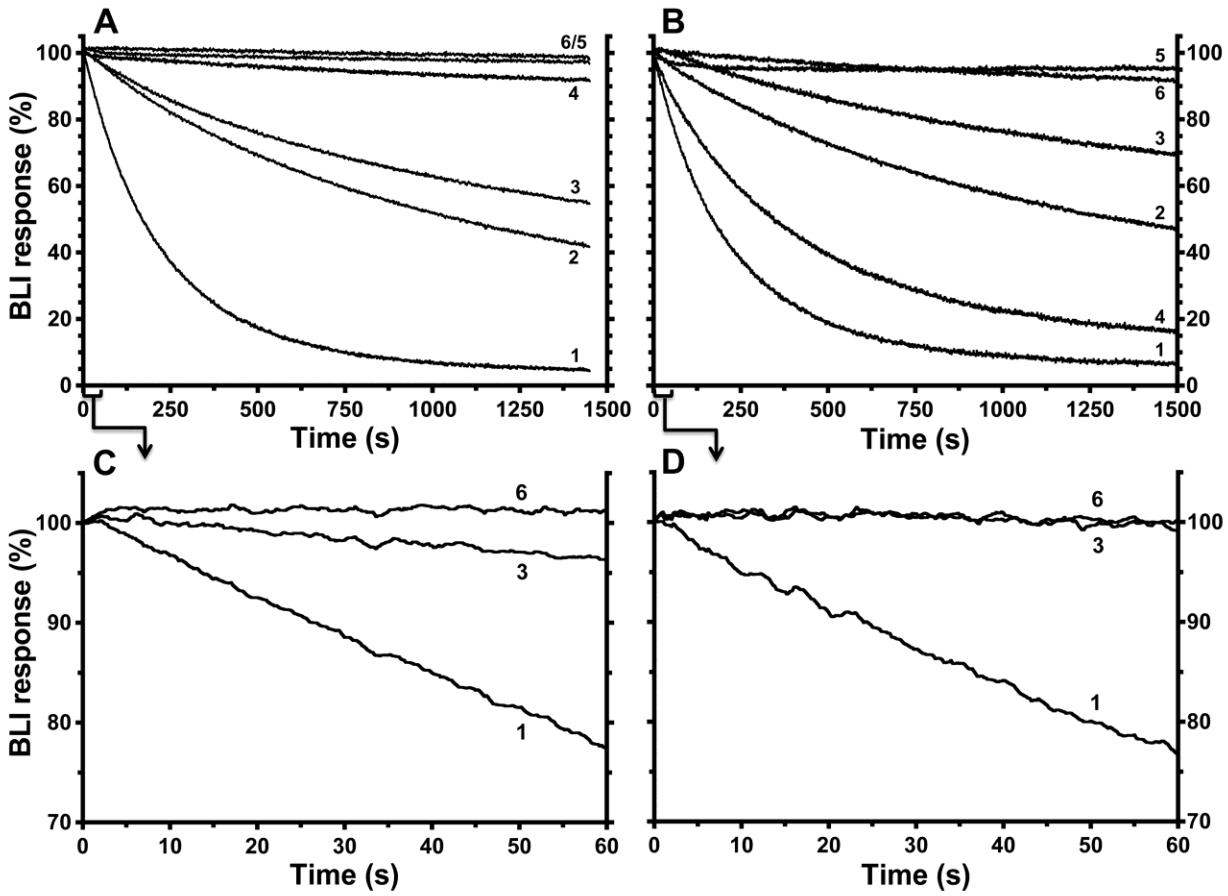

Figure 2.5. Effects of other ligands on dissociation of F_1 from sensor-bound wild-type ε. $F_1(-\delta\varepsilon)$ (50 nM) was incubated ~10 min in MTK8 +BSA buffer only (*A*) or plus 1 mM ATP:EDTA *(B)* and then incubated with BLI sensors containing WT $BapH_6$-ε to equilibrate $F_1 \cdot \varepsilon$ binding. Signals for bound $F_1(-\delta\varepsilon)$ varied slightly between sensors (6 to 9%), so data were normalized for display. Results show the kinetics of $F_1(-\delta\varepsilon)$ dissociation upon moving sensors into buffer with different ligands. Panels *C* and *D* show selected results from *A* and *B*, respectively, for the initial 60 s of dissociation. When present, Mg^{2+} was at 2 mM; all other ligands were at 1 mM. Curves: *1*, ATP:EDTA; *2*, MgADP; *3*, MgATP; *4*, buffer only; *5*, MgADP:Pi; *6*, Mg^{2+}:Pi.

This is consistent with access to the ε_X state when F_1 is in a post-hydrolysis conformation because isolated $F_1(-\delta\varepsilon)$ retained ~1.5 ADP (mol/mol) but negligible ATP at catalytic sites (see "Experimental Procedures"). Added MgADP/Pi (Fig. 2.5*A*, *curve 5*) appeared to stabilize the ε_X state, consistent with prior β-ε cross-linking results [55]. However, a similar effect was achieved by adding only Mg^{2+} and Pi (Fig. 2.5*A*, *curve 6*), suggesting that the endogenous ADP in isolated $F_1(-\delta\varepsilon)$ was sufficient to stabilize the ε_X state upon the addition of Mg^{2+} and Pi. The importance of Pi in stabilizing this state [55] was also observed here because MgADP alone (Fig. 2.5*A*, *curve 2*) allowed a significant fraction of F_1 to dissociate faster.

In contrast to slow $F_1{\cdot}\varepsilon$ dissociation under post-hydrolysis conditions, the addition of 1 mM ATP/EDTA caused ~94% of $F_1{\cdot}\varepsilon$ to dissociate ~80-fold faster (Fig. 2.5*A*, *curve 1*, $4.2 \times 10^{-3}\ s^{-1}$ ±0.1%) and with <3-s transition to faster dissociation (Fig. 2.5*C*). This effect is due to ATP because EDTA alone had a minimal effect on F_1 dissociation from immobilized WT ε (not shown). Further, by including 1 mM ATP/EDTA during association and dissociation phases, global analysis of $F_1{\cdot}\varepsilon$ binding/ dissociation shows that ATP/EDTA did not alter the $F_1{\cdot}\varepsilon$ binding rate but gave a dissociation rate and K_D similar to values for ε88stop (Table 2.2). The presence of nonhydrolyzable MgAMPPNP (2:1 mM) during the dissociation phase (not shown) also accelerated $F_1{\cdot}\varepsilon$ dissociation, indicating that nucleotide binding alone is sufficient to shift F_1 to a conformation that does not allow the εCTD to insert into F_1 and form the ε_X state. Also, the ability of MgADP/Pi to stabilize the inhibitory state of ε was readily reversible; even when $F_1(-\delta\varepsilon)$ was bound to WT ε/sensors for 45 min with MgADP/Pi present, switching the sensors to buffer with MgAMPPNP immediately caused >90% of $F_1(-\delta\varepsilon)$ to dissociate at the faster rate (not shown; 3.7×10^{-3}

s^{-1} ± 0.1%). For the experiment in Fig. 2.5*B*, $F_1(-\delta\varepsilon)$ was bound to immobilized WT ε in the presence of 1 mM ATP/EDTA, so that most $F_1{\cdot}\varepsilon$ complexes would not have ε in the slowly dissociating ε_X state at the time the sensors were moved to dissociation wells. As expected, F_1 dissociation was fast with ATP/EDTA present (Fig. 2.5*B*, *curve 1*). With buffer only (Fig. 2.5*B*, *curve 4*), most F_1 still dissociated fast. This could indicate that ATP bound during the $F_1{\cdot}\varepsilon$ association phase dissociated slowly or that endogenous ADP had dissociated from F_1 during the association phase due to the ATP/EDTA present. MgADP alone (Fig. 2.5*B*, *curve 2*) slowed dissociation of most F_1, but MgADP/Pi (Fig. 2.5*B*, *curve 5*) or Mg^{2+}/Pi (Fig. 2.5*B*, *curve 6*) effectively reversed the ATP/EDTA effect so that almost all F_1 dissociated very slowly. Mg^{2+} was essential for this effect; without it, F_1 dissociation in the presence of 1 mM Pi (not shown) was nearly identical to that in buffer alone (Fig. 2.5*B*, *curve 4*). The effect of Mg^{2+} was enhanced by submillimolar Pi (not shown, $K_{1/2}$ ~0.2mM Pi), similar to how Pi enhanced MgADP protection of F_1-bound ε from trypsin [55].

With Mg^{2+}/Pi, there was no apparent lag in reverting $F_1{\cdot}\varepsilon$ to slow dissociation (Fig. 2.5*D*, *curve 6*). This suggested that, after $F_1{\cdot}\varepsilon$ association with ATP/EDTA present, rapid reversion by Mg^{2+}/Pi to slow $F_1{\cdot}\varepsilon$ dissociation required hydrolysis of ATP that remained bound at a catalytic site. In the dissociation step, added Mg^{2+} could complex with the bound ATP, and hydrolysis would return F_1 to the catalytic dwell step, at which insertion of the εCTD into the central cavity appears to occur. The bound MgADP/Pi present would then stabilize F_1 with ε in the ε_X state. The experiment shown in Fig. 2.6 tested this possibility. With non-hydrolyzable MgAMPPNP present during $F_1{\cdot}\varepsilon$ association, dissociation of most $F_1{\cdot}\varepsilon$ was fast in the presence of MgAMPPNP (Fig. 2.6, *curve 1*) or in buffer alone (Fig.

Figure 2.6

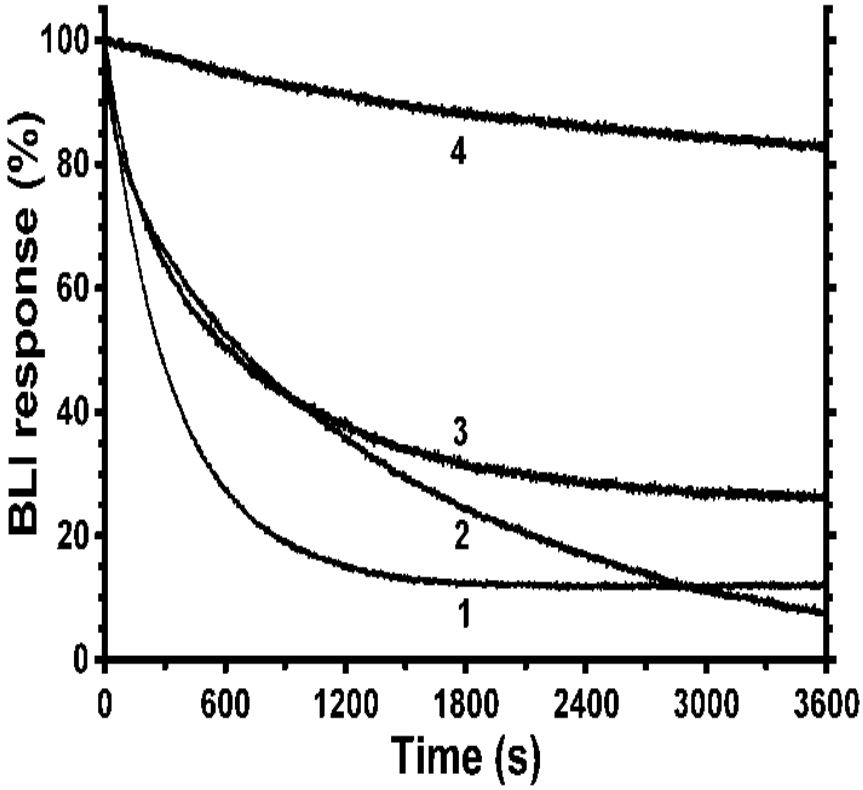
BLI response (%)
100
80
60
40
20
0
0
600
1200
1800
2400
3000
3600
Time (s)
4
3
2
1

Figure 2.6. Contrasting effects of Mg^{2+}:Pi on F_1/ε dissociation after preincubating F_1 with ATP:EDTA or MgAMPPNP. F_1(-δε) (50 nM) was incubated ~10 min in MTK8 buffer containing 2:1 mM MgAMPPNP (*curves 1-3*) or 1 mM ATP:EDTA (*curve 4*) and incubated with BLI sensors containing WT $BapH_6$-ε. BLI signals for bound F_1(-δε) were normalized as in Fig. 2.5. Kinetics of F_1 dissociation were monitored in the presence of 2:1 mM MgAMPPNP (*curve 1*), buffer only (*curve 2*), or 2:1 mM Mg^{2+}/Pi (*curves 3, 4*).

2.6, *curve 2*), similar to the effects of ATP/EDTA in Fig. 2.5*B*. However, with MgAMPPNP present during association, inclusion of Mg^{2+}/Pi during dissociation failed to prevent fast dissociation of most F_1 (Fig. 2.6, *curve 3*), in contrast to the parallel control with ATP/EDTA in association (Fig. 2.6, *curve 4*). These results indicate that, with catalytic nucleotide bound in a prehydrolysis state, the rotary conformation of F_1 does not allow insertion of the εCTD into the central rotor cavity, but hydrolysis at the catalytic dwell allows the εCTD access to insert and form the ε_X state. In the experiments of Fig. 2.5, hydrolysis conditions had complex effects on F_1·ε dissociation. With or without ATP/EDTA during F_1·ε binding, MgATP in the dissociation phase (*curve 3*) induced a small or negligible rate of F_1·ε dissociation during the initial 60 s (Fig. 2.5, *C* and *D*). Comparable with conditions for Fig. 2.5*B*, assays for ε inhibition of F_1-ATPase (Fig. 2.2) included an ATP/EDTA preincubation, and ε- saturated F_1 had initial ATPase activity (1–2 min, not shown) that was ~85% of the steady-state, inhibited rate. Thus, compared with fast F_1 dissociation in the continued presence of ATP/EDTA, hydrolysis of MgATP initially reverted F_1·ε complexes to slow dissociation, rapidly re-establishing the bias toward the inhibitory ε_X state (Fig. 2.5*D, curves 1* and *3*). This is consistent with noncompetitive inhibition of ε *versus* MgATP and, combined with other results above, indicates that ε accesses the inhibitory ε_X state following hydrolysis at the catalytic dwell step. On the longer time scale of Fig. 2.5 (*A* and *B*), hydrolysis conditions increased the dissociation rate for a fraction of F_1·ε complexes. As indicated by other experiments below, this slow effect on F_1·ε dissociation is probably due to gradual competitive transition of some active complexes to the ADP-inhibited state, which favors faster dissociation of ε. The fast dissociating fraction was substantially smaller for F_1·ε complexes formed in the

presence of ATP/EDTA (Fig. 2.5*B*), probably because the ATP/EDTA preincubation minimizes initial inhibition (not shown) due to ADP-inhibited complexes.

Inhibition of F_1(-δε) by Azide and the εCTD Are Competing Processes

The above results support prior SM mechanics studies [22–24, 26] that concluded that ε inhibition pauses rotation at the catalytic dwell position. In the absence of ε, long pauses at the catalytic dwell have been documented and attributed to inhibitory MgADP [57, 58]. However, there have been conflicting conclusions about the relationship between inhibitory MgADP and ε inhibition for F_1 of different bacterial species [22, 24, 25, 27]. We investigated this by testing interactions between ε inhibition and inhibition by sodium azide, which acts by stabilizing the MgADP-inhibited state [45, 59–61]. We first tested inhibition of F_1(-δε) by azide, with or without excess WT or mutant forms of H_6-ε present. Inhibition of F_1(-δε) alone showed a K_I of ~5 μM azide, whether assays were done with 2:1 mM Mg/ATP (Fig. 2.7) or with 1:2 mM Mg/ATP (not shown). Thus, for *E. coli* F_1, azide inhibition is separated from the step that confers sensitivity to inhibition by excess free Mg^{2+}. The K_I for azide was not altered by bound H_6-ε mutants that could not access the ε_X state due to truncation (ε88stop) or disulfide bonding (εA101C–L121C). The presence of 100 nM WT ε reduced the activity of F_1(-δε) ~10-fold, but the residual activity was still inhibited by excess azide. However, bound WT H_6-ε increased the K_I for azide ~5-fold (Fig. 2.7). Also, saturating F_1(-δε) with reduced H_6-εA101C/L121C, which was less inhibitory than WT H_6-ε, yielded an intermediate K_I value for azide inhibition. These results indicate that forming the inhibitory ε_X state competes with azide's capacity to inhibit F_1-ATPase. To test whether azide also competed with formation of the ε-inhibited state, F_1(-δε) was bound to immobilized WT BapH_6-ε in buffer alone, and F_1·ε dissociation was measured under hydrolysis conditions with varied concentrations of azide (Fig. 2.8*A*).

Increasing azide concentrations caused greater fractions of $F_1 \cdot \varepsilon$ to dissociate at a faster rate, and the hyperbolic dependence on azide (Fig. 2.8*B*) yielded a $K_{1/2}$ of ~14 μM, comparable with the mid-range of K_I values for azide inhibition with or without WT H_6-ε (Fig. 2.7). Taken together, the results of Figs. 2.7 and 2.8 show competition between (i) the ability of the εCTD to insert, forming the inhibitory ε_X state, and (ii) the ability of azide to bind to and stabilize the MgADP-inhibited state of F_1.

Figure 2.7

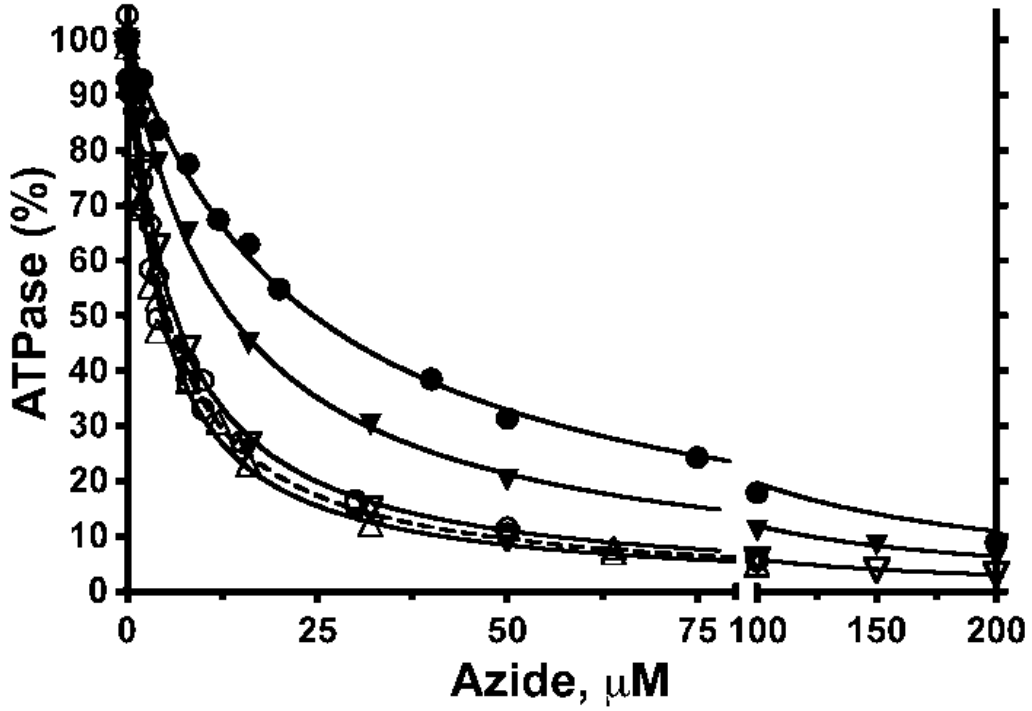
ATPase (%)
100
90
80
70
60
50
40
30
20
10
0
0
25
50
75
100
150
200
Azide, μM

Figure 2.7. Effects of excess ε variants on inhibition of F_1–ATPase by azide. Steady-state ATPase rates were measured for $F_1(-\delta\varepsilon)$ in the presence of varied concentrations of sodium azide. Assays were done in the absence of ε or in the presence of excess variants of H_6-ε. Each data set was fit to the equation $v = V/(1 + [\text{azide}]/K_I)$, then ATPase rates were normalized to V (μmol·min^{-1}·mg^{-1} $F_1(-\delta\varepsilon)$, without azide) = 100%. Without ε, similar K_I values (μM) were obtained for assays done with 2:1 mM ATP/Mg^{2+} (V = 78 ±3, K_I = 4.7 ± 0.7, not shown) or 1:2 mM ATP/Mg^{2+} (○; *dashed line*, V = 29.3 ± 0.5, K_I = 5.3 ± 0.3). Assays were done with 1:2 mM ATP/Mg^{2+} in the presence of 100 nM wild-type ε (●; V = 3.8 ± 0.04, K_I = 24.5 ± 0.9) or 100 nM ε88stop (△; V = 17.9 ± 0.3, K_I = 4.6 ± 0.2), or with 2:1 mM ATP/Mg^{2+} in the presence of 100 nM εA101C/L121C +5 mM DTT (▼; V = 30.9 ± 0.3, K_I = 13.5 ± 0.4) or in the presence of 300 nM disulfide-bonded εA101C/L121C (▽; V = 75.6 ± 0.7, K_I = 6.2 ± 0.2). In control assays (not shown), 5 mM DTT had no direct effect on ATPase activity of $F_1(-\delta\varepsilon)$.

Figure 2.8

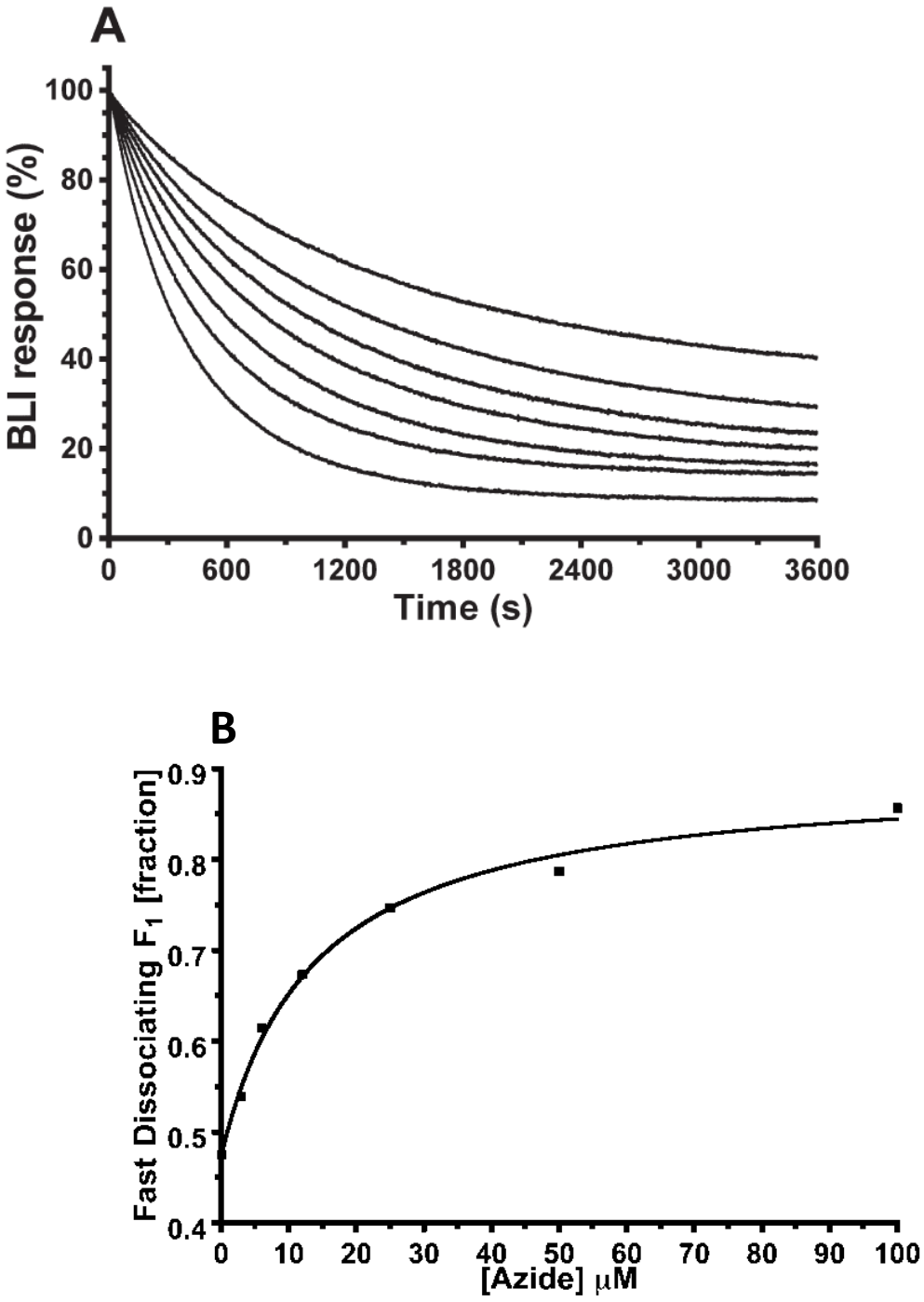
A
BLI response (%)
100
80
60
40
20
0
0
600
1200
1800
2400
3000
3600
Time (s)
B
Fast Dissociating F1 [fraction]
0.9
0.8
0.7
0.6
0.5
0.4
0
10
20
30
40
50
60
70
80
90
100
[Azide] μM

Figure 2.8. Effects of azide on dissociation of F_1 from sensor-bound, wild-type ε. *A*: Kinetics for $F_1 \cdot \varepsilon$ dissociation measured by BLI. Prior to the F_1 dissociation phase shown, BLI sensors had been loaded with biotinylated wild-type ε, then incubated for 900 s in buffer with 20 nM $F_1(-\delta\varepsilon)$; the normalized BLI signal at time 0 represents bound $F_1(-\delta\varepsilon)$. Dissociation of $F_1(-\delta\varepsilon)$ from immobilized ε was done in hydrolysis conditions (1 mM ATP, 2 mM Mg^{2+}) with increasing concentrations of azide, as indicated. Dissociation kinetics were biphasic, with 'fast' (1-2.5 $x10^{-3}$ s^{-1}) and 'slow' (0.8-1.6 $x10^{-4}$ s^{-1}) fractions (nonlinear regression fits not shown, but essentially superimpose with data at scale shown; $R^2 > 0.9995$ for all fits). *B*: The azide-dependence of F_1/ε dissociation. The fraction of complexes that dissociated fast *vs* slow shows hyperbolic dependence on azide concentration, with $K_{½}$ = 14 μM (± 2.3; $R^2 = 0.9935$).

2.4 Discussion

Correlating Results with Functional and Rotational States of the Enzyme—Hydrolysis by the three alternating catalytic sites of F_1 drives a full 360° rotation of the γ central rotary shaft, so hydrolysis of each ATP molecule involves a 120° rotation of γ relative to $\alpha_3\beta_3$. As depicted schematically in Fig. 2.9, SM microscopy studies of bacterial F_1-ATPases (reviewed in Refs. 62 and 63) have shown that each 120° rotation is comprised of two observable rotary substeps (*solid arrows*); MgATP binding at one alternating catalytic site drives an ~80° rotation of γ to the catalytic dwell angle, whereas the subsequent ~40° rotation is limited by the intrinsic rates of hydrolysis and Pi dissociation at the other alternating catalytic sites. At 120°, Mg^{2+} and ADP dissociate from one site before or in concert with binding of MgATP at another site to drive the next 80° substep. Fig. 2.9 also includes *bars* along the rotational arc that depict the observed angular position of γ (relative to $\alpha_3\beta_3$) in crystal structures of F_1 or F_1·**c**-ring complexes. This is based on alignment of structures by a structurally conserved, apparently stiff core of the γ subunit that we identified previously [8]. A recent analysis of MF_1 structures concluded that the position of γ could not be correlated with rotational angle during the catalytic cycle, arguing that the part of γ protruding below $\alpha_3\beta_3$ is variably displaced by lattice contacts in different crystals [64]. However, biophysical characterization of the stiffness of γ indicates that only the lowest portion of γ, near its interface with the **c**-ring of F_O, is extremely pliable [65]. Also, the 99 residues of γ that we identified as a structurally conserved "γ-core" include (i) most of the γ coiled-coil that is inside $\alpha_3\beta_3$, (ii) the first ~15 residues of the γ C-terminal helix that protrude below $\alpha_3\beta_3$, and (iii) 41 residues of the γ Rossmann fold domain that pack beside the protruding part of the γ C-terminal helix (see supplemental Figs. 4 and 5

Figure 2.9

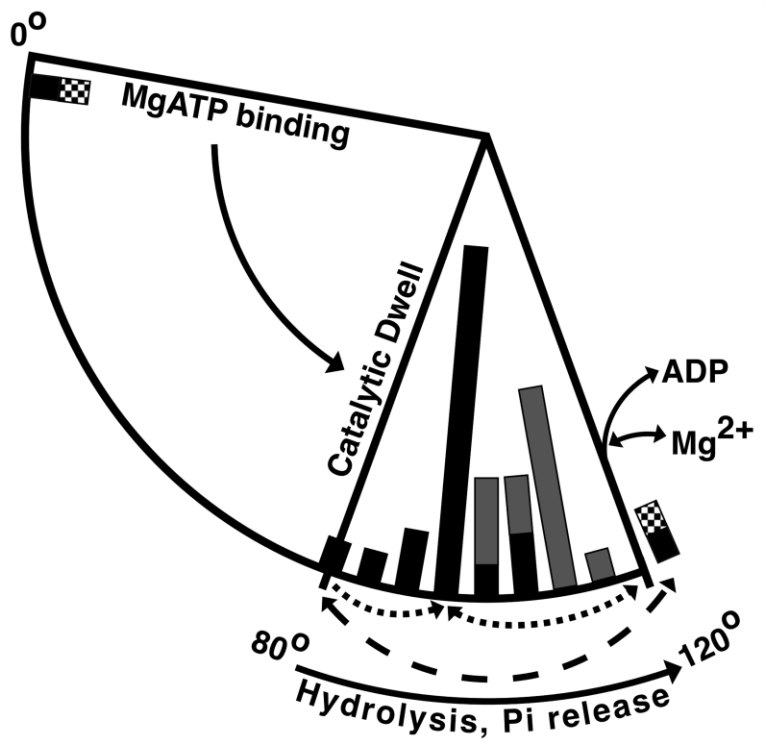
0°
MgATP binding
Catalytic Dwell
ADP
Mg2+
80°
120°
Hydrolysis, Pi release

Figure 2.9. Proposed paths for inhibition by εCTD or ADP/azide, relative to rotary catalytic sub-steps and estimated angular positions of γ in F_1 structures. A 120° segment is shown for γ's rotational cycle, corresponding to net hydrolysis of 1 ATP. Two rotary substeps, observed by SM microscopy, are depicted by *solid arrows* (direction is for γ's rotation during hydrolysis). *Bars* along the inner edge of the 80° to 120° *arc* indicate γ's approximate rotary angle in 34 F_1 crystal structures (see supplemental Table S-I). *Bars* are spaced every 5°, and the *height* represents the number of F_1 structures aligned near each angle (±2.5°); the *shortest bar*, one structure, *longest bar*, 12 structures. *Bars* are *shaded* for structures of bovine F_1 (*black*), yeast F_1 (*gray*) and *E. coli* F_1 (*checkered*). The *dotted arrows* below the *bars* indicate the proposed paths to and from the ADP-inhibited state, as stabilized by azide at ~95° [61]. The *dashed arrow* shows the ~40° rotary shift proposed to occur during transition into (*counterclockwise*) or out of (*clockwise*) the ε-inhibited state. The two F_1 aligned past 120° are also shown near 0°, as this position should be near the starting point for the next 120° turn.

of Ref. 8). We have updated our analysis of the rotational angle of γ to include 34 F_1 or F_1·**c**-ring structures and find that all γ subunits superimpose well with the γ-core (supplemental Table S-I). Thus, the distribution of F_1 structures along the rotary arc of γ in Fig. 2.9 should be useful for comparing structural states with functional and rotational data.

Although there is no current consensus for correlating the rotary position of γ in known structures with the dwell states observed in SM assays after 80 and 40° substeps [63, 66, 67], we assign γ to be at 80° for one MF_1 structure, with all three catalytic sites filled with nucleotide (Protein Data Bank entry 1H8E), because structural considerations [68] and molecular dynamics simulations [69] suggest that it is closest to the catalytic dwell state. Most MF_1 structures have no nucleotide in the β_E site due to an open conformation that distorts the nucleotide- binding pocket, but 1H8E has a "half-closed" conformation of β_E with bound MgADP and SO_4^{2-} (thought to mimic Pi binding). Another recent MF_1 structure (Protein Data Bank entry 4ASU) also has a nucleotide in all three catalytic sites, but its β_E is much closer to the open conformation and has ADP but no bound SO_4^{2-} (or Pi) or Mg^{2+} [64]. The 4ASU structure was proposed to represent the catalytic intermediate from which final products Mg^{2+} and ADP dissociate, and its rotary position at ~123° (Fig. 2.9) correlates with SM studies indicating that ADP dissociates after ~40° rotation to one of the 120° dwell positions [70–72]. The structural indication that Mg^{2+} dissociates before ADP [64] suggests that the inhibitory effect of free Mg^{2+} occurs at the 120° position. This can explain results showing that excess free Mg^{2+} does not affect inhibitory transitions that occur at the catalytic dwell step at 80°; free Mg^{2+} does not affect the rate at which actively rotating *E. coli* F_1(-ε) switches to the ADP-inhibited (paused) state [22], and, as shown here, free Mg^{2+} does not alter inhibition of *E. coli* F_1 by εCTD or azide.

Although our results indicate that ADP and ε inhibition begin as competing processes after hydrolysis at the catalytic dwell, F_1 structures of these inhibited states have γ positioned at angles that are distinct from the catalytic dwell; in Fig. 2.9, azide-inhibited MF_1 [61] has γ at 93°, and ε-inhibited *E. coli* F_1 [8] has γ rotated much further to 123° (*checkered bar*). In contrast, SM studies concluded that both ADP and ε inhibition cause long paused/inactive states at the catalytic dwell at 80° [22–24, 57]. With a bead attached to γ or ε, it is possible that SM microscopy could have overlooked dynamic oscillations between 80 and 120° because those assays can exhibit broad angular distributions of events. For example, during long paused periods (up to 1–2 s) without net rotation, a γ-attached bead on *E. coli* F_1 (-ε) showed rapid, ongoing angular fluctuations spanning at least ±30° (Fig. 2.3*A* in Ref. 22). This could represent dynamic rotational oscillations in *E. coli* F_1 or could be a technical limitation because the bead was attached to γ by a single cysteine, allowing for significant flexibility in the linkage. On the other hand, there is prior evidence that functional rotation is needed for transition to and from the ε-inhibited state; with *E. coli* F_OF_1 in liposomes, a chemical treatment that blocks rotation of F_O also prevented nucleotide-dependent changes in the conformation of ε [54]. With F_1 exposed to MgADP/Pi, conditions that stabilize the ε-inhibited state (Fig. 2.5), cryoelectron microscopy of *E. coli* F_1 showed a unique, ε-dependent position of γ and a unique position of ε relative to $\alpha_3\beta_3$ [73]. Also, with F_OF_1-liposomes, SM fluorescence assays showed a shift in the position of the εNTD relative to the F_O stator for active *versus* inactive complexes [74]. Thus, we propose that the εCTD begins inserting into bacterial F_1 near the catalytic dwell (80°) but then induces partial rotation to ~120° to achieve the final ε-inhibited state, with the last half of the εCTD buried in the central cavity of F_1 [8]. This is

similar to a proposal that insertion of the mitochondrial inhibitor protein (IF_1) into MF_1 involves rotational steps [75], and I F_1-inhibited MF_1 has γ rotated ~27° past the catalytic dwell in Fig. 2.9. The transitions of azide-inhibited MF_1 and ε-inhibited *E. coli* F_1 to distinct rotary angles may help explain the competition between these inhibitory paths. Azide-inhibited MF_1 has azide bound with MgADP in the closed, high affinity β_D site, but azide inhibition is unlikely to occur in the ε-inhibited state of *E. coli* F_1 because insertion of the εCTD and rotation of γ shift β_D to a distinct "half-closed" conformation. Conversely, if *E. coli* F_1 first shifted to the ADP-inhibited state, azide would probably stabilize the closed β_D state and so prevent opening of the $\alpha_E\beta_D$ interface with γ that is necessary to allow insertion of the εCTD. In Fig. 2.9, the *broken lines below* the *arc* indicate the proposed rotational paths leading to and from ADP- or ε-inhibited states. In SM tests of forced rotation, TF_1 was preferentially activated from the ADP-inhibited state (paused at ~93°; Fig. 2.9) by >40° rotation forward, and, consistent with proposed release of ADP near 120° (Fig. 2.9), added ADP suppressed or reversed rotational activation [76]. In contrast, forced rotation of up to 120° in either direction failed to reactivate ε-paused TF_1 [26]. Based on the asymmetric insertion of εCTD within F_1 [8], we suspect that reactivation from the ε_X-inhibited state (Fig. 2.9, near 120°) occurs with the lowest activation barrier by reverse rotation of γ/εNTD toward the catalytic dwell angle at 80° (Fig. 2.9, *dashed arrow*). Such reactivation by rotation in the direction of ATP synthesis may be indicated by a study with *E. coli* F_OF_1-liposomes; with MgADP and Pi present, prior exposure to proton motive force activated the initial rate of subsequent ATPase activity up to 9-fold [77].

Dynamics of ε Conformational Changes and the Influence of Nucleotides/Ligands— Under conditions for ATP hydrolysis, SM assays with a 60-nm gold bead attached to γ showed

that *E. coli* F_1 complexes switch back and forth between actively rotating and paused states every few seconds, with or without ε bound to F_1 [22]. Our results on F_1·ε dissociation kinetics are consistent with such rapid exchange between active and inactive states. As shown in Fig. 2.5 (*C* and *D*), there were no more than a few seconds lag in ligand-dependent switching between the slowest and fastest modes of F_1·ε dissociation. Exposure to saturating nucleotide without hydrolysis (ATP/EDTA or MgAMPPNP) induced the fastest and essentially monophasic F_1·ε dissociation (Figs. 2.5 and 2.6), indicating that few F_1·ε complexes remained in or could regain access to the ε_X-inhibited state. However, most F_1·ε complexes still dissociated slowly upon exposure to hydrolysis conditions (Fig. 2.5), consistent with noncompetitive inhibition by ε *versus* ATP for *E. coli* F_1 [29, 44]. Also, the K_I for ε inhibition of steady-state hydrolysis (Table 2.1, ~0.5 nM) is similar to the K_D for F_1·ε binding (Table 2.2, 0.24 nM), which was measured without added nucleotides. Thus, it is unlikely that catalytic binding of ATP or MgAMPPNP directly increases the rate at which the ε_X-paused state returns to an active form. Rather, we propose that the intrinsic rates to and from the ε_X-inhibited state are fast enough (seconds or less) to allow ligands to influence subsequent conformational changes once F_1 exits from the ε-inhibited state. Once the εCTD escapes from the central cavity of F_1 near 80°, F_1 would be most likely to rotate forward, completing an active 40° step (Fig. 2.9, *solid arrow*). At that point, binding of nucleotide would drive an ~80° step toward the next catalytic dwell but, without hydrolysis, would trap F_1 in a conformation and rotary position that would not allow the εCTD to reinsert; thus, F_1·ε complexes would dissociate at the faster rate observed with only γ/εNTD interactions. With hydrolysis conditions, each return to a catalytic dwell step would provide the same low probability for insertion of the εCTD, and, as indicated by SM

studies [22], the long durations of the paused/inhibited states (1 to 3.5 s) relative to the limiting catalytic steps (1–2 ms) would result in a large fraction of inhibited complexes during steady-state hydrolysis.

In an SM study with *E. coli* F_1 [22], the presence of ε did not alter the duration time of active complexes (0.5–1 s), but ε-paused states had longer duration times (up to 3.5 s) than ADP-paused states (~1 s). This is consistent with other indications that ε inhibition predominates over ADP inhibition. Oxyanions, which are thought to activate F_1 by promoting release of inhibitory ADP [78], activate *E. coli* F_1 more if ε is absent [28], and recently it was shown that the oxyanion selenite optimally activates ε-depleted *E. coli* F_1 ~10-fold[4] with excess free Mg^{2+} present but only activates ε-saturated F_1 2–2.5-fold [79]. Also, because our results show that inhibition by the εCTD is distinct from the ADP-inhibited transition, the unaffected duration of the active state [22] suggests that a prior common step is rate limiting for transitions to either ADP- or ε-inhibited states. This common step is probably the end of hydrolysis that precedes Pi release because ε reduces the rate of Pi release ~15-fold following "unisite" hydrolysis [28]. Pi stabilizes F_1 with ε in the ε_X state, which could mean that Pi rebinds to β_D (with bound MgADP) and delays an active 40° rotation, allowing more time for a possible transition to the ε_X-inhibited state. However, we cannot rule out that the Pi effect could be due in part to binding to other β(s), which show SO_4^{3-} bound at the "P-loop" in ε-inhibited F_1 [8].

Conclusions—This study sheds further light on how the CTD of subunit ε inhibits the catalytic F_1 complex of a bacterial ATP synthase. Most significantly, results reveal that ATP hydrolysis is required for insertion of the inhibitory εCTD into F_1 at the catalytic dwell step and that ε inhibition competes with conversion to an ADP-inhibited state of the

enzyme. With insertion of the εCTD starting at the catalytic dwell (~80°), the dynamic response of the conformation of ε to catalytic site ligands and the structurally observed ε angle of ~123° in ε-inhibited F_1 suggest dynamic, reversible rotation over the 40° substep. Our results also show that the εCTD has a small energetic contribution to net binding of ε to F_1. Thus, there is potential for antibiotic development by discovering or designing compounds that enhance or mimic ε inhibition of bacterial ATP synthases. The BLI assays established here for kinetics of F_1·ε binding and dissociation should be valuable in further analyzing which εCTD residues and interactions are critical for ε inhibition in F_1-ATPase from *E. coli* and other bacteria. Of course, the BLI assay cannot be used to study ε inhibition in membrane-bound ATP synthase because ε does not dissociate from intact F_OF_1. The extent of ε inhibition can vary widely for membranes isolated from different bacteria. For example, *E. coli* membranes exhibit substantial ATPase activity, whereas mycobacterial membranes are devoid of ATPase activity but can be activated by treatment that probably damages the ε subunit [80]. Thus, additional approaches will be needed to determine what other factors influence ε inhibition in ATP synthases of different bacterial species.

2.5 Experimental Methods

Plasmid Constructs for Affinity-tagged E. coli ε Subunit—A plasmid described previously [30] (noted here as $pH_6\varepsilon$) encodes a His_6-tagged ε (H_6-ε), with a tobacco etch virus protease cleavage site following the N-terminal His_6 tag. Site-directed mutagenesis was used to create the following mutations in H_6-ε. A pair of Cys mutations, εA101C/L121C, was created on $pH_6\varepsilon$ using the QuikChange Multi site-directed mutagenesis kit (Stratagene) with primers 5'-CATGGAAGCGA-AACGTAAGTGTGAAGAGCACATTAGGAG-3' (εA101C) and 5'-GCTCAGGCGTCTGCGG-AATGCGCCAAAGCGATC-3' (εL121C). H_6-ε that expresses only the εNTD (H_6-ε88stop; see Ref. 31) was created with the QuikChange-II XL kit (Stratagene) (forward primer, 5'-CAATTCGCGGCCAGTAAGTCGACGAAGCG-3'). Plasmid pBKH2 was created to add a biotin acceptor peptide (Bap) before the N-terminal His6 tag on H_6-ε. This BapH_6-ε has 49 residues before the native initial Met of ε, and tobacco etch virus cleavage would yield ε with three extra N-terminal residues (GAM). It was created with $pH_6\varepsilon$ as a template, using PCR to generate a 514-bp amplicon with restriction sites added before (XhoI) and after (BamHI) the gene for H_6-ε (primers, 5'-CGACTCGAGCATGTCGTACTA-CCATCACC-3' and 5'-CTCGGATCCTTACATCGCTTTTTTGGTCAAC-3'). Following cleavage with XhoI and BamHI, this amplicon was cloned into the same sites of pDW363 [32], replacing the *malE* gene, to create pBKH2. *BirA* (*E. coli* biotin holoenzyme synthetase) is co-expressed from pBKH2, allowing *in vivo* biotinylation of the biotin acceptor peptide on BapH_6-ε [32]. BapH_6-ε expressed with ε88stop or εA101C/L121C had poor protein yields, so ε was also expressed as a fusion protein following an N-terminal maltose-binding protein (MBP), a cleavage site for PreScission protease (GE Healthcare), and the Bap tag. This MBP-Bap-ε has a 31-residue segment between MBP and the initial Met of ε, and after

cleavage by PreScission protease, Bap-ε would retain a 25-residue N-terminal Bap tag. The vector for this construct, pMal-PPase, was derived from pMALc2e (New England Biolabs), with a PreScission protease cleavage sequence after *malE* [33], and an NdeI site was removed by cleavage and polymerase fill-in. The sequence encoding the Bap tag was PCR-amplified from pDW363, with flanking restriction sites before (StyI) and after (NdeI and BamHI) the Bap sequence (primers, 5'-CATCCCAAGGCTGGAGGCCTGAACGATATTTTC-3' and 5'-CTCGGATCCCATATGGCCACCAGTGTCCTCGTG-3'). After cleavage with StyI and BamHI, this amplicon was inserted into StyI-BamHI sites of pMal-PPase to generate pMAL-PP-Bap. The *atpC* gene for WTε was extracted from p3U [34] as a 625-bp NdeI-XbaI fragment and ligated into the same sites of pMAL-PP-Bap to create pBKH8, encoding a fusion protein of MBP-Bap-ε. Plasmids encoding MBP-Bap-ε with mutation ε88stop (pBKH9) or εA101C/L121C (pBKH10) were produced in the same way, but the NdeI-XbaI inserts were 799 bp (extra sequence downstream of *atpC*) because those mutant *atpC* genes had been passed through an intermediate vector.

Purification of Proteins—SDS-PAGE [35] (Bio-Rad Ready Gels, 12% or 4–15%) was used to analyze the purity of all protein preparations, with staining by SYPRO Orange (Invitrogen) and scanning on a Typhoon 9410 imager (GE Healthcare; 488-nm laser excitation, 526-nm SP emission filter). With gels to test for internal disulfide bonding in Bap-εA101C/L121C, concentrated gel sample buffer contained 0.5 mM *N*-ethylmaleimide instead of 2-mercaptoethanol (βME). Concentration of protein samples was determined by a modified Lowry assay [36]. *E. coli* F_OF_1 was expressed, and F_1 was purified and depleted of subunit δ to form F_1(-δ) as described [8]. F_1(-δ) was depleted of subunit ε by

immunoaffinity chromatography [37], using three passages of 5–7 mg of F_1-δ through an anti-ε column (3 ml). At this stage, upon dilution and passage through two sequential centrifuge columns, luciferase assays [8] showed that F_1(-δε) had the following endogenous nucleotide content (mol/mol F_1(-δε) ± S.E. from four different samples): noncatalytic sites, 0.89 ± 0.13 ATP and 0.83 ± 0.04 ADP; catalytic sites, 0.1 ± 0.08 ATP and 1.49 ± 0.17 ADP.

Wild-type and mutant forms of H_6-ε were expressed in *E. coli* BL21 strain "T7 Express lysY" (New England Biolabs). H_6-ε was purified by affinity chromatography (column with 10 ml of TALON resin; Clontech) as described [30] but with ε-buffer at pH 7.5 (20 mM Tris-HCl, 100 mM NaCl, pH 7.5). After loading, the column was washed with buffer + 10 mM imidazole (10 column volumes) and buffer + 15 mM imidazole (4 column volumes) before elution with buffer + 100 mM imidazole (4 column volumes). Residual impurities were removed from H_6-ε by gel filtration (HiPrep-16/60, Sephacryl S100 HR, GE Healthcare Life Sciences), and pure H_6-ε was exchanged into ε-buffer + 10% (v/v) glycerol before storage at -80 °C. For some experiments, the His_6 tag was removed by treatment with 25 units/ml AcTEVTM protease (Life Technologies) protease for 6 h. The sample was then loaded on the TALON column, and untagged ε was collected in the flow-through, concentrated, and frozen in ε-buffer+ 10% glycerol.

BapH_6-ε was expressed from pBKH2 in *E. coli* strain BL21. Cells were grown at 22 °C in a medium containing Luria broth, biotin (12.2 mg/liter), 4.5 M sorbitol, and 1 M betaine. Protein expression was induced by adding isopropyl 1-thio-β-D-galactopyranoside when the *A*595 reached 0.5. Cells were grown for 4 h after induction until the *A*595 reached ~1.0. BapH_6-ε was partially purified by TALON chromatography (as forH_6-ε).

Fractionation with ammonium sulfate was then used; $BapH_6$-ε that precipitated between 25 and 55% saturation was dissolved in ε-buffer + 10% glycerol. Finally, $BapH_6$-ε was purified by gel filtration (Sephadex G-50 column, 44 cm x 1-cm diameter), concentrated by ultrafiltration (Vivaspin 6 concentrator, 5000 molecular weight cutoff), frozen in liquid N_2, and stored at -80 °C.

To express biotinylated MBP-Bap-ε mutants, *E. coli* strain DH5α was co-transformed with pBirAcm (which expresses BirA; Avidity (Aurora, CO)) and either pBKH9 (MBP-Bap-ε88stop) or pBKH10 (MBP-Bap-εA101C/L121C). Each strain was grown overnight at 37 °C in LB with ampicillin (100 μg/ml) and chloramphenicol (25 μg/ml). Overnight cultures were used to inoculate 2 liters of the same medium plus 0.4% glucose and 0.1 mM biotin. Cells were grown at 37 °C to *A*595 ~0.5, 0.4 mM isopropyl 1-thio-β-D-galactopyranoside was added to induce expression of MBPBap-ε and BirA, and growth continued for ~3.5 h at 37 °C. Cells were harvested by centrifugation and washed once with column buffer (20 mM Tris-HCl, pH 7.5, 200 mM NaCl, 1 mM EDTA). Cells were lysed by sonication and centrifuged at 11,290 x *g* for 30 min, and the supernatant was passed through a 0.45-μm filter. This sample was mixed with 5 ml of amylose-agarose resin (New England Biolabs; pre-equilibrated with column buffer) and incubated at 4 °C, with rocking, for 2 h. The amylose resin was then sedimented (1000 x *g*, 3 min), the supernatant was discarded, and the resin was washed five times by centrifugation with 40 ml of column buffer + 5mM βME. For the εA101C/L121C mutant, 5mM βME was present throughout purification. The resin was incubated with 0.1 mg of PreScission Protease (4 °C, 3 h, in 15 ml of column buffer + 5mM βME) to release Bap-ε, which was collected in the supernatant and in a subsequent wash of the resin with 10 ml of column buffer + 5 mM

βME. Ultrafiltration (Vivaspin-20, 5000 molecular weight cut-off) was used to concentrate the Bap-ε from 25 to 1 ml and exchange it into ε buffer + 10% glycerol, including 1 mM βME for Bap-εA101C/L121C. Concentrated Bap-ε was frozen in liquid N_2 and stored at -80 °C. For some experiments, His_6- or Bap-tagged εA101C/L121C was treated with 5,5'-dithiobis(2-nitrobenzoate) (DTNB) to induce disulfide bonding between closely approaching cysteines [38]. The sample was first passed through a Biogel P6 centrifuge column [39] (pre-equilibrated with 20 mM MOPS-Tris, 50 mM KCl, pH 8 (MTK8)) to remove βME. Tagged εA101C/L121C (~30 μM) was then incubated with 50 μM DTNB for 15 min or less at room temperature and passed through a second centrifuge column to remove excess DTNB.

ATPase Assays—A coupled enzyme assay [40] was used for continuous monitoring of ATP hydrolysis, and assays were done at 30 °C. Decrease in NADH concentration was monitored at 340 nm in a Hewlett-Packard 8453 spectrophotometer. The standard assay buffer was MTK8 supplemented with 1 mM phosphoenolpyruvate and 0.3 mM NADH. MgATP substrate was added from stock solutions of Mg acetate and Na_2ATP; concentrations and ratios of Mg^{2+}/ATP are noted for specific experiments. Pyruvate kinase (rabbit muscle, Roche Applied Science catalog number 109045) and lactate dehydrogenase (Porcine heart, Calbiochem catalog number 427211) were each present at 0.1 mg/ml in assays with excess Mg^{2+} *versus* ATP; for assays with excess ATP *versus* Mg^{2+}, pyruvate kinase was 0.2 mg/ml. In some assays, hydrolysis of GTP was measured rather than ATP. For assays measuring inhibition by ε, BSA (fatty-acid free) was added at 0.5 mg/ml, EDTA was added to 0.1 mM, and F_1(-δε), ε, and ATP were added to final concentrations and preincubated at 30 °C for 10 min; the assay was initiated by adding magnesium acetate

from a concentrated stock and mixing. Hydrolysis rates were measured at steady state, typically 12–15 min after adding Mg^{2+}. For each data set varying ε concentration, a fixed concentration of F_1(-δε) was used (F_T = 0.6 or 1.2 nM), and hydrolysis rates were fit by nonlinear regression (Prism, GraphPad, Inc.) to the following equation,

$$A_i = A_0 - (A_0 - A_e)\left(\frac{K_I + \varepsilon_i + F_T - \sqrt{(K_I + \varepsilon_i + F_T)^2 - 4\cdot \varepsilon_i \cdot F_T}}{2\cdot F_T}\right) \qquad \text{(Eq. 1)}$$

where A_0 is the rate measured for F_1(-δε) alone, A_i is the rate measured at each ε concentration, ε_i, A_e is the rate fitted for ε-saturated F_1(-δε), and K_I is the apparent dissociation constant fitted for F_1·ε binding. For assays of inhibition by azide, magnesium acetate, ATP, sodium azide, and ε (if any) were added first, and the assay was initiated by adding F_1(-δε) from a concentrated stock; steady-state rates were measured as above.

Kinetic Assays of Binding and Dissociation between F_1(-δε) and Biotinylated ε, Using Biolayer Interferometry (BLI)—An Octet-RED system and streptavidin-coated sensors (Forte´Bio, SA biosensors, catalog number 18-5019) were used to monitor BLI kinetics of protein-protein binding and dissociation, analogous to surface plasmon resonance techniques [41]. MTK8 buffer included 0.5 mg/ml BSA to minimize nonspecific binding of proteins to the sensors and as carrier protein for nanomolar dilutions of F_1(-δε) or ε. All steps were done at 30 °C, with each sensor stirred in 0.2 ml of sample at 1000 rpm and a standard measurement rate of 5 s^{-1}. Wild-type or mutant forms of biotinylated ε ($BapH_6$-ε, or Bap-ε after cleavage from MBP-Bap-ε) were immobilized on SA biosensors. Levels of *in vivo* biotinylation varied between ε samples, so preliminary BLI titrations were done for each biotinylated ε to determine the Bap-ε concentration and loading time needed for

optimal BLI kinetic responses in subsequent binding of $F_1(-\delta\varepsilon)$ to the ε-loaded sensors. Minimal loading of ε was found to be favorable for kinetic responses to $F_1(-\delta\varepsilon)$ binding, so most subsequent experiments loaded biotinylated ε to yield 0.2–0.4 nm of BLI signal per sensor. Use of reference sensors with immobilized biotinylated ε but without added $F_1(-\delta\varepsilon)$ confirmed that added ligands (nucleotides, Mg^{2+}, EDTA, and azide) did not alter the BLI signal for immobilized ε. To correct for BLI baseline drift and minimal nonspecific binding of $F_1(-\delta\varepsilon)$ to sensors, all BLI experiments included one or more reference sensors in parallel for which biotinylated ε was omitted from the ε-loading step, but $F_1(-\delta\varepsilon)$ was included in the association step, usually at the highest concentration of $F_1(-\delta\varepsilon)$ used for each experiment. Forte´Bio's analysis software (version 6.4) was used for reference subtraction, Savitsky-Golay filtering, and global fitting of kinetic rates for $F_1{\cdot}\varepsilon$ binding and dissociation.

2.6 Acknowledgements and credits

We thank Y. M. Milgrom for stimulating discussions and for sharing unpublished results. We thank Profs. Richard L. Cross and Stephan Wilkens for critical reading of the manuscript. We thank Prof. Robert K. Nakamoto (University of Virginia) for plasmid pH$_6$ε. Plasmid constructs for biotinylated ε were created by Dr. Brian Haarer. Dr. Haarer also expressed and purified biotinylated WT ε and ε88stop. His-tagged ε versions were expressed and purified by Mr. Marcus Hutcheon. Inhibition assays with WT ε and His-tagged ε versions were carried out by Mr. Hutcheon (Data contributing to Fig. 2.2 and Table 2.1). All remaining experiments were done by Mr. Naman Shah.

Footnotes: [1] To whom correspondence should be addressed: Dept. of Biochemistry and Molecular Biology, SUNY Upstate Medical University, 750 E. Adams St. Syracuse, NY 13210. Tel.: 315-464-8711; Fax: 315-464-8750; E-mail: duncant@upstate.edu.

[2] The abbreviations used are: NTD, N-terminal domain; CTD, C-terminal domain; ε_C and ε_X, compact and extended conformations of ε (Fig. 1); BLI, biolayer interferometry; Bap, biotin acceptor peptide; βME, 2-mercaptoethanol; DTNB, 5,5'-dithiobis(2-nitrobenzoate); MF$_1$, mitochondrial F$_1$-ATPase; TF1, F1-ATPase of thermophilic *Bacillus* sp. *PS3*; SM, single-molecule; H$_6$-ε, His$_6$-tagged ε; MBP, maltose-binding protein; AMPPNP, 5'-adenylyl-β,γ-imidodiphosphate.

[3]The original study with εA101C/L121C (21) showed that an εA101C–L121C disulfide bond could be formed in membrane-bound F$_O$F$_1$ but did not appear to alter ATPase activity. We tested membranes expressing F$_O$F$_1$ with εA101C/L121C and showed that removing DTT from the sample activated

ATPase 2-fold; this is the same activation seen originally (21) after inducing a disulfide between the εCTD and εNTD (εM49C-A126C). We believe that their ATPase assays did

not include reductant for the nonoxidized sample of F_OF_1 + εA101C/L121C and that the disulfide formed quickly and spontaneously, as we have observed (Fig. 3). Thus, they would not have observed activation of ATPase by oxidation of εA101C–L121C if the disulfide had also formed in the non-oxidized sample.

[4]Y. M. Milgrom, personal communication.

2.7 References

1. Boyer, P. D. (1997) The ATP synthase. A splendid molecular machine. *Annu. Rev. Biochem*. 66, 717–749
2. Duncan, T. M. (2004) The ATP Synthase. Parts and Properties of a Rotary Motor. *The Enzymes*, Vol. XXIII, 3rd Ed. (Hackney, D. D., and Tamanoi, F., eds) pp. 203–275, Elsevier Academic Press, New York
3. Spetzler, D., Ishmukhametov, R., Hornung, T., Martin, J., York, J., Jin-Day, L., and Frasch, W. D. (2012) *Energy Transduction by the Two Molecular Motors of the F_OF_1 ATP Synthase* (Eaton-Rye, J. J., Tripathy, B. C., and Sharkey, T. D., eds) pp. 561–590, Springer, Dordrecht, Netherlands
4. Cox, G. B., Devenish, R. J., Gibson, F., Howitt, S. M., and Nagley, P. (1992) The structure and assembly of ATP synthase. *Molecular Mechanisms in Bioenergetics* (Ernster, L., ed) pp. 283–315, Elsevier Science, New York
5. Andries, K., Verhasselt, P., Guillemont, J., Go¨hlmann, H. W., Neefs, J. M., Winkler, H., Van Gestel, J., Timmerman, P., Zhu, M., Lee, E., Williams, P., de Chaffoy, D., Huitric, E., Hoffner, S., Cambau, E., Truffot-Pernot, C., Lounis, N., and Jarlier, V. (2005) A diarylquinoline drug active on the ATP synthase of *Mycobacterium tuberculosis*. *Science* 307, 223–227
6. Koul, A., Vranckx, L., Dendouga, N., Balemans, W., Van den Wyngaert, I., Vergauwen, K., Go¨hlmann, H. W., Willebrords, R., Poncelet, A., Guillemont, J., Bald, D., and Andries, K. (2008) Diarylquinolines are bactericidal for dormant mycobacteria as a result of disturbed ATP homeostasis. *J. Biol. Chem*. 283, 25273–25280

7. Diacon, A. H., Pym, A., Grobusch, M., Patientia, R., Rustomjee, R., Page- Shipp, L., Pistorius, C., Krause, R., Bogoshi, M., Churchyard, G., Venter, A., Allen, J., Palomino, J. C., De Marez, T., van Heeswijk, R. P., Lounis, N., Meyvisch, P., Verbeeck, J., Parys, W., de Beule, K., Andries, K., and McNeeley, D. F. (2009) The diarylquinoline TMC207 for multidrug-resistant tuberculosis. *N. Engl. J. Med.* 360, 2397–2405

8. Cingolani, G., and Duncan, T. M. (2011) Structure of the ATP synthase catalytic complex (F_1) from *Escherichia coli* in an autoinhibited conformation. *Nat. Struct. Mol. Biol.* 18, 701–707

9. Feniouk, B. A., Suzuki, T., and Yoshida, M. (2006) The role of subunit ε in the catalysis and regulation of F_OF_1-ATP synthase. *Biochim. Biophys. Acta* 1757, 326–338

10. Richter, M. L. (2004) γ-ε interactions regulate the chloroplast ATP synthase. *Photosynth. Res.* 79, 319–329

11. Campanella, M., Casswell, E., Chong, S., Farah, Z., Wieckowski, M. R., Abramov, A. Y., Tinker, A., and Duchen, M. R. (2008) Regulation of mitochondrial structure and function by the F_1F_O-ATPase inhibitor protein, IF_1. *Cell Metab.* 8, 13–25

12. Iino, R., Hasegawa, R., Tabata, K. V., and Noji, H. (2009) Mechanism of inhibition by C-terminal α-helices of the ε subunit of *Escherichia coli* F_OF_1-ATP synthase. *J. Biol. Chem.* 284, 17457–17464

13. Masaike, T., Suzuki, T., Tsunoda, S. P., Konno, H., and Yoshida, M. (2006) Probing conformations of the β subunit of F_OF_1-ATP synthase in catalysis. *Biochem. Biophys. Res. Commun.* 342, 800–807

14. Stocker, A., Keis, S., Vonck, J., Cook, G. M., and Dimroth, P. (2007) The Structural basis for unidirectional rotation of thermoalkaliphilic F_1- ATPase. *Structure* 15, 904–914

15. Gibbons, C., Montgomery, M. G., Leslie, A. G., and Walker, J. E. (2000) The structure of the central stalk in bovine F_1-ATPase at 2.4 Å resolution. *Nat. Struct. Biol.* 7, 1055–1061

16. Kabaleeswaran, V., Puri, N., Walker, J. E., Leslie, A. G., and Mueller, D. M. (2006) Novel features of the rotary catalytic mechanism revealed in the structure of yeast F_1 ATPase. *EMBO J.* 25, 5433–5442

17. Uhlin, U., Cox, G. B., and Guss, J. M. (1997) Crystal structure of the ε subunit of the proton-translocating ATP synthase from *Escherichia coli*. *Structure* 5, 1219–1230

18. Wilkens, S., and Capaldi, R. A. (1998) Solution structure of the ε subunit of the F_1-ATPase from *Escherichia coli* and interactions of this subunit with β subunits in the complex. *J. Biol. Chem*. 273, 26645–26651

19. Yagi, H., Kajiwara, N., Tanaka, H., Tsukihara, T., Kato-Yamada, Y., Yoshida, M., and Akutsu, H. (2007) Structures of the thermophilic F_1- ATPase ε subunit suggesting ATP-regulated arm motion of its C-terminal domain in F_1. *Proc. Natl. Acad. Sci. U.S.A.* 104, 11233–11238

20. Watt, I. N., Montgomery, M. G., Runswick, M. J., Leslie, A. G., and Walker, J. E. (2010) Bioenergetic cost of making an adenosine triphosphate molecule in animal mitochondria. *Proc. Natl. Acad. Sci. U.S.A.* 107, 16823–16827

21. Schulenberg, B., and Capaldi, R. A. (1999) The ε subunit of the F_1F_O complex of *Escherichia coli*. Cross-linking studies show the same structure *in situ* as when isolated. *J. Biol. Chem*. 274, 28351–28355

22. Sekiya, M., Hosokawa, H., Nakanishi-Matsui, M., Al-Shawi, M. K., Nakamoto, R. K., and Futai, M. (2010) Single molecule behavior of inhibited and active states of *Escherichia coli* ATP synthase F_1 rotation. *J. Biol. Chem*. 285, 42058–42067

23. Konno, H., Murakami-Fuse, T., Fujii, F., Koyama, F., Ueoka-Nakanishi, H., Pack, C. G., Kinjo, M., and Hisabori, T. (2006) The regulator of the F_1 motor. Inhibition of rotation of cyanobacterial F_1-ATPase by the ε subunit. *EMBO J*. 25, 4596–4604

24. Tsumuraya, M., Furuike, S., Adachi, K., Kinosita, K., Jr., and Yoshida, M. (2009) Effect of ε subunit on the rotation of thermophilic *Bacillus* F_1- ATPase. *FEBS Lett.* 583, 1121–1126

25. Konno, H., Isu, A., Kim, Y., Murakami-Fuse, T., Sugano, Y., and Hisabori, T. (2011) Characterization of the relationship between ADP- and ε-induced inhibition in cyanobacterial F_1-ATPase. *J. Biol. Chem*. 286, 13423–13429

26. Saita, E. I., Iino, R., Suzuki, T., Feniouk, B. A., Kinosita, K., Jr., and Yoshida, M. (2010) Activation and stiffness of the inhibited states of F_1-ATPase probed by single-molecule manipulation. *J. Biol. Chem*. 285, 11411–11417

27. Feniouk, B. A., Suzuki, T., and Yoshida, M. (2007) Regulatory interplay between proton motive force, ADP, phosphate, and subunit ε in bacterial ATP synthase. *J. Biol. Chem*. 282, 764–772

28. Dunn, S. D., Zadorozny, V. D., Tozer, R. G., and Orr, L. E. (1987) ε subunit of *Escherichia coli* F_1-ATPase. Effects on affinity for aurovertin and inhibition of product release in unisite ATP hydrolysis. *Biochemistry* 26, 4488–4493

29. Weber, J., Dunn, S. D., and Senior, A. E. (1999) Effect of the ε-subunit on nucleotide binding to *Escherichia coli* F_1-ATPase catalytic sites. *J. Biol. Chem.* 274, 19124–19128

30. Andrews, S. H., Peskova, Y. B., Polar, M. K., Herlihy, V. B., and Nakamoto, R. K. (2001) Conformation of the γ subunit at the γ-ε-c interface in the complete *Escherichia coli* F_1-ATPase complex by site-directed spin labeling. *Biochemistry* 40, 10664–10770

31. Cipriano, D. J., and Dunn, S. D. (2006) The role of the ε subunit in the *Escherichia coli* ATP synthase. The C-terminal domain is required for efficient energy coupling. *J. Biol. Chem.* 281, 501–507

32. Tsao, K.-L., DeBarbieri, B., Michel, H., and Waugh, D. S. (1996) A versatile plasmid expression vector for the production of biotinylated proteins by site-specific, enzymatic modification in *Escherichia coli*. *Gene* 169, 59–64

33. Bhardwaj, A., Walker-Kopp, N., Wilkens, S., and Cingolani, G. (2008) Foldon-guided self-assembly of ultra-stable protein fibers. *Protein Sci.* 17, 1475–1485

34. Duncan, T. M., Zhou, Y., Bulygin, V. V., Hutcheon, M. L., and Cross, R. L. (1995) Probing interactions of the *Escherichia coli* F_OF_1 ATP synthase β and γ subunits with disulphide cross-links. *Biochem. Soc. Trans.* 23, 736–741

35. Laemmli, U. K. (1970) Cleavage of structural proteins during the assembly of the head of bacteriophage T4. *Nature* 227, 680–685

36. Peterson, G. L. (1977) A simplification of the protein assay method of Lowry *et al.* which is more generally applicable. *Anal. Biochem*. 83, 346–356

37. Dunn, S. D. (1986) Removal of the ε subunit from *Escherichia coli* F_1- ATPase using monoclonal anti-ε antibody affinity chromatography. *Anal. Biochem*. 159, 35–42

38. Duncan, T. M., Bulygin, V. V., Zhou, Y., Hutcheon, M. L., and Cross, R. L. (1995) Rotation of subunits during catalysis by *Escherichia coli* F_1-ATPase. *Proc. Natl. Acad. Sci. U.S.A.* 92, 10964–10968

39. Penefsky, H. S. (1977) Reversible binding of Pi by beef heart mitochondrial adenosine triphosphatase. *J. Biol. Chem*. 252, 2891–2899

40. Pullman, M. E., Penefsky, H. S., Datta, A., and Racker, E. (1960) Partial resolution of the enzymes catalysing oxidative phosphorylation. I. Purification and properties of soluble dinitrophenyl-stimulated adenosine triphophatase. *J. Biol. Chem*. 235, 3322–3329

41. Abdiche, Y., Malashock, D., Pinkerton, A., and Pons, J. (2008) Determining kinetics and affinities of protein interactions using a parallel real-time label-free biosensor, the Octet. *Anal. Biochem*. 377, 209–217

42. Tozer, R. G., and Dunn, S. D. (1986) Column centrifugation generates an intersubunit disulfide bridge in *Escherichia coli* F_1-ATPase. *Eur. J. Biochem*. 161, 513–518

43. Dunn, S. D. (1982) The isolated γ subunit of *Escherichia coli* F_1 ATPase binds the ε subunit. *J. Biol. Chem*. 257, 7354–7359

44. Sternweis, P. C., and Smith, J. B. (1980) Characterization of the inhibitory ε subunit of the proton-translocating adenosine triphosphatase from *Escherichia coli*. *Biochemistry* 19, 526–531

45. Hyndman, D. J., Milgrom, Y. M., Bramhall, E. A., and Cross, R. L. (1994) Nucleotide-binding sites on *Escherichia coli* F_1-ATPase. Specificity of noncatalytic sites and inhibition at catalytic sites by MgADP. *J. Biol. Chem*. 269, 28871–28877

46. Kato, Y., Sasayama, T., Muneyuki, E., and Yoshida, M. (1995) Analysis of time-dependent change of *Escherichia coli* F_1-ATPase activity and its relationship with apparent negative cooperativity. *Biochim. Biophys. Acta* 1231, 275–281

47. Jault, J. M., Matsui, T., Jault, F. M., Kaibara, C., Muneyuki, E., Yoshida, M., Kagawa, Y., and Allison, W. S. (1995) The $\alpha 3\beta 3\gamma$ complex of the F_1- ATPase from thermophilic *Bacillus PS3* containing the αD261N substitution fails to dissociate inhibitory MgADP from a catalytic site when ATP binds to noncatalytic sites. *Biochemistry* 34, 16412–16418

48. Drobinskaya, I. Y., Kozlov, I. A., Murataliev, M. B., and Vulfson, E. N. (1985) Tightly bound adenosine diphosphate, which inhibits the activity of mitochondrial F_1-ATPase, is located at the catalytic site of the enzyme. *FEBS Lett*. 182, 419–424

49. Milgrom, Y. M., and Boyer, P. D. (1990) The ADP that binds tightly to nucleotide-depleted mitochondrial F_1-ATPase and inhibits catalysis is bound at a catalytic site. *Biochim. Biophys. Acta* 1020, 43–48

50. Murataliev, M. B., Milgrom, Y. M., and Boyer, P. D. (1991) Characteristics of the combination of inhibitory Mg^{2+} and azide with the F_1 ATPase from chloroplasts. *Biochemistry* 30, 8305–8310

51. Guerrero, K. J., Xue, Z. X., and Boyer, P. D. (1990) Active/Inactive state transitions of the chloroplast F_1 ATPase are induced by a slow binding and release of Mg^{2+}. Relationship to catalysis and control of F_1 ATPases. *J. Biol. Chem*. 265, 16280–16287

52. Jault, J. M., Divita, G., Allison, W. S., and Di Pietro, A. (1993) Glutamine 170 to tyrosine substitution in yeast mitochondrial F_1 β-subunit increases catalytic site interaction with GDP and IDP and produces negative cooperativity of GTP and ITP hydrolysis. *J. Biol. Chem*. 268, 20762–20767

53. Xiong, H., Zhang, D., and Vik, S. B. (1998) Subunit ε of the *Escherichia coli* ATP synthase. Novel insights into structure and function by analysis of thirteen mutant forms. *Biochemistry* 37, 16423–16429

54. Mendel-Hartvig, J., and Capaldi, R. A. (1991) Nucleotide-dependent and dicyclohexylcarbodiimide-sensitive conformational changes in the ε subunit of *Escherichia coli* ATP synthase. *Biochemistry* 30, 10987–10991

55. Mendel-Hartvig, J., and Capaldi, R. A. (1991) Catalytic site nucleotide and inorganic phosphate dependence of the conformation of the δ subunit in *Escherichia coli* adenosinetriphosphatase. *Biochemistry* 30, 1278–1284

56. Dallmann, H. G., Flynn, T. G., and Dunn, S. D. (1992) Determination of the 1-ethyl-3-[(3-dimethylamino)propyl]-carbodiimide-induced cross-link between the β and ε subunits of *Escherichia coli* F_1-ATPase. *J. Biol. Chem*. 267, 18953–18960

57. Hirono-Hara, Y., Noji, H., Nishiura, M., Muneyuki, E., Hara, K. Y., Yasuda, R., Kinosita, K., Jr., and Yoshida, M. (2001) Pause and rotation of F_1- ATPase during catalysis. *Proc. Natl. Acad. Sci. U.S.A.* 98, 13649–13654

58. Nakanishi-Matsui, M., Kashiwagi, S., Ubukata, T., Iwamoto-Kihara, A., Wada, Y., and Futai, M. (2007) Rotational catalysis of *Escherichia coli* ATP synthase F_1 sector. Stochastic fluctuation and a key domain of the β subunit. *J. Biol. Chem.* 282, 20698–20704

59. Vasilyeva, E. A., Minkov, I. B., Fitin, A. F., and Vinogradov, A. D. (1982) Kinetic mechanism of mitochondrial adenosine triphosphatase. Inhibition by azide and activation by sulphite. *Biochem. J.* 202, 15–23

60. Murataliev, M. B., and Boyer, P. D. (1992) The mechanism of stimulation of MgATPase activity of chloroplast F_1-ATPase by non-catalytic adeninenucleotide binding. Acceleration of the ATP-dependent release of inhibitory ADP from a catalytic site. *Eur. J. Biochem.* 209, 681–687

61. Bowler, M. W., Montgomery, M. G., Leslie, A. G., and Walker, J. E. (2006) How azide inhibits ATP hydrolysis by the F-ATPases. *Proc. Natl. Acad. Sci. U.S.A.* 103, 8646–8649

62. Noji, H., Okuno, D., and Ikeda, T. (2011) Mechanochemistry of F_1 motor protein. *Chem. Sci.* 2, 2086–2093

63. Kinosita, K., Jr. (2012) F_1-ATPase. A prototypical rotary molecular motor. *Adv. Exp. Med. Biol.* 726, 5–16

64. Rees, D. M., Montgomery, M. G., Leslie, A. G., and Walker, J. E. (2012) Structural evidence of a new catalytic intermediate in the pathway of ATP hydrolysis by F_1-

ATPase from bovine heart mitochondria. *Proc. Natl. Acad. Sci. U.S.A.* 109, 11139–11143

65. Sielaff, H., Rennekamp, H., Wa¨chter, A., Xie, H., Hilbers, F., Feldbauer, K., Dunn, S. D., Engelbrecht, S., and Junge, W. (2008) Domain compliance and elastic power transmission in rotary F_O F_1-ATPase. *Proc. Natl. Acad. Sci. U.S.A.* 105, 17760–17765

66. Okuno, D., Fujisawa, R., Iino, R., Hirono-Hara, Y., Imamura, H., and Noji, H. (2008) Correlation between the conformational states of F_1-ATPase as determined from its crystal structure and single-molecule rotation. *Proc. Natl. Acad. Sci. U.S.A.* 105, 20722–20727

67. Sielaff, H., Rennekamp, H., Engelbrecht, S., and Junge, W. (2008) Functional halt positions of rotary F_OF_1-ATPase correlated with crystal structures. *Biophys. J.* 95, 4979–4987

68. Menz, R. I., Walker, J. E., and Leslie, A. G. (2001) Structure of bovine mitochondrial F_1-ATPase with nucleotide bound to all three catalytic sites. Implications for the mechanism of rotary catalysis. *Cell* 106, 331–341

69. Pu, J., and Karplus, M. (2008) How subunit coupling produces the γ-subunit rotary motion in F_1-ATPase. *Proc. Natl. Acad. Sci. U.S.A.* 105, 1192–1197

70. Nishizaka, T., Oiwa, K., Noji, H., Kimura, S., Muneyuki, E., Yoshida, M., and Kinosita, K., Jr. (2004) Chemomechanical coupling in F_1-ATPase revealed by simultaneous observation of nucleotide kinetics and rotation. *Nat. Struct. Mol. Biol.* 11, 142–148

71. Adachi, K., Oiwa, K., Nishizaka, T., Furuike, S., Noji, H., Itoh, H., Yoshida, M., and Kinosita, K., Jr. (2007) Coupling of rotation and catalysis in F_1- ATPase revealed by single-molecule imaging and manipulation. *Cell* 130, 309–321

72. Shimo-Kon, R., Muneyuki, E., Sakai, H., Adachi, K., Yoshida, M., and Kinosita, K., Jr. (2010) Chemo-mechanical coupling in F_1-ATPase revealed by catalytic site occupancy during catalysis. *Biophys. J.* 98, 1227–1236

73. Wilkens, S., and Capaldi, R. A. (1994) Asymmetry and structural changes in EC F_1 examined by cryoelectronmicroscopy. *Biol. Chem. Hoppe-Seyler* 375, 43–51

74. Zimmermann, B., Diez, M., Zarrabi, N., Graber, P., and Borsch, M. (2005) Movements of the ε-subunit during catalysis and activation in single membrane-bound H^+-ATP synthase. *EMBO J.* 24, 2053–2063

75. Gledhill, J. R., Montgomery, M. G., Leslie, A. G., and Walker, J. E. (2007) How the regulatory protein, IF_1, inhibits F_1-ATPase from bovine mitochondria. *Proc. Natl. Acad. Sci. U.S.A.* 104, 15671–15676

76. Hirono-Hara, Y., Ishizuka, K., Kinosita, K., Jr., Yoshida, M., and Noji, H. (2005) Activation of pausing F_1 motor by external force. *Proc. Natl. Acad. Sci. U.S.A.* 102, 4288–4293

77. Fischer, S., Graber, P., and Turina, P. (2000) The activity of the ATP synthase from *Escherichia coli* is regulated by the transmembrane proton motive force. *J. Biol. Chem*. 275, 30157–30162

78. Milgrom, Y. M., and Cross, R. L. (1993) Nucleotide binding sites on beef heart mitochondrial F_1-ATPase. Cooperative interactions between sites and specificity of noncatalytic sites. *J. Biol. Chem*. 268, 23179–23185

79. Bulygin, V. V., and Milgrom, Y. M. (2009) A bi-site mechanism for *Escherichia coli* F_1-ATPase accounts for the observed positive catalytic cooperativity. *Biochim. Biophys. Acta* 1787, 1016–1023

80. Haagsma, A. C., Driessen, N. N., Hahn, M. M., Lill, H., and Bald, D. (2010) ATP synthase in slow- and fast-growing mycobacteria is active in ATP synthesis and blocked in ATP hydrolysis direction. *FEMS Microbiol. Lett*. 313, 68–74

81. Pettersen, E. F., Goddard, T. D., Huang, C. C., Couch, G. S., Greenblatt, D. M., Meng, E. C., and Ferrin, T. E. (2004) UCSF Chimera.Avisualization system for exploratory research and analysis. *J. Comput. Chem*. 25, 1605–1612

2.8 Supplementary Data

Figures and Tables

Figure S2.1

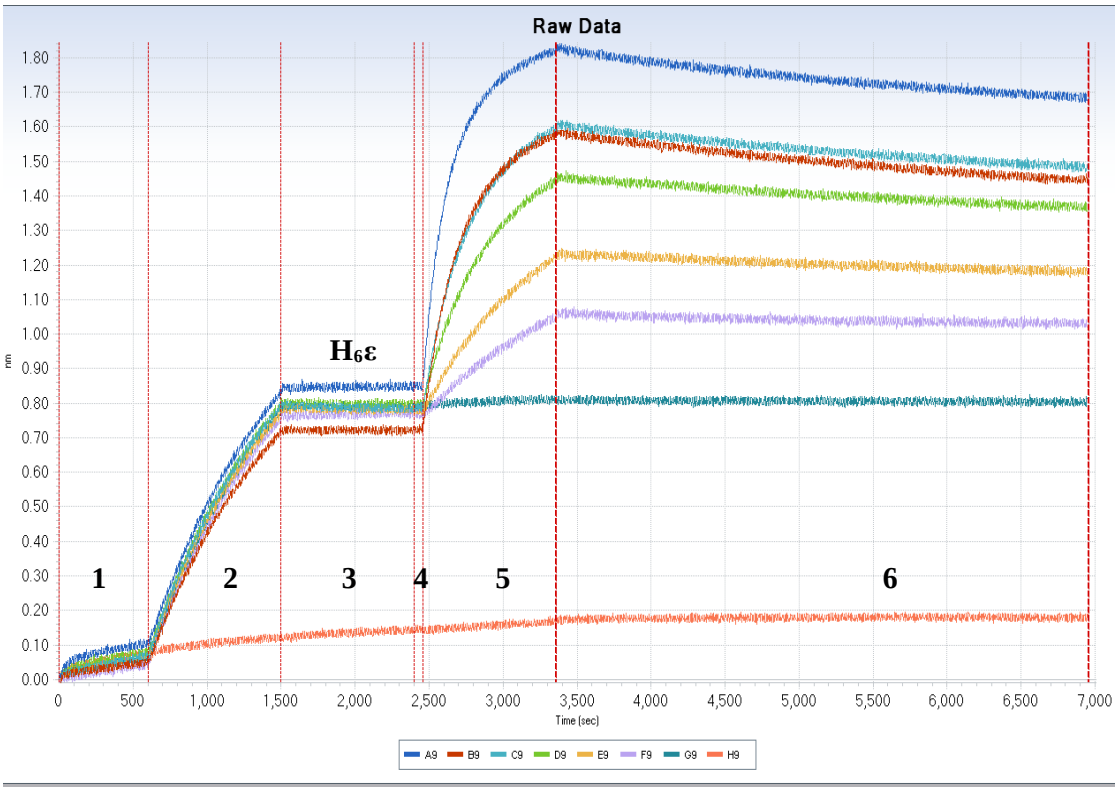

Figure S2.1. Example of raw BLI data showing immobilization of biotinylated ε on sensors and subsequent binding and dissociation of F_1 (-δε). Screen-capture image from a typical BLI experiment on the Octet-RED. A set of 8 streptavidin-coated sensors were pre-wet with buffer (MTK8 + 0.5 mg BSA/ml) in wells of a 96-well micro titer plate. All steps used 0.2 ml sample per well. Each vertical red line denotes the start of a distinct step in which the sensors were shifted to the next row of wells. Steps 1, 3 and 4 = baseline (buffer only); step 2 = 50 nM Bap-ε used to load the sensors; step 5 = F_1/ε association, with varied concentrations of F_1(-δε) (listed by right axis); step 6 = F_1/ε dissociation (buffer only). After F_1/ε association (step 5), step 6 returned sensors to the row of buffer wells used in step 4, which aided in signal corrections for optical variations between wells.

Table S2.1

PDB code	# γ-core residues	RMSD (Cα, Å)	Rotary Angle (deg)
1H8E	99	0.81	80.0
1E79	99	0.65	85.9
2XND	99	0.78	88.3
2JDI	99	[ref]	92.1
1W0J	99	0.62	93.0
2CK3	99	0.36	93.0
1E1Q	68	0.68	93.7
1H8H	68	0.65	94.2
1COW	68	0.65	94.2
1BMF	68	0.62	94.3
1E1R	68	0.62	94.5
2JIZ	99	0.61	95.0
1W0K	68	0.73	95.2
2JJ1	90	0.57	95.2
1EFR	68	0.62	96.6
2JJ2	99	0.63	96.6
1NBM	68	0.64	99.1
3OEH-2	99	0.92	100.5
3OEE-2	99	0.96	102.0
2HLD-2	99	0.99	102.2
3OE7-2	99	0.91	103.1
2WSS	96	0.84	104.0
2V7Q	99	0.74	106.8
3FKS	99	1.10	107.5
3OEH-1	99	0.90	108.7
3OFN-1	99	0.96	108.8
2HLD-1	99	0.97	109.2
3OE7-1	99	0.89	109.7
3OFN-2	99	0.97	111.2
2XOK	99	0.96	111.6
3OEE-1	99	0.88	111.9
2WPD	95/99	0.97/1.04	113.0/112.6
3OAA	99	1.11	123.3
4ASU	95/99	0.83/0.96	123.7/123.0

Table S2.1: Rotational position of γ within F_1 or F_1/c-ring crystal structures. The 8 PDB codes in bold were part of the original γ structural alignment used to identify the 99 conserved γ-core residues (Cingolani & Duncan, 2011, Nat. Struc. Mol. Biol. 18, 701-707). For all other F_1 structures, the γ-core residues were superimposed (Cα atoms) to the corresponding residues in the 2JDI 'ground state' structure of mitochondrial F_1, and column 2 lists the number of γ residues superimposed. Note that 8 structures have only 68 residues superimposed and 2 other structures have only 90 or 96, since other γ-core residues were not resolved. Even the structures with only 68 aligned γ-core residues had 1 aligned segment (9-10 residues) that was not in the coiled-coil domain. For 2WPD and 4ASU, it was noted that the first 4 γ-core residues, near the start of the N-terminal helix, showed poor superimposition to the reference; both were analyzed ± those 4 residues as shown, but the change in rotary angle was minimal. Relative to the surrounding α3β3 complex, the rotary position of γ is thought to be closest to the catalytic dwell for structure 1H8E, so its rotary angle was designated as 80°. For other structures, the rotary angle relative to 1H8E was measured by rotating the structure from its γ-core alignment with 2JDI to the best alignment of one of its β subunits with the equivalent chain in 1H8E (using Chimera's MatchMaker). This was done for each of the 3 equivalent β chains superimposed to the same chain of 1H8E (i.e., chain D to D, E to E, or F to F), and the rotary angle reported is the mean value; all mean angles have standard deviations <2°. The optimal superimposition of many βs spanned the whole β sequence, but always included most residues of the N-terminal domain and the upper region of the nucleotide-binding domain. For all mitochondrial structures, a minimum of 57% β sequence superimposed (Cα), with RMSD typically <0.6 Å. For E. coli F_1 (3OAA), optimal superimposition of each β with the

equivalent chain of 1H8E included the following %residues (RMSD): chain D = 44% (1.0 Å); E = 57% (0.9 Å); F = 83% (0.9 Å). The three measurements agreed well, as the mean angle measured for 3OAA had a standard deviation of ±1.1°.

Chapter Three

Aerobic Growth of *Escherichia coli* is Reduced and *In vitro* ATP Synthesis is Selectively Inhibited by Deleting Five C-terminal residues from the ATP Synthase's ε Subunit.

Naman B. Shah and Thomas M. Duncan

Department of Biochemistry and Molecular Biology, State University of New York Upstate Medical University, 750 East Adams Street, Syracuse, New York 13210

3.1 Abstract

The F-type ATP synthase is a rotary nanomotor involved in cellular energy metabolism in eukaryotes and eubacteria. In most bacteria, the ATP synthase can be auto-inhibited by the C-terminal domain of its ε subunit (εCTD), but the importance of ε inhibition *in vivo* is unclear. Functional rotation is blocked by insertion of the latter half of the εCTD into the enzyme's central cavity. The εCTD's final segment is deeply buried but has few specific interactions with other subunits in the *Escherichia coli* enzyme, and is variable or absent in other bacteria that exhibit strong ε-inhibition *in vitro*. Here, respiratory growth was reduced ~60% by genetically deleting the last 5 residues of the εCTD (εΔ5) but only by ~20% in the complete absence of the εCTD. With isolated membranes, neither εΔ5 nor ε88stop truncations led to a significant proton leak through F_O. However, ATP synthase lacking the εCTD was highly active in hydrolysis and synthesis of ATP, but the εΔ5 truncation differentially increased ε's inhibition of ATP synthesis nearly 3-fold *vs* hydrolysis. Further, the εΔ5 truncation had little effect on ε's affinity for the isolated catalytic F_1 complex, but reduced ε's maximal inhibition of F_1-ATPase from >90% to ~20%. The results suggest that the εCTD may have distinct regulatory interactions with F_1 when rotary catalysis operates in opposite directions for hydrolysis *vs* synthesis of ATP.

3.2 Introduction

The F-type ATP synthase is critical for efficient energy metabolism in eukaryotes and eubacteria. It is a self-contained rotary motor enzyme that is composed of a membrane–embedded F_O complex (ab_2c_{8-15}) and an external F_1 complex ($\alpha_3\beta_3\gamma\delta\varepsilon$) [1, 2]. The structural assembly of subunits in F_1 includes a hexamer of alternating α and β subunits that surround the central rotor stalk region of the asymmetric γ subunit. The ε subunit is near the foot of γ with its N-terminal domain in contact with both the γ subunit and the c-ring. A peripheral stator stalk between F_1 and F_O is formed by F_1 subunit δ along with the b_2 dimer of F_O. In addition to subunit a and dimer b_2, the F_O domain contains a ring of c subunits that rotates in tandem with the γε stalk. For ATP synthesis, Proton Motive Force generated by the electron transport chain drives the rotation of the c-ring which is coupled with the rotation of γ within F_1. Rotation of the asymmetric γ subunit helps drive conformational changes in α and β subunits that are crucial for cooperative, alternating catalysis at the three catalytic nucleotide binding sites located mainly on the β subunits. *In vitro*, F_1 can dissociate from F_O as a soluble, rotary ATPase.

ATP synthases can also rotate in the reverse direction by hydrolyzing ATP to generate PMF under certain conditions. In mitochondria, this ATPase–driven proton pumping can be blocked by a mitochondria-specific inhibitor protein called IF_1 [3, 4]. In contrast, most bacterial ATP synthases can be auto-inhibited by the C-terminal domain (CTD) of the ε subunit [2, 5]. The CTD of ε can transition between at least two observed states: a compact conformation (ε_C) that allows coupled functions [6] and an extended conformation (ε_X) that inhibits synthesis and hydrolysis of ATP [7, 8]. In the ε_C state, the two α-helices of the εCTD form a hairpin coiled-coil that packs against the εNTD, as observed with isolated ε

from 2 species [9, 10] and in 1 bacterial F_1 structure [11]. In mitochondrial F_1 structures, the ε homolog is locked in the ε_C conformation by a unique mitochondrial subunit [12]. Thus far, the ε_X state has only been observed in the crystal structure of *E. coli* F_1 [13], in which the latter half of the εCTD inserts into the central cavity of F_1 and has extensive contacts with other subunits. The second α-helix of the ε_X state (ε112-125) contacts five other subunits, with apparent H-bonds and/or salt bridges to α1, α2, β1 and γ subunits. The terminal segment of εCTD (ε126-138) was called the εhook in the ε_X state, as it bends around γ and contacts the CTD of another catalytic subunit, β3. The ε-hook buries extensive surface area within F_1 but has minimal specific interactions, with perhaps one H-bond (εI131 amide to β3-D372 sidechain). The final C-terminal segment of ε varies significantly in sequence and length between diverse bacterial species [5]. High-resolution structures have been determined for bacterial ε from two other species, *Bacillus PS3* [10] and *Caldalkalibacillus thermarum* TA2.A1 [11]; both superimpose well with the ε_C conformation of *E. coli* ε, but are shorter at the C-terminus by 4 and 3 residues, respectively. Despite this, activity of each ATP synthase can be strongly inhibited by the shorter εCTD [7, 14, 15]. Thus, we postulated that the final segment of the ε-hook might be dispensable or even destabilizing for inhibition by the εCTD. Inhibition by ε is not essential for respiratory growth of *E. coli*, as significant growth on a non-fermentable carbon source can be achieved with the entire εCTD genetically truncated [16, 17]. Interestingly, however, an early mutagenic study with *E. coli* found that combined deletion of 4 C-terminal and 15 N-terminal residues disrupted oxidative phosphorylation, but the N- and C-terminal truncations were not tested separately [18] . In this study, we genetically deleted just the final five amino acids of εCTD (ε134-138) to generate an *E. coli* εΔ5

mutant. Growth on a non-fermentable carbon source was reduced ~60% by εΔ5, whereas complete deletion of the εCTD (ε88stop) reduced growth by ~20%. With isolated membranes, εΔ5 reduced the ATP synthesis rate by >2.7-fold, but did not alter ε's inhibition of ATPase activity. Since a new class of effective antibacterial agents have been found to target the ATP synthase [19], our results show that regulation by the εCTD provides a bacteria-specific target for future development of antibacterials against the ATP synthase.

3.3 Experimental Methods

Plasmids and mutagenesis.

Plasmid p3DC [20], which encodes subunits β and ε, was used as template to truncate the terminal five amino acids of εCTD via site-directed mutagenesis [21]. Primer 5'-CAGCTGCGCGTTATCGAG-TTG**TAATAA**AAAGCGATGTAACACCGGC-3' (mutations underlined) was used to replace codons for εT134/K135 with two ochre stop codons (bold). DNA sequencing (Upstate Medical University's core facility) was used to confirm that only the desired mutations were created. DNA encoding ε with the stop codons (εΔ5) was extracted in a *NdeI-XbaI* restriction fragment and used to replace the corresponding fragment of pAU1 [20] to obtain pAU1εΔ5. The *NdeI-XbaI* fragment was also used to move εΔ5 into pBKH8 [22], creating pBKH8εΔ5. The ε88stop truncation was also moved in a *NdeI-XbaI* fragment from pBKH9 [22] into pAU1. Mutation βM209L was originally a gift from A.E. Senior [23] and was transferred to pAU1 in a *SacI-EagI* fragment.

Phenotypic assay for respiratory growth.

F_OF_1, either WT or with the mutants noted (Fig. 3.1, Table 3.1), was expressed from the *atp* operon on low-copy plasmid pAU1. For most phenotypic growth tests, pAU1 constructs were transformed into strain LE392Δ(*atpI-C*) [24]. Individual bacterial colonies were inoculated into 10 ml Luria Bertani broth (LB; Lennox type, Sigma Aldrich) + ampicillin (0.1 mg/ml), and grown overnight at 37°C, with shaking at 200 rpm in a 125 ml Erlenmeyer flask. Cells were then diluted into 10 ml of fresh LB + ampicillin to obtain an optical density (OD, 600 nm) of 0.1. When growth reached OD ~0.8, cells were diluted 100-fold into defined minimal salts medium [25] including 1 mM $MgSO_4$, 0.1% v/v trace

elements [25], 0.06% cas-amino acids (BD Difco), 6 μM thiamine, 0.1 mg/ml ampicillin, 50 μg/ml methionine, and 30 mM succinate as the non-fermentable carbon source. Growth at 37°C was measured with 0.4 ml of culture per well in a 48-well transparent microtiter plate with lid (Nunc), with triplicate samples for each distinct pAU1 construct. Growth was monitored every 15 min by optical density (600 nm), using a plate reader (Biotek Synergy HT or TECAN Infinite F200). Plates were shaken at 88.6 rpm (TECAN) or at "slow" setting (Biotek) for 20 to 30 hours. Some assays were repeated with the same plasmids in a distinct *atp*-deletion strain, DK8 [26], so the defined growth medium included 0.3 mM isoleucine and valine and omitted methionine. The DK8 strain showed less stringent differences in growth between WT and negative controls in initial tests. For more consistent performance, defined medium for DK8 had reduced cas-amino acids (0.03%) and succinate (6 mM). Also, to reduce carry-over of LB, DK8 cells from overnight cultures were sedimented and resuspended with defined medium before final dilution into defined medium for the assay.

Isolation of inverted membrane vesicles. Strain LE392Δ(*atpI-C)* containing pAU1 (WT or ε mutants) was inoculated from individual colonies into 10 ml LB + ampicillin (0.1 mg/ml) and grown overnight in a 125 ml Erlenmeyer flask at 37°C with shaking (200 rpm). Cells were then diluted into 2 L of defined minimal salts medium [25] to obtain a starting OD_{600} of ~0.05. Additions were as noted earlier except that, rather than succinate, 30 mM Glucose and 1% Glycerol were the carbon sources. The cells were grown at 37ºC with constant aeration and were harvested during logarithmic growth phase. Inverted membrane vesicles (IMV) were prepared as described before [27].

Expression and purification of proteins

WT-F_OF_1 was expressed, purified, and depleted of subunits δ and ε as before [22, 28]. For expression of biotinylated ε as an MBP-Bap-ε fusion protein, pBKH8 (WT or εΔ5) was transformed into strain DH5α [29]. Biotinylated ε (Bap-ε WT or Bap-εΔ5) was purified as before [22]. Concentrations and purity of proteins were determined by a modified Lowry assay [30] and SDS-PAGE [31].

Detection of F_OF_1 content in membrane vesicles by immunoblotting

IMVs and known amounts of purified F_1 were subjected to SDS-PAGE [31] on pre-cast 4-20% gradient polyacrylamide gels (Bio-Rad), at 200 V for 33 minutes. Proteins on the gel were then transferred to a polyvinylidene difluoride membrane (Invitrogen) in a Bio-Rad Mini Trans-Blot cell at 200 mA for 1 hour using 1X electrophoresis buffer + 10% (v/v) methanol. The blotted membrane surface was blocked with TBST (TBS, 10 mM Tris-Cl, 150 mM NaCl, pH 8, 0.05% Tween-20) + 5% (w/v) non-fat dried milk, and then washed 3 x 5 minutes with TBST + 0.3 M NaCl. The membrane was then incubated for one hour with the primary rabbit anti-β antibody (1:200) in TBST + 10 mg/ml bovine serum albumin; this anti-β antibody (Agrisera, # AS05-85) was previously tested for this purpose with *E. coli* membranes [32]. Membrane washes with TBST + 0.3 M NaCl were repeated, followed by one hour incubation with a fluorescent goat anti-rabbit secondary antibody (1:1000) (Thermo Scientific, #35553). The blot was air dried and fluorescence was detected on a Typhoon 9410 imager (GE Healthcare Life Sciences) with a 532 nm laser and 526 nm short-pass filter. Signals for β from known amounts of F_1 provided a linear response range that was used to quantify the amount of β in different membrane samples.

ATP hydrolysis

ATP hydrolysis rates were measured with a coupled enzymes assay [33] as described [22]. Reactions were done at 30°C. Assays with IMVs contained 5 mM KCN to inhibit NADH consumption by the electron transport chain.

ATP synthesis

Assays of ATP synthesis by IMVs were modified from [34]. The IMVs were diluted to 0.105 mg/ml final in 1910 µl of synthesis reaction buffer (50 mM MOPS-Tris, pH 7.5 + 10 mM MgOAc) in a 1x1 cm cuvette. Aeration was achieved throughout the assay by stirring with a round magnetic stirrer with cross-cut channels. Reactions were done at ambient temperature (~22°C). Membranes were allowed to equilibrate for two minutes after dilution into the cuvette. NADH (50 µl of 0.1 M stock) was added to 2.5 mM final and, after one minute to allow PMF formation, ATP synthesis was started by adding 40 µl of ADP/Pi mixture to obtain 1 mM ADP and 3 mM Pi final (Total assay volume, 2.0 ml). Over four minutes, 100 µl of reaction was withdrawn at one minute intervals, added to 400 µl of ice-cold stop solution (1% TCA, 2 mM EDTA) with vortexing, and the quenched samples kept on ice. For each quenched sample in duplicate, 10 µl was added to 390 µl of ice-cold luciferase assay buffer (0.1 M Tris-acetate, 2 mM EDTA, pH7.5). Samples of ATP standards were treated with stop solution and diluted as above to provide a linear response over 0.25 pmol to 12 pmol in the final measurement. Samples could be frozen at this point, if needed. For each neutralized sample, 100 µl was transferred to a well of a white, opaque 96-well microtiter plate (Nunc F96 Microwell plates, Thermo Scientific #136101), which was then equilibrated to ambient temperature. The plate was placed in a Synergy HT microplate reader (Biotek) equipped with autoinjector. For each sequential sample well, 50

μl of luciferase reagent (ATP Bioluminescence Assay kit CLS II, Roche Diagnostics) was injected and luminescence was measured for 10 s (top path; integration, 1 s; gain, 135). All membranes assayed showed linear rates of ATP synthesis over the assay period (not shown).

Proton pumping assay

Proton pumping activity of IMV was measured by monitoring fluorescence quenching of 9-amino-6-chloro-2-methoxyacridine (ACMA; 1 μM), which reflects ΔpH [35]. Assays were done at 30°C on a Fluoromax-4 or Fluorolog-3 (Horiba Scientific) with the following settings: excitation/emission wavelengths (nm) of 430/560; excitation/emission slits of 5/4 nm; gratings set at 1200; integration time of 0.5 s; and interval time of 7.5 s.

BioLayer Interferometry (BLI) assay

BioLayer Interferometry was used to study the interactions between isolated F_1(-δε) and biotinylated ε variants. Experiments were done in an Octet RED system (Pall ForteBio) as described [22, 36].

3.4 Results

Effects of εCTD truncations on aerobic growth

To observe whether ε-CTD truncations affect *in vivo* function of the ATP synthase, bacteria expressing wild-type (WT) or mutant forms of F_OF_1 were grown with a nonfermentable carbon source, succinate, so growth required oxidative phosphorylation [37]. As a negative control, mutation βM209L was used, which allows assembly of normal levels of ATP synthase on the membrane but renders it essentially inactive [23, 38]. As shown in Fig. 3.1 and Table 3.1, growth on succinate was negligible for cells expressing F_OF_1 with βM209L; similar negligible growth also occurred with cells expressing no F_OF_1 (LE392Δ(*atpI-C*) + vector pACYC177, not shown). Deletion of the entire εCTD (ε88stop) reduced respiratory growth yield only ~20% with little effect on growth rate. This is consistent with another group's study in which ε88stop allowed respiratory growth on acetate and caused a minimal decrease in growth yield on limiting glucose [16]. In contrast, deleting only 5 C-terminal amino acids from ε (εΔ5) reduced growth yield and growth rate (Table 3.1) by ~60%. The assay was repeated with the same plasmids expressed in a distinct *Δatp*-operon host strain, DK8, and similar results were obtained (not shown). The DK8 strains were able to utilize succinate better than LE392Δ and show higher growth probably with the help of C_4-dicarboxylate transporter [39]. To obtain more stringent conditions, succinate was reduced to a limiting concentration (see method). The greater phenotypic defect of εΔ5 is not simply due to mis-assembly of F_OF_1 since εΔ5 membranes showed higher F_OF_1 content than for ε88stop (Table 3.1). Thus, the entire εCTD can be removed with minimal effects, but the small εΔ5 truncation

Figure 3.1

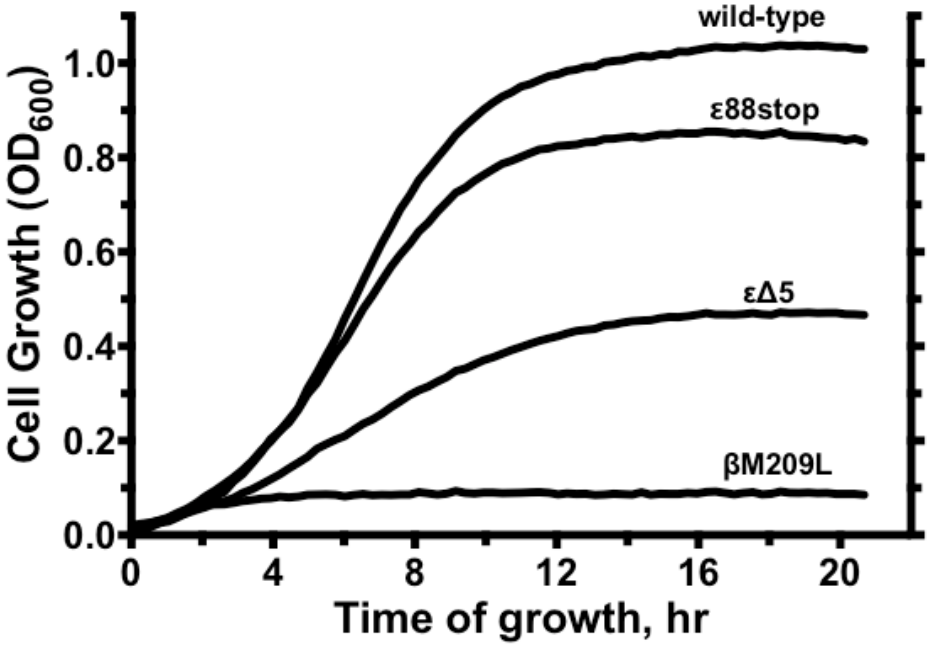
wild-type
ε88stop
εΔ5
βM209L
Cell Growth (OD_{600})
1.0
0.8
0.6
0.4
0.2
0.0
0
4
8
12
16
20
Time of growth, hr

Figure 3.1. Phenotypic assay for growth of *E. coli* by respiration. LE392(Δ*atpI-C*) cells expressing F_OF_1 from pAU1were grown on defined medium with succinate as the sole carbon source. Mutations present are noted for each culture.

Table 3.1

Strain	**Growth Yield**, % WT ±SEM[a]	**Growth Rate, OD_{600}/Hr** ±SEM	**Relative $F_O F_1$ content[e]**
WT	100% ±9 (5)[b]	0.2 ± 0.01 (5)	1
ε88stop	78% ±13 (4)	0.14 ± 0.03 (4)	0.23
εΔ5	38% ±4 (6)	0.08 ± 0.01 (6)	0.54
βM209L	4% ± 2 (3)	NS[c]	ND[d]

Table 3.1. Effect of εCTD truncations on aerobic growth on succinate. Growth yield is the maximal OD at 600nm and is normalized. [a]SEM = standard error of mean. [b]number of independent assays. [c]Not significant. [d]Not determined. [e]Amounts of F_OF_1 in membrane were quantified by anti-β antibody; values were normalized with respect to WT.

appears to perturb the εCTD's regulatory interactions in a way that significantly degrades the capacity for *in vivo* oxidative phosphorylation.

Effects of εCTD truncations on in vitro functions of membrane-bound ATP synthase

To further examine why εΔ5 is more deleterious than ε88stop *in vivo*, IMVs were isolated and tested for effects of εCTD truncations on activities of F_OF_1 *in vitro*. ATP hydrolysis by IMVs was measured with excess uncoupler FCCP present in all conditions, to ensure that F_OF_1 activity was not inhibited by 'backpressure' from PMF. Nearly all ATPase activity of WT and mutant membranes was due to F_OF_1 since sodium azide, a catalytic site inhibitor, reduced ATPase by at least 98% (not shown). In direct comparison, εΔ5 and ε88stop membranes showed 63% and 60% ATPase activity *vs* WT (Table 3.2). However, when results were normalized for the F_OF_1 content in membranes, intrinsic ATPase activity was 2.6-fold higher in the complete absence of the εCTD (ε88stop). This is consistent with prior demonstrations that WT membrane ATPase activity doubled when ε inhibition was disrupted by (i) trypsin cleavage of the εCTD [40] or (ii) by trapping ε in the compact ε_C state by a disulfide crosslink between εCTD/εNTD [41]. In contrast, the εΔ5 truncation did not significantly alter the intrinsic ATPase activity of F_OF_1 in membranes. This is also supported by the effects of LDAO, a detergent that is known to activate ATPase of *E. coli* F_OF_1 & F_1 mostly by disrupting ε inhibition [42, 43]: LDAO activated ATPase activity to the same extent for WT and εΔ5 membranes (Table 3.1). These results suggest that the loss of ε's 5 C-terminal residues does not significantly alter the inherent energetic balance between active and ε-inhibited forms of F_OF_1 in membranes.

As suggested previously for ε88stop [16], it is possible that partial functional uncoupling of F_1 from F_O contributes to the *in vivo* phenotypic defect of εΔ5. One result of this could

Table 3.2

Membranes	**ATPase**[b] ±SEM	**Relative ATPase**[c]	**DCCD Inhibition of ATPase**[d] ±SEM	**LDAO stimulation of ATPase**[e] ±SEM	**ATP synthesis**[f] ±SEM	**Maximal NADH-driven pumping**[g] ±SEM
WT	5.2 ±0.3 (7)[a]	1.0	77% ±4 (5)	1.9 ±0.3 (7)	105 ±7 (8)	70%±2.5 (8)
εΔ5	3.3 ±0.3 (9)	1.1	68% ±4 (2)	2.1 ±0.1 (9)	38 ±2 (5)	77%±3.7 (3)
ε88stop	3.1 ±0.6 (3)	2.6	81% ±5 (3)	1.4 ±0.04 (3)	100 ±8 (4)	59%±1.5 [h] (5)

Table 3.2. Effects of truncation on the *in vitro* activities of membranes. [a]number of independent assays. [b]μmol/min/mg membrane protein, Mean±SEM (see Methods). [c]values normalized to relative levels of catalytic β subunit in membranes. [d]%Inhibition after preincubation of membranes with DCCD, Mean±SEM (see Methods). [e]Ratio of activity +/– LDAO in assay, Mean±SEM (see Methods). [f]nmol ATP/min/mg membrane protein, Mean±SEM. Parenthetic values are number of independent experiments for each assay. [g]% fluorescence quenching, Mean±SEM. [h]difference between ε88stop and other results is significant. Student t-test vs WT and εΔ5 gave P-values ≤ 0.0255.

be that some ATPase activity is not thermodynamically linked to PMF; under respiratory conditions that would drive net ATP synthesis through well-coupled F_OF_1, unregulated ATP hydrolysis would create a futile cycle that reduces the efficiency of cellular energy conversion. To test for this, ATPase activity was measured after treating membranes with dicyclohexylcarbodiimide (DCCD), a covalent modifier of the ***c***-ring that blocks proton transport through F_O. For well coupled F_OF_1 complexes, blocking proton transport also inhibits ATPase activity [44]**.** As shown in Table 3.2, the ε88stop truncation did not significantly alter the sensitivity of membrane ATPase to DCCD, although the original study by Cipriano and Dunn [16] showed slightly reduced DCCD inhibition for ε88stop membranes. The εΔ5 truncation did result in a small but significant decrease in inhibition by DCCD (Table 3.2). Further tests would be needed to determine if this ~10% greater fraction of uncoupled ATPase is sufficient to contribute to the reduced aerobic growth caused by εΔ5.

Membranes were also tested for possible effects of εCTD truncations on ATP synthesis activity. As shown in Table 3.2, εΔ5 membranes showed a >2.7-fold lower capacity for ATP synthesis. This was not due to reduced PMF, as NADH-driven respiration generated similar ΔpH gradients for WT and εΔ5 membranes (Fig. 3.2, Table 3.2). The lower ATP synthesis rate is also not due to the ~50% lower F_OF_1 content in εΔ5 membranes since both ε88stop & WT-haploid membranes (not shown) had even lower F_OF_1 content (Table 3.1) but had ATP synthesis rates similar to that of WT pAU1 membranes (Table 3.2). This is consistent with prior studies showing that F_OF_1 content of haploid membranes exceeds that necessary for ATP synthesis rates *in vivo* [45] and *in vitro* [46]. In fact, since εΔ5 membranes had more F_OF_1 than ε88stop or WT haploid membranes, their 2.7-fold lower

Figure 3.2

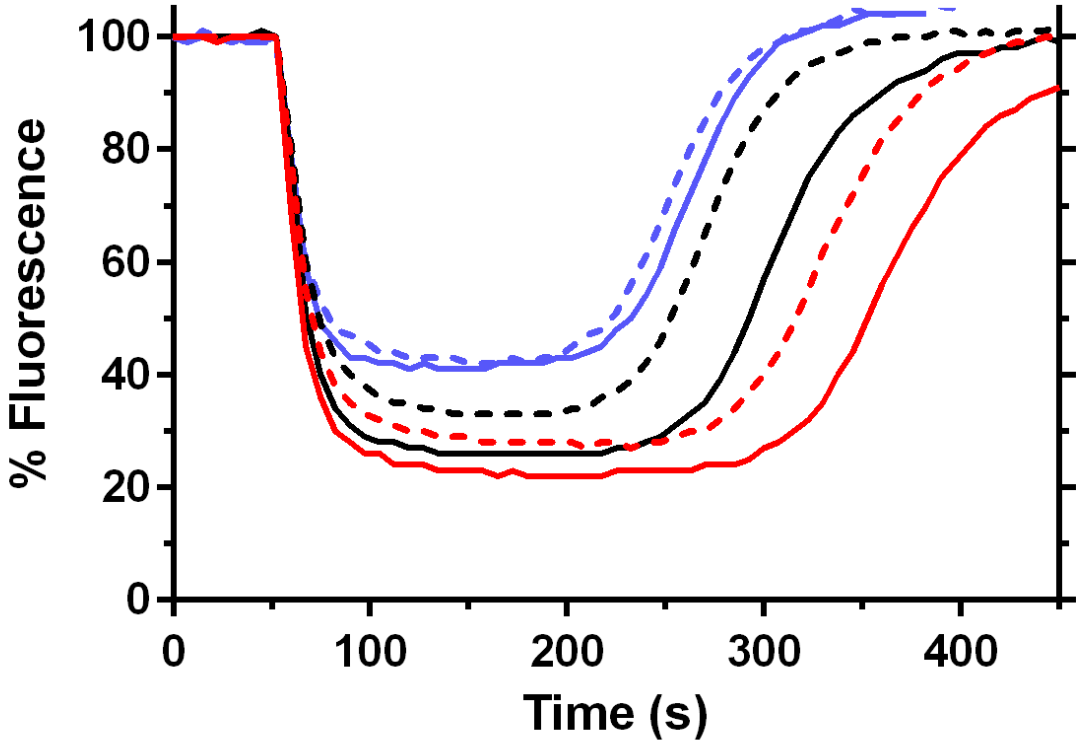

Figure 3.2. Respiratory generation of Proton Motive Force by membranes. Proton pumping was measured by quenching of fluorescence of the dye ACMA (see methods). Respiration was initiated by addition of NADH to 0.5 mM. Dotted lines represent proton pumping by untreated ε88stop (*blue*), εΔ5 (*red*) and WT (*black*) membranes. Solid lines represent proton pumping by the same membranes after treatment with DCCD to block possible proton transport through F_O.

synthesis rate probably reflects an even greater intrinsic inhibition of ATP synthesis by the εΔ5 subunit. Control assays were also included to test whether reduced ATP synthesis by εΔ5 membranes was due in part to any uncoupled ATPase activity. The ATP synthesis rates of εΔ5 or WT membranes were not significantly altered by the presence of AMPPNP, which inhibits ATPase but not ATP synthesis [47, 48] (not shown). Together, these results indicate that the εΔ5 truncation has a direct effect in increasing ε's inhibition of ATP synthesis by F_OF_1. However, this does not rule out a possible contribution of uncoupled ATPase to the εΔ5 growth defect on succinate (as suggested by the reduced inhibition of εΔ5 membrane ATPase by DCCD); ADP is in large excess over ATP produced in the *in vitro* synthesis assay, but *in vivo* respiration typically drives high ATP/ADP ratios, at which uncoupled ATPase could be more significant.

Another test for possible coupling defects between F_1 and F_O is to monitor the kinetics of H^+-pumping by isolated, everted membranes. Altered coupling between F_1 and F_O might allow uncontrolled, passive flux of protons, which would decrease the capacity to generate PMF by respiration or by ATPase-driven proton pumping. This was tested by comparing WT and mutant membranes for NADH-driven proton pumping. As shown in Table 3.2 and Fig. 3.2, with NADH-driven respiration, εΔ5 membranes generated similar or better PMF than did WT, but ε88stop membranes generated partially reduced PMF. To test for F_O-specific proton leaks, membranes were treated with DCCD before addition of NADH. DCCD caused a shift (50-60 s for WT and εΔ5; 15 s for ε88stop) in the amount of time the membranes were able to maintain PMF. Both WT pAU1 and εΔ5 membranes showed similar shifts with DCCD treatment (Fig. 3.2). The ε88stop membranes showed a smaller time shift than both WT pAU1 and εΔ5 membranes. These results show that the εCTD

truncations do not cause any increased leak through F_O. In the case of ε88stop, the membrane capacity to drive gradient was reduced (Table 3.2, Fig. 3.2) but it was not due to increased leak through F_O. Although the PMF was lower, the synthesis rates by ε88stop membranes were as high as for WT (Table 3.2). Overall, our proton pumping results show that the truncations have not adversely affected the membrane coupling and the low growth of the mutants is not due to the inability to generate PMF. Next, the effects of the truncations were tested when PMF was generated by ATP hydrolysis *via* F_1. Here εΔ5 showed similar ATPase-driven proton pumping. Only ε88stop membranes generated lower PMF than WT membranes. Cipriano and Dunn observed markedly slower PMF generation by ε88stop membranes. We saw a similar effect in our studies; however, it may be due to lower total expression of F_OF_1 is lower (Table 3.1).

Effects of εΔ5 truncation on interactions of εCTD with isolated F_1

Previously, we used Biolayer Interferometry (BLI) kinetic assays of protein-protein interactions to show that the εNTD is responsible for initial binding and for most of the binding energy between F_1 and ε, whereas the conformation of the εCTD controls ε dissociation from F_1[22]. Dissociation of ε probably does not occur at all when it adopts the extended conformation (ε_X) in which part of the εCTD is buried within the central cavity of F_1 [22, 28]. Ligands influence the overall dissociation rate of εCTD by stabilizing the ε_X state that leads to slow dissociation (MgADP/Pi) or by preventing ε from entering the ε_X state, leading to fast dissociation (ATP/EDTA). Here, BLI was used to determine whether the εΔ5 truncation changes the kinetics or energetics of interactions of εCTD with F_1. With F_1 bound to immobilized εΔ5 in buffer alone, >90% of F_1/εΔ5 complexes dissociated very slowly in buffer only (not shown, k_d ~$5x10^{-5}$ s^{-1}), which is similar to the behavior of F_1/WT-ε [22]. This shows that εΔ5 is still strongly biased towards tight binding, but any difference in dissociation rates between εΔ5 and WT-ε is not discernible by BLI at these slow rates. When the dissociation step included ATP/EDTA to mimic pre-hydrolysis condition, faster, essentially monophasic dissociation of both F_1/WT-ε and F_1/εΔ5 (~94%) occurred with no noticeable lag (Fig. 3.3). However, F_1/εΔ5 dissociated with a ~6-fold slower rate (6.3×10^{-4} s^{-1}). This suggests that the εCTD of εΔ5 either (i) binds more tightly to F_1 in the extended, inhibitory conformation or (ii) adopts a distinct tight-binding mode. When F_1/WT-ε were bound in the presence of ATP/EDTA, preventing access to tight binding, subsequent exposure to Mg^{2+} in the dissociation phase allowed hydrolysis and rapid switching to the ε-inhibited state at the catalytic dwell, and post-hydrolysis conditions (MgADP/Pi) in the dissociation step stabilized ε in the tightly-bound form (Fig. 3.3, *red*

and *green*) [22]. F_1/εΔ5 complexes also showed this rapid reversal to a tightly-bound state on switching from ATP/EDTA during F_1/εΔ5 association to MgADP/Pi in the dissociation phase (Fig. 3.3, *green*). Greater than 95% of complexes dissociated very slowly for WT-ε and εΔ5. Overall, these results indicate that, while the εCTD can still undergo dynamic transitions between different conformations, the absence of 5 terminal residues from the εCTD significantly stabilizes a tightly-bound state of ε on F_1 relative to the dissociable state.

The ATPase activity of isolated *E. coli* F_1 is inhibited >90% by bound WT-ε [5, 22]. Since, εΔ5 showed an increased bias towards tight binding, we investigated whether the tighter binding correlates with greater inhibition. We have shown that the Bap-tag on ε does not affect its inhibition of isolated F_1 [22]. ATPase assays were used to measure the K_I for inhibition of F_1(-δε) by Bap-εΔ5, as done before for WT-ε and ε88stop [22]. The K_I of 0.7 nM determined for Bap-εΔ5 is similar to the K_I for WT-ε (0.5 nM), but does not reflect the increased stability of the tightly-bound state as indicated by the BLI assays of F_1/εΔ5 binding. Furthermore, εΔ5 exhibited maximal inhibition of only ~20% (Fig. 3.4). This is similar to the ~24% maximal inhibition by ε88stop under the same conditions, although the K_I for ε88stop is nearly 20-fold weaker due to absence of the εCTD [22]. This surprising finding suggests that the shorter εCTD of εΔ5 still contributes to tight binding to F_1, but it no longer binds in a way that contributes to strong inhibition of F_1-ATPase activity, although it does inhibit ATP synthesis by F_OF_1 on membranes (Table 3.2).

Figure 3.3

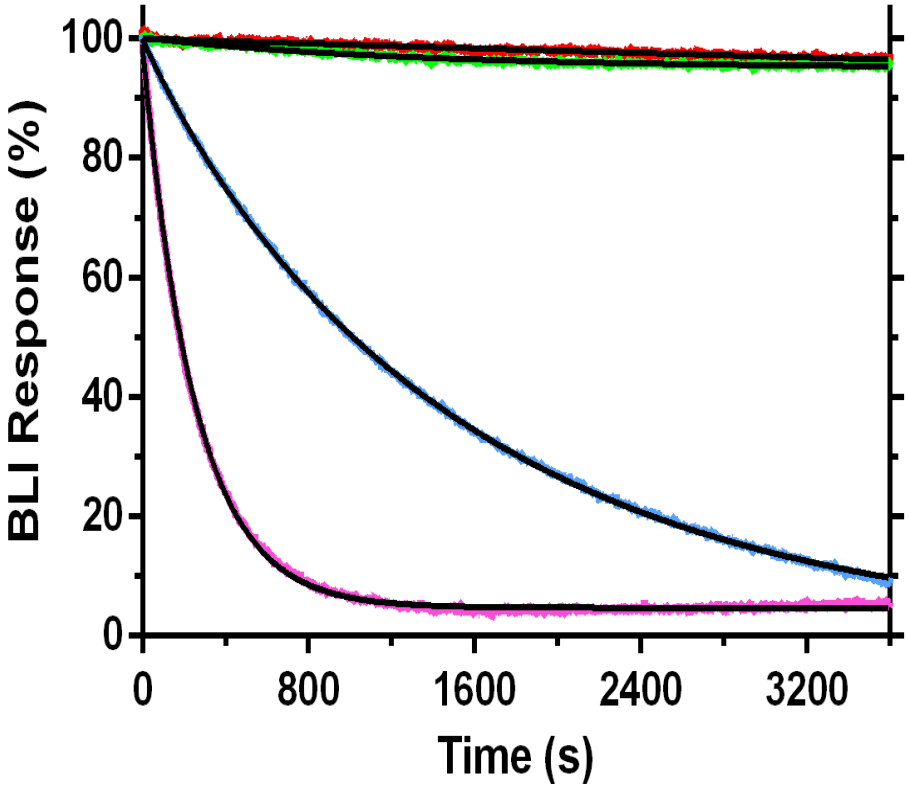

Figure 3.3 Effects of εΔ5 on dissociation of F_1/ε complexes. Only the dissociation phase of a BLI assay is shown. In previous steps, similar amounts of biotinylated ε (Bap-ε, WT or εΔ5) were immobilized on streptavidin-coated BLI sensors, then sensors were incubated with excess F_1(-δε) to form F1/ε complexes. For the red (WT-ε) and green (εΔ5) datasets, F_1(-δε) was bound in the presence of ATP/EDTA (1 mM each), then allowed to dissociate in presence of MgADP/Pi (2 mM Mg^{2+}, 1 mM ADP, 1 mM Pi); dissociation rates for both curves (assuming 1 exponential phase) were $\leq 1 \times 10^{-6}$ s^{-1}, the technical lower limit under these conditions. For the pink (WT-ε) and blue (εΔ5) datasets, the binding step contained only buffer and F_1 was allowed to dissociate in presence of ATP/EDTA (1 mM each), and dissociation rates were determined by nonlinear regression (GraphPad Prism) for two phases of exponential decay. Results: WT ε (*Pink*), 95% of complexes dissociated with $k_d = 4 \times 10^{-3}$ s^{-1} (95% confidence interval = 3.98×10^{-3} to 4×10^{-3}) and εΔ5 (*Blue*), 94% complexes dissociated with $k_d = 6.3 \times 10^{-4}$ s^{-1} (95% confidence interval = 6.29×10^{-4} to 6.31×10^{-4}). R^2 was ≥ 0.999 for both fits.

Figure 3.4

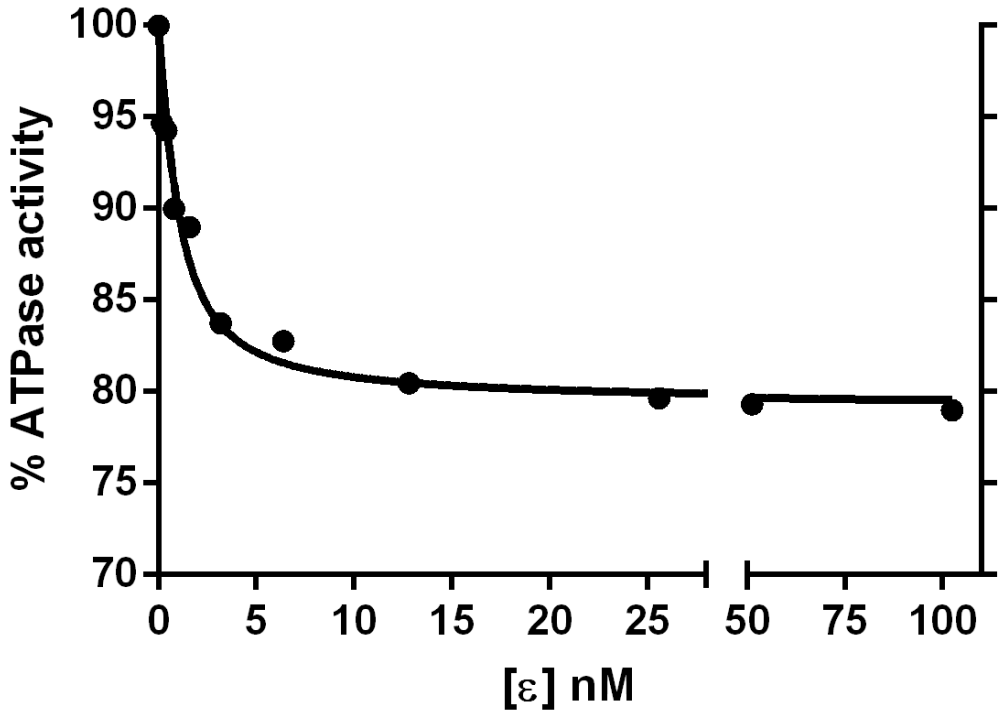

Figure 3.4. Inhibition of F_1-ATPase activity by εΔ5. ATPase activity was measured with titration of different concentrations of εΔ5 with F_1(-δε). The uninhibited ATPase activity (with 0 nM εΔ5) was 60.9 μmol/min/mg. Maximal inhibition of F_1(-δε) by εΔ5 = 20% (95% confidence interval: 19% to 22%) calculated by the quadratic equation shown here [22]. K_I = 0.68 nM. (95% = 0.33 to 1.02 nM). R^2 = 0.972.

3.5 Discussion

We have shown that a small truncation at ε's C-terminus affects respiratory growth of *E. coli*. Truncations of ε's final five residues (εΔ5) caused >2.5-fold reduction in aerobic growth yield, but deletion of the entire εCTD (ε88stop) had much less impact on aerobic growth (Figure 3.1). *In vitro* assays showed that in membranes expressing F_OF_1 with εΔ5 or ε88stop, there was no increased proton leak through F_O when PMF was generated by NADH. However, ε88stop membranes were unable to generate the same level of PMF as εΔ5 or WT. Hence, the reduction in growth is not due to misassembly or membrane leak that prevents the electron transport chain from generating PMF. Furthermore, εΔ5 truncation selectively inhibits the ATP synthesis activity as we observed a small effect on coupled ATPase activity but >2.7-fold reduction in ATP synthesis activity. In contrast, ATP synthesis rates remained unaffected in membranes with the entire εCTD deleted (ε88stop). ATPase activity of isolated F_1 showed minimal inhibition by εΔ5 (20%; similar to inhibition by ε88stop [22]) as compared to WT-ε (>90%) although εΔ5 bound to F_1 as tightly as WT-ε. While further tests are required to determine if the uncoupled ATPase could cause enough futile cycle to contribute to the *in vivo* effect, our studies indicate that ε has different mechanisms of regulating the enzyme when the enzyme rotates in the direction of ATP synthesis vs ATP hydrolysis. Overall, our results show that perturbing the interactions of εCTD with F_OF_1 can disrupt optimal cellular energy conversion.

Many studies have shown that the ATPase activity of bacterial F_1 is inhibited by the ε subunit [42, 49-52]. Tsunoda et al. [53] showed that εCTD inhibited ATPase activity of membranes by adopting an extended conformation, but no effect was seen on the ATP synthesis activity. However, it was recently reported that εCTD removal led to a three-fold

increase in maximal ATP synthesis rates [54]. Thus, εCTD can inhibit both synthesis and hydrolysis by ATP synthase. Our results show that altering the εCTD interactions with F_1 can significantly bias regulation towards preferential inhibition of ATP synthesis.

Correlation between phenotypic growth defect and low ATP synthesis rate

We found that reduced ATP synthesis rate was the most significant functional defect with εΔ5 membranes, but is it sufficient to account for the phenotypic growth defect? Early study of phenotypic growth on succinate showed that, with F_OF_1 overexpressed similar to our system, reducing F_OF_1 expression 3-4 fold to 'normal' or haploid levels did not decrease the growth yield on succinate, indicating F_OF_1 function is in excess capacity even at haploid level of expression for respiratory growth [45]. We believe that εΔ5 introduces a greater energy barrier for activation of ATP synthesis by ε-inhibited F_OF_1. Our membrane assays of ATP synthesis used NADH, but succinate (substrate for growth) could only generate a lower maximal PMF due to the reduced H^+/e- ratio for this substrate. Thus, in the εΔ5 cells grown on succinate, even more F_OF_1 complexes might remain ε-inhibited than indicated by our *in vitro* assays driven by NADH. As excess capacity of over-expressed εΔ5 F_OF_1 might moderate the effect on net ATP synthesis, εΔ5 might cause an even larger decrease in phenotypic growth in a strain expressing lower, haploid levels of F_OF_1. We are currently reengineering our expression system to test for this. We also observed that εΔ5 slightly reduced inhibition of membrane ATPase by DCCD, so we cannot rule out a contribution of uncoupled ATPase in εΔ5 membranes, which could cause a futile cycle of hydrolysis of ATP.

Prior studies [40, 41] and our results with ε88stop membranes show that *E. coli* membranes typically have ~50% of F_OF_1 in ε-inhibited state. Results here (Table 3.2) show that εΔ5

truncation does not significantly change this level of ATPase inhibition on the membranes. ATP synthesis rate of εΔ5 membranes is >2.7-fold slower than for WT membranes and likely reflects a greater fraction of F_OF_1 complexes that are ε-inhibited in these assay conditions. This reduction is not due to reduced PMF driving force since NADH-driven H^+-pumping assays show similar kinetics and steady-state gradients (ΔpH) for WT and εΔ5 membranes. Our proton pumping data showed lower NADH-driven H^+-pumping by ε88stop membranes. At the same time, the ATPase was activated. Our results are consistent with another study that had shown that ε88stop membranes had reduced ATPase-driven H^+-pumping even though ATPase was activated [16]. We believe that the deletion of entire εCTD results in a decrease in proton pumping by the electron transport chain resulting in lower PMF since there is no evidence for worse leak through the F_O domain. Ideally, this lower PMF should result in decreased ATP synthesis rates. However, it is possible that with the CTD deleted, inhibition of ATP synthesis by ε is absent, resulting in more active complexes. This leads to net ATP synthesis rates that are comparable to WT membranes.

Although εΔ5 did not alter inhibition of membrane ATPase, BLI tests showed a significant effect of εΔ5 on ε's interactions with the isolated F_1 complex. The ~6-fold slower dissociation of F_1/εΔ5 upon exposure to ATP/EDTA indicates that εΔ5 enhances the stability of tightly-bound state(s) of F_1/ε relative to dissociable states. The strong binding of εΔ5 with isolated F_1 but lower inhibition of its ATPase activity is surprising. One possibility is that the εΔ5 subunit, in some extended state, is able to access a yet unknown site during turnover that it does not lead to inhibition of isolated F_1-ATPase. While F_1 is bound to F_O on the membrane, this site may be inaccessible as the mutant shows similar ATPase inhibition as for WT-ε. This shows dissimilar behavior of ε in intact F_OF_1 and on

soluble F_1. Thus, ε may interact with the F_1 in different ways that are directly impacted by whether ε is interacting with F_O.

The differential effect of εΔ5 on membrane functions of F_OF_1 suggests that the εCTD forms distinct inhibitory interactions when the enzyme is rotating in the opposite directions for ATP hydrolysis versus synthesis. This is consistent with the bi-directional ratchet mechanism proposed by Cipriano et al. [55]. By this mechanism, ε's distinct states for εCTD are based on the type of nucleotide(s) interacting with the catalytic site(s) of F_1. Binding of ATP or ADP would lead ε to adopt a conformation that would allow rotation of γ only in ATP hydrolysis or ATP synthesis direction, respectively. We have observed that εΔ5 inhibits ATP synthesis much more than ATP hydrolysis by intact F_OF_1. Binding of ADP to the catalytic sites may lead εΔ5 to adopt a conformation that allows tighter binding and higher inhibition when the enzyme rotates in ATP synthesis direction. When ATP is bound, the truncated ε may adopt a conformation that allows faster dissociation from F_1 just like WT ε [22]. On the other hand, our single molecule FRET data has shown three distinct conformations of ε on membranes but only two conformations of ε on isolated F_1 [56]. This indicates that ε may be adopting more than two distinct conformations or interacting with sites that are not known yet. It is possible that in presence of ATP, εΔ5 adopts an alternate conformation that is distinct from the ε_X observed in *E. coli* F_1 structure [13]. As a result, it may have access to a distinct, unknown site that allows slower dissociation from F_1 than WT ε (Fig. 3.3). However, the slower dissociation does not result in stronger inhibition of ATPase. In intact F_OF_1, εΔ5 may be capable of adopting the alternate conformation upon binding of ATP at catalytic site. However, the presence of the

F_O subunits may favor εΔ5 to adopt the normal inhibitory conformation as observed with WT ε. Hence, level of inhibition of ATPase activity remains similar to WT ε.

The changes in ε's interactions with the enzyme due to the εΔ5 truncation were examined to understand the preferential inhibition of ATP synthesis vs hydrolysis. For the ε_C conformation of *E. coli* ε, truncating the terminal five residues from εCTD should have minimal effects on the εNTD/εCTD interface, since εΔ5 removes only one residue (εT134) that contacts the εNTD. On the other hand, for the ε_X conformation, the residues removed by εΔ5 are responsible for ~64% of the surface area buried between the ε-hook and β_3. The loss of contacts and surface area may give rise to these mechanistic possibilities that can account for selective inhibition of ATP synthesis:

i. The truncation further biases εCTD towards a distinct interaction (not ε_X) with F_OF_1 that selectively inhibits ATP synthesis.
ii. The truncation causes mechanical 'slip' between F_O proton-transport rotation and $F_1(\gamma\varepsilon)$ rotation driving net synthesis of ATP.
iii. The truncation alters interactions of the extended (ε_X) state so that the activation energy barrier is higher for ATP synthesis direction but low for ATP hydrolysis direction.

Other inhibitors have been reported that selectively inhibit the enzyme in one direction over the other. For example, sodium azide preferentially inhibits ATP hydrolysis by bacterial, chloroplast and mitochondrial enzymes but has no effect on ATP synthesis [48, 57]. Similarly, a structural analogue of ATP, Adenylyl-imidodiphosphate (AMPPNP), inhibits ATP hydrolysis but not ATP synthesis in bacteria and mitochondria [47, 48]. Whereas, other structural analogs of ADP, 3-O-[1-(5-dimethylamino)-naphthoyl] ADP (F-

ADP) and 3-O-(1-naphthoyl) ADP (N-ADP) inhibit ATP synthesis much more strongly than hydrolysis [48]. εΔ5 now offers another example that ATP synthesis can be selectively inhibited more than ATP hydrolysis.

Overall, our results are consistent with the idea that εCTD may be fine-tuned in different bacterial species to adapt the regulation of ATP synthesis/hydrolysis functions to the distinct metabolic/environmental demands of each species [2, 5]. In *E. coli* ε, the terminal 'hook' region appears to make minimal specific interactions with other subunits in the observed ε-inhibited state. We showed here that a minor truncation of this hook resulted in selective inhibition of ATP synthesis and reduced the capacity for cell growth on a nonfermentable carbon source. Other bacterial species have shown stronger inhibition of ATPase with shorter εCTD [7, 14, 15]. For example, *Mycobacterium tuberculosis* ATP synthase contains the ε subunit with the CTD shorter by 15 residues [58] but its ATPase activity is highly ε-inhibited in *M. tuberculosis* [59]. Similarly, in *Mycobacterium phlei,* the ATPase activity is highly inhibited [59].This inhibition is probably mediated by ε as the ATPase was activated with trypsin treatment. Thus, the effects of truncation at ε's C-terminal domain may correlate with stronger inhibition of enzyme activity seen in other bacterial species.

3.6 Conclusion

Our results have demonstrated the importance of the interactions of εCTD with other subunits for efficient aerobic growth of *E. coli*. When these interactions are perturbed, they lead to reduced ATP synthesis rate resulting in lower aerobic growth. This is a 'proof of principle' that altering ε's regulatory interactions can provide means to disrupt bacterial energy metabolism. The regulatory functions of ε are likely to be conserved within a broad range of pathogenic bacteria. As a result, there is a high probability that disruption of ε's regulatory interactions in many of these bacteria will yield similar results of low growth. With ATP synthase already validated as a drug target against *Mycobacterium tuberculosis*, ε subunit thus provides an attractive target for further antibiotic development.

3.7 References

1. Boyer PD: The ATP synthase--a splendid molecular machine. *Annual Review of Biochemistry* 1997, 66:717-749.
2. Duncan TM: The ATP Synthase: Parts and Properties of a Rotary Motor. In: *The Enzymes, vol XXIII: Energy Coupling and Molecular Motors*. *Volume 23*, 3rd edition.
3. Harris DA, Das AM: Control of mitochondrial ATP synthesis in the heart. *Biochem J* 1991, 280:561-573.
4. Walker JE: The regulation of catalysis in ATP synthase. [Review]. *Current Opinion in Structural Biology* 1994, 4(6):912-918.
5. Feniouk BA, Suzuki T, Yoshida M: The role of subunit ε in the catalysis and regulation of F_OF_1-ATP synthase. *Biochimica et Biophysica Acta* 2006, 1757(5-6):326-338.
6. Tsunoda SP, Aggeler R, Yoshida M, Capaldi RA: Rotation of the c subunit oligomer in fully functional F_1F_O ATP synthase. *Proceedings of the National Academy of Sciences of the United States of America* 2001, 98(3):898-902.
7. Masaike T, Suzuki T, Tsunoda SP, Konno H, Yoshida M: Probing conformations of the beta subunit of F_OF_1-ATP synthase in catalysis. *Biochem Biophys Res Commun* 2006, 342(3):800-807.
8. Iino R, Hasegawa R, Tabata KV, Noji H: Mechanism of inhibition by C-terminal alpha-helices of the epsilon subunit of Escherichia coli F_OF_1-ATP synthase. *J Biol Chem* 2009, 284(26):17457-17464.

9. Wilkens S, Capaldi RA: Solution structure of the ε subunit of the F_1-ATPase from *Escherichia coli* and interactions of this subunit with β subunits in the complex. *Journal of Biological Chemistry* 1998, 273(41):26645-26651.

10. Yagi H, Kajiwara N, Tanaka H, Tsukihara T, Kato-Yamada Y, Yoshida M, Akutsu H: Structures of the thermophilic F_1-ATPase ε subunit suggesting ATP-regulated arm motion of its C-terminal domain in F_1. *Proc Natl Acad Sci USA* 2007, 104(27):11233-11238.

11. Stocker A, Keis S, Vonck J, Cook GM, Dimroth P: The Structural Basis for Unidirectional Rotation of Thermoalkaliphilic F_1-ATPase. *Structure* 2007, 15(8):904-914.

12. Gibbons C, Montgomery MG, Leslie AG, Walker JE: The structure of the central stalk in bovine F_1-ATPase at 2.4 Å resolution. *Nature Structural Biology* 2000, 7(11):1055-1061.

13. Cingolani G, Duncan TM: Structure of the ATP synthase catalytic complex (F(1)) from Escherichia coli in an autoinhibited conformation. *Nat Struct Mol Biol* 2011, 18(6):701-707.

14. Kato-Yamada Y, Bald D, Koike M, Motohashi K, Hisabori T, Yoshida M: Epsilon subunit, an endogenous inhibitor of bacterial F(1)-ATPase, also inhibits F(0)F(1)-ATPase. *Journal of Biological Chemistry* 1999, 274(48):33991-33994.

15. Keis S, Stocker A, Dimroth P, Cook GM: Inhibition of ATP hydrolysis by thermoalkaliphilic F_1F_o-ATP synthase is controlled by the C terminus of the ε subunit. *J Bacteriol* 2006, 188(11):3796-3804.

16. Cipriano DJ, Dunn SD: The role of the epsilon subunit in the Escherichia coli ATP synthase. The C-terminal domain is required for efficient energy coupling. *J Biol Chem* 2006, 281(1):501-507.

17. Kuki M, Noumi T, Maeda M, Amemura A, Futai M: Functional domains of epsilon subunit of Escherichia coli H+-ATPase (F_OF_1). *J Biol Chem* 1988, 263:17437-17442.

18. Jounouchi M, Takeyama M, Noumi T, Moriyama Y, Maeda M, Futai M: Role of the amino terminal region of the epsilon subunit of Escherichia coli H(+)-ATPase (F_OF_1). *Arch Biochem Biophys* 1992, 292:87-94.

19. Andries K, Verhasselt P, Guillemont J, Göhlmann HWH, Neefs J-M, Winkler H, Van Gestel J, Timmerman P, Zhu M, Lee E *et al*: A Diarylquinoline Drug Active on the ATP Synthase of Mycobacterium tuberculosis. *Science* 2005, 307(5707):223-227.

20. Duncan TM, Zhou Y, Bulygin VV, Hutcheon ML, Cross RL: Probing interactions of the Escherichia coli F_OF_1 ATP synthase beta and gamma subunits with disulphide cross-links. *Biochem Soc Trans* 1995, 23(4):736-741.

21. Braman J, Papworth C, Greener A: Site-Directed Mutagenesis Using Double-Stranded Plasmid DNA Templates. In: *In Vitro Mutagenesis Protocols*. *Volume 57*.

22. Shah NB, Hutcheon ML, Haarer BK, Duncan TM: F_1-ATPase of Escherichia coli: THE ϵ-INHIBITED STATE FORMS AFTER ATP HYDROLYSIS, IS DISTINCT FROM THE ADP-INHIBITED STATE, AND RESPONDS DYNAMICALLY TO CATALYTIC SITE LIGANDS. *Journal of Biological Chemistry* 2013, 288(13):9383-9395.

23. Wilke-Mounts S, Pagan J, Senior AE: Mutagenesis and reversion analysis of residue Met-209 of the beta-subunit of Escherichia coli ATP synthase. *Arch Biochem Biophys* 1995, 324(1):153-158.

24. Schaefer EM, Hartz D, Gold L, Simoni RD: Ribosome-binding sites and RNA-processing sites in the transcript of the *Escherichia coli unc* operon. *J Bacteriol* 1989, 171(7):3901-3908.

25. Gibson F, Cox GB, Downie JA, Radik J: Partial diploids of Escherichia coli carrying normal and mutant alleles affecting oxidative phosphorylation. *Biochem J* 1977, 162(3):665-670.

26. Klionsky DJ, Brusilow WS, Simoni RD: In vivo evidence for the role of the epsilon subunit as an inhibitor of the proton-translocating ATPase of Escherichia coli. *J Bacteriol* 1984, 160:1055-1060.

27. Wise JG: Site-directed mutagenesis of the conserved β subunit tyrosine 331 of *Escherichia coli* ATP synthase yields catalytically active enzymes. *J Biol Chem* 1990, 265:10403-10409.

28. Cingolani G, Duncan TM: Structure of the ATP synthase catalytic complex (F(1)) from Escherichia coli in an autoinhibited conformation. *Nat Struct Mol Biol* 2011, 18(6):701-707.

29. Grant SG, Jessee J, Bloom FR, Hanahan D: Differential plasmid rescue from transgenic mouse DNAs into Escherichia coli methylation-restriction mutants. *Proceedings of the National Academy of Sciences* 1990, 87(12):4645-4649.

30. Lowry OH, Rosebrough NJ, Farr AL, Randall RJ: Protein Measurement with the Folin Phenol Reagent *J Biol Chem* 1951, 193(1):265-275.

31. Laemmli UK: Cleavage of structural proteins during the assembly of the head of bacteriophage T4. *Nature* 1970, 227(259):680-685.

32. Fang Z, Doig C, Rayner A, Kenna DT, Watt B, Forbes KJ: Molecular evidence for heterogeneity of the multiple-drug-resistant Mycobacterium tuberculosis population in Scotland (1990 to 1997). *J Clin Microbiol* 1999, 37(4):998-1003.

33. Pullman ME, Penefsky HS, Datta A, Racker E: Partial resolution of the enzymes catalysing oxidative phosphorylation. I. Purification and properties of soluble dinitrophenyl-stimulated adonosine triphophatase. *J Biol Chem* 1960, 235:3322-3329.

34. Tomashek JJ, Glagoleva OB, Brusilow WS: The Escherichia coli F_1F_O ATP synthase displays biphasic synthesis kinetics. *J Biol Chem* 2004, 279(6):4465-4470.

35. Vik SB, Cain BD, Chun KT, Simoni RD: Mutagenesis of the a subunit of the F_1F_O-ATPase from Escherichia coli. Mutations at Glu-196, Pro-190, and Ser-199. *J Biol Chem* 1988, 263:6599-6605.

36. Shah N, Duncan T.: Bio-layer interferometry for measuring kinetics of protein-protein interactions and allosteric ligand effects. *Journal of Visualized Experiments* 2014, 18(84).

37. Gibson F: The introduction of Escherichia coli and biochemical genetics to the study of oxidative phosphorylation. *Trends in Biochemical Sciences* 2000, 25(7):342-344.

38. Duncan TM, Senior AE: The defective proton-ATPase of *uncD* mutants of Escherichia coli. Two mutations which affect the catalytic mechanism. *J Biol Chem* 1985, 260:4901-4907.

39. Boogerd FC, Boe L, Michelsen O, Jensen PR: atp Mutants of Escherichia coli Fail To Grow on Succinate Due to a Transport Deficiency. *J Bacteriol* 1998, 180(22):5855-5859.

40. Mendel-Hartvig J, Capaldi RA: Nucleotide-dependent and dicyclohexylcarbodiimide-sensitive conformational changes in the epsilon subunit of Escherichia coli ATP synthase. *Biochemistry* 1991, 30(45):10987-10991.

41. Schulenberg B, Capaldi RA: The ε subunit of the F_1F_O complex of *Escherichia coli*. Cross-linking studies show the same structure *in situ* as when isolated. *Journal of Biological Chemistry* 1999, 274(40):28351-28355.

42. Lotscher HR, deJong C, Capaldi RA: Interconversion of high and low adenosinetriphosphatase activity forms of Escherichia coli F_1 by the detergent lauryldimethylamine oxide. *Biochemistry* 1984, 23:4140-4143.

43. Dunn SD, Tozer RG, Zadorozny VD: Activation of Escherichia coli F_1-ATPase by lauryldimethylamine oxide and ethylene glycol: relationship of ATPase activity to the interaction of the epsilon and beta subunits. *Biochemistry* 1990, 29:4335-4340.

44. Hermolin J, Fillingame RH: H_+-ATPase activity of *Escherichia coli* F_1F_0 is blocked after reaction of dicyclohexylcarbodiimide with a single proteolipid (subunit c) of the F_0 complex. *J Biol Chem* 1989, 264:3896-3903.

45. Jensen PR, Westerhoff HV, Michelsen O: Excess capacity of H(+)-ATPase and inverse respiratory control in Escherichia coli. *EMBO Journal* 1993, 12(4):1277-1282.

46. Etzold C, Deckers-Hebestreit G, Altendorf K: Turnover number of Escherichia coli F_OF_1 ATP synthase for ATP synthesis in membrane vesicles. *Eur J Biochem* 1997, 243(1-2):336-343.

47. Penefsky HS: Differential Effects of Adenylyl Imidodiphosphate on Adenosine Triphosphate Synthesis and the Partial Reactions of Oxidative Phosphorylation. *Journal of Biological Chemistry* 1974, 249(11):3579-3585.

48. Hong S, Pedersen PL: ATP Synthase and the Actions of Inhibitors Utilized To Study Its Roles in Human Health, Disease, and Other Scientific Areas. *Microbiology and Molecular Biology Reviews : MMBR* 2008, 72(4):590-641.

49. Aggeler R, Mendel Hartvig J, Capaldi RA: Monoclonal antibody modification of the ATPase activity of Escherichia coli F_1 ATPase. *Biochemistry* 1990, 29:10387-10393.

50. Smith JB, Sternweis PC: Purification of membrane attachment and inhibitory subunits of the proton translocating adenosine triphosphatase from Escherichia coli. *Biochemistry* 1977, 16:306-311.

51. Laget PP, Smith JB: Inhibitory propeties of endogenous subunit e in the Escherichia coli F_1 ATPase. *Arch Biochem Biophys* 1979, 197:83-89.

52. Dunn SD, Tozer RG: Activation and inhibition of the Escherichia coli F_1-ATPase by monoclonal antibodies which recognize the epsilon subunit. *Arch Biochem Biophys* 1987, 253:73-80.

53. Tsunoda SP, Rodgers AJ, Aggeler R, Wilce MC, Yoshida M, Capaldi RA: Large conformational changes of the epsilon subunit in the bacterial F_1F_O ATP synthase provide a ratchet action to regulate this rotary motor enzyme. *Proceedings of the*

National Academy of Sciences of the United States of America 2001, 98(12):6560-6564.

54. Iino R, Hasegawa R, Tabata KV, Noji H: Mechanism of inhibition by C-terminal α-helices of the ε subunit of *Escherichia coli* F_OF_1-ATP synthase. *J Biol Chem* 2009, 284(26):17457-17464.

55. Cipriano DJ, Bi Y, Dunn SD: Genetic fusions of globular proteins to the epsilon subunit of the Escherichia coli ATP synthase: Implications for in vivo rotational catalysis and epsilon subunit function. *J Biol Chem* 2002, 277(19):16782-16790.

56. Duncan TM, Düser MG, Heitkamp T, McMillan DGG, Börsch M: Regulatory conformational changes of the ε subunit in single FRET-labeled F(o)F(1)-ATP synthase. *Proceedings - Society of Photo-Optical Instrumentation Engineers* 2014, 8948:89481J.

57. Bald D, Amano T, Muneyuki E, Pitard B, Rigaud JL, Kruip J, Hisabori T, Yoshida M, Shibata M: ATP synthesis by F_OF_1-ATP synthase independent of noncatalytic nucleotide binding sites and insensitive to azide inhibition. *Journal of Biological Chemistry* 1998, 273(2):865-870.

58. Biuković G, Basak S, Manimekalai MSS, Rishikesan S, Roessle M, Dick T, Rao SPS, Hunke C, Grüber G: Variations of Subunit ε of the Mycobacterium tuberculosis F_1F_O ATP Synthase and a Novel Model for Mechanism of Action of the Tuberculosis Drug TMC207. *Antimicrobial Agents and Chemotherapy* 2013, 57(1):168-176.

59. Haagsma AC, Driessen NN, Hahn MM, Lill H, Bald D: ATP synthase in slow- and fast-growing mycobacteria is active in ATP synthesis and blocked in ATP hydrolysis direction. *FEMS Microbiol Lett* 2010, 313(1):68-74.

60. Higashi T, Kalra VK, Lee SH, Bogin E, Brodie AF: Energy-transducing membrane-bound coupling factor-ATPase from Mycobacterium phlei. I. Purification, homogeneity, and properties. *Journal of Biological Chemistry* 1975, 250(16):6541-6548.

Chapter Four

Bio-Layer Interferometry for Measuring Kinetics of Protein-Protein Interactions and Allosteric Ligand Effects

Naman B. Shah and Thomas M. Duncan

Department of Biochemistry and Molecular Biology, State University of New York Upstate Medical University, 750 East Adams Street, Syracuse, New York 13210

This research was originally published in Journal of Visualized Experiments. Naman B. Shah, and Thomas M. Duncan. **Bio-layer Interferometry for Measuring Kinetics of Protein-protein Interactions and Allosteric Ligand Effects.** *Journal of Visualized Experiments*. 2014, **18** (84)

4.1 Abstract

We describe the use of Bio-layer Interferometry to study inhibitory interactions of subunit ε with the catalytic complex of *Escherichia coli* ATP synthase. Bacterial F-type ATP synthase is the target of a new, FDA-approved antibiotic to combat drug-resistant tuberculosis. Understanding bacteria-specific auto-inhibition of ATP synthase by the C-terminal domain of subunit ε could provide a new means to target the enzyme for discovery of antibacterial drugs. The C-terminal domain of ε undergoes a dramatic conformational change when the enzyme transitions between the active and inactive states, and catalytic-site ligands can influence which of ε's conformations is predominant. The assay measures kinetics of ε's binding/dissociation with the catalytic complex, and indirectly measures the shift of enzyme-bound ε to and from the apparently nondissociable inhibitory conformation. The Bio-layer Interferometry signal is not overly sensitive to solution composition, so it can also be used to monitor allosteric effects of catalytic-site ligands on ε's conformational changes.

4.2 Introduction

Protein-protein interactions are important for many biological processes, and label-free optical methods like Surface Plasmon Resonance (SPR) have been used *in vitro* to study kinetics of binding and dissociation [1]. Most label-free methods immobilize one biomolecule on a sensor surface and use an optical signal to detect a binding partner from solution as it associates with the immobilized biomolecule [1]. While SPR is a highly sensitive method, it is prone to interference due to changes in the refractive index of the solution flowing over the sensor [2]. Although not as sensitive as SPR, Bio-Layer Interferometry (BLI) is less affected by changes in sample composition [1, 3]. BLI uses fiber optic biosensors that have a proprietary biocompatible coating at the tip. The system used here (Octet-RED96) contains eight spectrophotometers. White light is piped to a row of probes that move on a robotic arm. Fiber optic sensors are picked up by the probes and moved to a 96-well plate containing samples. One of the target molecules is immobilized on the biosensor surface. Then sensors are moved to wells containing the binding partner in solution. BLI monitors association of the binding partner with the immobilized molecule, and then monitors dissociation after moving the sensors to solution without the binding partner. Binding of molecules to the biosensor surface leads to changes in optical interference between light waves that reflect back to the spectrophotometers from an internal surface and from the external interface between sensor and solution. These changes in interference can be quantified and used to determine kinetic rates of binding and dissociation, as summarized in the animation of Figure 4.1.

We have applied BLI to measure interactions between the catalytic complex of bacterial ATP synthase and its ε subunit, which can auto-inhibit the enzyme. ATP synthase is a

membrane- embedded rotary nanomotor that catalyzes synthesis and hydrolysis of ATP [4]. The catalytic complex (F_1) can be isolated in a soluble form that works as an ATPase. Subunit ε has two domains: the N-terminal domain (NTD) is necessary for proper assembly and functional coupling of the enzyme but does not interact directly with the catalytic subunits; the C-terminal domain (CTD) can inhibit the enzyme by interacting with multiple catalytic subunits [5, 6]. This ε-mediated regulation is specific to bacterial ATP synthases and is not observed in the mitochondrial homologue. ATP synthase has emerged as a target for antibacterial drugs, as shown by recent FDA approval of bedaquiline to treat drug-resistant tuberculosis [7]. Thus, targeting ε's inhibitory role for drug discovery could yield antibacterials that do not inhibit the mitochondrial ATP synthase. With the isolated catalytic complex (F_1), ε becomes a dissociable subunit. However, with ε bound to F_1, the εCTD can undergo a dramatic conformational change, partially inserting into the enzyme's central cavity and forming an inhibitory state that is unlikely to dissociate directly [6, 8]. We use BLI to measure kinetics of F_1/ε binding and dissociation, and indirectly, to examine allosteric effects of catalytic-site ligands on ε's conformation.

In our system, ε was chosen for immobilization on the sensor surface since BLI signal (like SPR) is sensitive to the mass of the molecules binding at the surface. The ε subunit is small (~15 kDa) relative to the main F_1 complex (~347 kDa). Thus, a larger BLI signal will result from binding of F_1 to immobilized ε. In order to monitor F_1/ε dissociation, which can be very slow, ε must be strongly immobilized. Thus we chose to biotinylate ε and immobilize it on streptavidin-coated biosensors. Proteins can be biotinylated by (i) random modification of surface lysines [9], (ii) reaction of a unique native or engineered cysteine with a biotin-maleimide reagent [10] or (iii) genetically adding a specific biotin-acceptor

peptide that is enzymatically biotinylated during *in vivo* expression of the tagged protein [11]. In our system, ε is biotinylated using method (iii) [8]. Once biotin-tagged ε is immobilized on streptavidin sensors, BLI can measure the binding and dissociation of F_1 that has been depleted of subunit ε (F_1(-ε)). For the experiments described here, preliminary assays had been done to determine reasonable amounts of the biotinylated protein to immobilize on the sensors. This can vary, depending on the molecular weight of the protein and its binding partner, but the goal is to determine a minimal amount of immobilized protein that provides (i) acceptable signal-to-noise for binding kinetics with a low concentration of the binding partner (below K_D) and (ii) minimal distortion of binding kinetics with near-saturating concentration of the binding partner. Also, stoichiometry of biotinylation may vary (but avoid >1 mol biotin/mol protein), so some initial assay may be needed for each new lot of biotinylated protein to confirm that a consistent BLI signal can be achieved during immobilization on the streptavidin-coated sensors.

4.3 Results

Real time binding and dissociation BLI kinetics are shown in **Figure 4.3**. This experiment was done with assay buffer in association and dissociation. This experiment was started with a 10 min baseline step since the sensors had been prewet only briefly. Next, biotinylated ε was loaded on the sensors. No detectable dissociation of ε occurred throughout all remaining steps as seen from the reference curve (G) which had no binding partner added. A second reference sensor (H) was devoid of immobilized protein and showed low nonspecific binding of the binding partner. Various concentrations of F_1(-ε) were used in the association step for sensors A-F in order to fit results globally and get the best values for k_a, k_d, and K_D. Results were processed as in the protocol, yielding the data traces (blue) in **Figure 4.4**. In this case, reference sensor trace H was subtracted from sample traces to correct for nonspecific binding of the binding partner and system signal drift. In the data analysis step, all curves were globally fit with a 1:1 model (single k_a, single k_d); the "Global (Full)" fit assumes complete dissociation of the binding partner (signal will return to zero at infinite time) (**Figure 4.4**, red). Note that, for the two highest concentrations of F_1(-ε), there are small but significant deviations of the data from the global, 1:1 model. Low levels of immobilized ligand (biotinylated "ε" subunit) were used, and the fit was not improved by including a mass transport factor in the model (not shown). However, F_1(-"ε") is a large complex (~350 kDa), and other experiments (not shown) suggest that these deviations are due to reduced binding accessibility of a fraction of immobilized ligand; *i.e.* an F_1 bound to one "ε" may sterically hinder access to another biotinylated "ε" bound on the same streptavidin tetramer.

Figure 4.5 shows a different experiment in which the enzyme was bound to sensor-immobilized ε in the presence of 1 mM ATP/EDTA; this predisposes most F_1/"ε" complexes to assume the noninhibitory conformation, which dissociates readily [8]. Sensors were then moved to dissociation wells containing assay buffer with different ligands. This demonstrates the effects of different ligands on the conformation of ε. For example, exposure to MgADP/Pi dramatically slowed net dissociation, indicating that ε shifted conformation to the tightly-bound, inhibitory state. Complex dissociation kinetics were observed since different ligands caused different shifts in the fraction of F_1.ε complexes with ε in the active (dissociable) or inhibitory (nondissociable) conformations. It is also possible that substantial conformational changes of bound proteins contribute directly to changes in BLI signal but, in our studies, this appears to be negligible compared to the signal for binding/dissociation of the large F_1 complex (see Shah *et al.* [8], Figure 4.5D; transition to curves 3 and 6 show very similar behavior, although their conditions favor distinct conformations of bound F_1). The Data Analysis software was not designed for such complex dissociation kinetics. Thus, we exported the data to text files for nonlinear regression analysis with other software.

4.4 Discussion

Currently available instruments for BLI allow significant throughput and flexibility in assays for biomolecular interactions. Various solution samples are dispensed in wells of a black microtiter plate, and a set of parallel BLI sensors are programmed to move back and forth between columns of wells on the plate. The samples are stirred by orbital shaking throughout the assay. The system used here has 8 sensors and uses a 96-well sample plate, but another system uses 16 sensors and a 384-well sample plate. Thus, interaction between a sensor-immobilized biomolecule and its binding partner in solution can be tested under different conditions with multiple sensors in parallel. For example, in the first assay presented here with the immobilized inhibitory ε subunit, interactions were measured with six different concentrations of the enzyme (binding partner) in parallel (**Figures 4.3** and **4.4**). This allowed a global analysis to determine a single pair of rate constants (k_a, k_d) for net binding and dissociation, and thus an equilibrium dissociation constant ($KD = k_d/k_a$), which agrees closely with the inhibitory constant (K_I) determined from solution assays of enzyme inhibition by ε [8]. A second type of experiment (**Figure 4.5**) demonstrated that BLI can also monitor allosteric effects of small ligands on the interactions between two proteins; the effects of different ligands were compared in parallel. There are limitations for detecting effects of allosteric ligands, since BLI signal depends on the mass of the binding molecule, and can directly detect binding of small compounds under optimized conditions [13]. However, in the assay of **Figure 4.5**, the binding partner, F_1, was a large protein complex (~347 kDa), so the BLI signal for its binding/dissociation was not significantly affected by additional binding of small ligands such as ATP (~500 Da) to the F_1 complex. This was confirmed with assays in which these ligands did not affect the BLI

signal for F_1 bound to a truncated form of ε lacking the inhibitory CTD [8]. Thus, assays of allosteric effects must consider the mass of the allosteric ligand relative to the masses of the interacting proteins, and preferably include controls to test for direct BLI response to the binding of the ligand.

Note that certain steps and modifications in the experimental protocol can be critical for achieving better results and more accurate analysis. For example, as in the protocol described here (see steps 1.2.3, 1.2.5), an assay intended for global analysis of binding and dissociation rate constants should include an extra baseline step (see step 1.2.3) in a new column of buffer wells (**Figure 4.2**, column 4) before the Association step, and the sensors should be returned to that same column of buffer wells for the Dissociation step (see step 1.2.5). Having each sensor in the same well (with the same optical properties) before and after the Association step can improve the inter-step correction (step 3.4) for Association/Dissociation steps, and this facilitates global kinetic fitting of multiple data traces (as in **Figure 4.4**). Also, for assays that are more preliminary than shown here, the program has an option to shorten or extend the time of any step during the assay (while it is the active step). This is useful, for example, if the optimal loading signal is not already known, or if more time is needed to allow enough dissociation to achieve a good fit for the dissociation rate.

Nonspecific binding of the binding partner to the sensor surface can be a problem for label-free methods such as SPR and BLI. In our assays, this was effectively minimized by including BSA in the assay buffer. As in immunoblotting protocols, proteins other than BSA could be used, and low concentrations of detergent may also minimize nonspecific binding (Tween20 is used in kinetics buffer from the supplier). Even with minimal

nonspecific binding, most assays should include at least one control sensor without immobilized protein but with the highest concentration of binding partner in the Association step (see **Figure 4.3**, sensor H); subtraction of the residual nonspecific binding (and its decay during the Dissociation step) can significantly improve kinetic analyses for the specific binding/dissociation being studied. On the other hand, once initial assays confirm that the biotinylated protein remains stably bound after the Loading step (see **Figure 4.3**, sensor G), that control can be omitted and that sensor can be used for a sample condition.

For robust determination of association and dissociation rate constants using BLI, multiple concentrations of binding partner should be used and all the data traces should be fit by global analysis, if possible (as in **Figures 4.3** and **4.4**). Ideally, the range of concentrations should span ~10-fold above and below the estimated K_D. In our case, with a high-affinity interaction (K_D =0.25 nM), the signal-to-noise was poor for binding kinetics with sub-K_D concentrations. Thus, concentrations of binding partner above the K_D were used such that significant changes in observed rates and levels of binding were obtained (see **Figure 4.3**). Also, a long dissociation step was used to improve the confidence in fitting the slow dissociation rate. With high affinity interactions, it is also possible that slow dissociation is exaggerated by rebinding during the dissociation step, since BLI assays are done in a stirred sample rather than continued flow over the sensor, as for SPR. This potential artifact can be tested with assays in which the dissociation buffer contains a 'sink' of excess competitive protein that binds dissociated binding partner and prevents it from rebinding to the sensor-immobilized protein [14]. In our system, this was done by comparing results with and without nonbiotinylated (>10-fold above K_D) in the dissociation well, and we

confirmed that rebinding was not a significant problem [8]. Finally, if sets of kinetic results are not fit well by global analysis (1:1 or 2:1 models available), there are other analysis options for troubleshooting. For example, instead of choosing "Global (Full)" (in step 4.2), "Local" can be chosen to fit each sensor trace independently. If binding follows a simple 1:1 model, plotting the observed binding rates (k_{obs}) *vs* the concentrations of binding partner should show a linear dependence, with the slope equal to the second-order, intrinsic binding rate. The Analysis tab of the software has an "X-Y graph" window that allows quick visualization of this relationship.

One limitation of the instrument that we used is the available temperature range. With a range of 2 °C above ambient temperature to 40 ºC, only molecules that are stable in that range can be used. Moreover, thermodynamic analysis is limited by the narrow temperature range. Another general limitation is that the maximum assay time is ~4 hr; after this, artifacts develop due to evaporation of samples from the open microtiter plate.

BLI involves a relatively simple arrangement compared to SPR. The sensors are moved between columns of wells with fixed volumes, rather than a constant flow of sample over the sensor. Although not as sensitive as SPR, BLI is less affected by changes in refractive index due to changes in sample composition. Overall, with this relative ease of use and flexibility of the instrument in shifting between assay conditions, BLI provides a versatile tool for *in vitro* assays of biomolecular interactions.

4.5 Protocol

1. Programming the Instrument for BLI Assay

Turn on the instrument at least one hour in advance to allow the lamp to warm up; this is necessary to minimize noise and drift in optical signal during the experiment. Set the desired temperature via the instrument tab to prewarm the sample plate holder. Then set up the experimental design in the Data Acquisition software. Select "New Kinetics Experiment" in the Experiment Wizard tab. This presents a tabbed menu with all steps that must be defined.

1.1. Plate Definition

Define the columns to be used on the 96-well sample plate. Assign columns to contain buffer, immobilized protein or binding partner. For each association well, enter the concentration of binding partner to be used. Note: the plate definition shown in **Figure 4.2** has options for distinct assays.

1.2. Assay Definition

Define all steps needed for the assay. These include (i) Baseline (several), (ii) Loading, (iii) Association and (iv) Dissociation of binding partner. Then, as described below, link individual assay steps with columns of wells on the sample plate by selecting the assay step and then double clicking on the respective column. This programs the sensors to be moved from one column of wells to the next during the assay.

1. **Baseline**

Begin with a brief baseline step (≥60 sec), with sensors in assay buffer (**Figure 4.2**, column 1), to establish initial BLI signals in the 96-well plate.

2. **Loading** (immobilizing the biotinylated protein on the sensors)

Assign sensors to wells that will contain the biotinylated protein (**Figure 4.2**, column 2). Use the threshold function to achieve a predetermined level of binding (see Introduction). Set the threshold option so that all sensors will be moved to the next column of wells when any one of the sensors reaches the threshold.

3. **Baseline**

Include another baseline step in buffer (**Figure 4.2**, column 3; typically >5 min) to wash away nonimmobilized biotinylated proteins from the sensors and establish new, stable baseline signals. For basic binding/dissociation assays only (as in **Figure 4.3**), include an extra baseline step (60 sec) with sensors in new wells of buffer (**Figure 4.2**, column 4) before the Association step.

4. **Association** (of the binding partner to the immobilized protein)

For a basic binding/dissociation assay (as in **Figure 4.3**), select a range of concentrations of binding partner to be used for different sensors/wells (**Figure 4.2**, column 5). Adjust the step time so that at least a saturating concentration of the binding partner should approach equilibrium binding signal. For an assay to test allosteric effects of small ligands on dissociation of the protein-protein complex (as in **Figure 4.5**), select a single high concentration of binding partner (~10-fold above the estimated K_D) for use in all association wells.

5. **Dissociation** (of the binding partner)

For a basic binding/dissociation assay only (as in **Figure 4.3**), designate the sensors to return to column 4 (**Figure 4.2**), the same buffer wells as used for the extra baseline before Association. For an assay to test allosteric effects of small ligands, instead designate

sensors to move to column 6 (**Figure 4.2**), where each well can contain buffer plus different allosteric ligands.

1.3. Sensor Assignment

Indicate the locations in the sensor tray that will contain prewetted sensors for the assay. Identify any empty positions since the experiment will fail if no sensors are picked up.

1.4. Review Experiment

Visualize all planned steps to check for mistakes and go back to correct them.

1.5. Run Experiment

Enter necessary details, including location of data files. Enter the desired temperature for the experiment. If sensors still require prewetting, select the option to delay starting the experiment. Finally, once all sample preparation is complete (step 2) and both the sample plate and sensor tray are loaded in the instrument, click the Go button to run the assay.

2. Sample Preparation

1. Prepare an appropriate assay buffer. Buffer used for experiments shown in **Figures 4.3** and **4.5**: 20 mM MOPS (3-(N-Morpholino)propanesulfonic acid), Tris (Tris(hydroxymethyl)amino-methane) (added to adjust pH to 8.0), 50 mM KCl. Include BSA (bovine serum albumin, fatty-acid free, 0.5 mg/ml final) in the buffer for all assay steps and for all dilutions of the biotinylated protein or binding partner to minimize nonspecific binding of proteins to the sensors.

2. Dilute the biotinylated protein (ε) in assay buffer to an appropriate concentration (see Introduction).

3. Prepare dilutions of the binding partner (F_1(-ε)) in assay buffer (see Discussion for range of concentrations to use).

4. Prewet the streptavidin-coated sensors for at least 10 min to remove their protective sucrose coating. Remove the sensor-containing rack from the sensor tray and insert a 96-well plate in the bottom of the tray, sliding one corner of the plate into the orienting notch on the tray. For the column of sensors to be used, add 200 µl of assay buffer per well in that column of the 96-well plate. Return the rack of sensors to the tray in the correct orientation (with tabs in slots).

5. As assigned during programming in Step 1, fill wells of the sample plate with assay buffer or the appropriate protein dilutions, as in **Figure 4.2**. Avoid introducing bubbles, as they can cause noise in the optical signal. Include one or more reference wells that omit either (i) biotinylated protein or (ii) binding partner.

6. Open the door of the instrument and insert the sensor tray onto the stage (left), with the tray's tabs inserted into the slots of the stage. Insert the sample plate into the plate holder (right); make sure that the plate is seated flat and in the correct orientation, as indicated on the plate holder. Close the door and start the assay from the Data Acquisition program (step 1.5).

3. Data Processing

1. After the assay has run, open the Data Analysis software and load the folder containing the data. Click the "Processing" tab to see a stepwise Processing menu (at left) and the raw kinetic data, with each sensor (A-H) assigned a different color (see **Figure 4.3**).

2. Under "Data Selection", click the "Sensor Selection" button. On the "Sample Plate Map", designate the wells for 1 or 2 control sensors (G, H in assay of **Figure 4.3**) as reference wells. On the Processing menu, check the "Subtraction" box and select "Reference Wells" to subtract reference signal (single or averaged) from every other sensor's signal.

3. Align all traces to Y=0 by using the "Align Y Axis" step. Select "Baseline" as the alignment step (this being the last baseline before the Association step). For "Time Range", enter the last 10 sec of that baseline (*i.e.* 50-60 sec for a 60-sec baseline, as in **Figure 4.3**).

4. Check the "Inter-step Correction" box to minimize signal shifts between the Association and Dissociation steps. Select align to Baseline or Dissociation.

5. Select Savitzky-Golay filtering function in most cases and click "Process Data!" to proceed. Visually inspect the final processed data (lower right panel). With assays intended for global data analysis (as in **Figure 4.4**), if signal traces show a significant shift between Association and Dissociation steps, change the selection of Dissociation or Baseline for the "Inter-step Correction" and reprocess the data before proceeding to Data Analysis.

4. Data Analysis

Click the "Analysis" tab in Data Analysis to begin. Note: the example steps below are for global analysis of multiple binding/dissociation curves (as in **Figure 4.3**).

1. For "Step to Analyze", choose Association and Dissociation. For "Model", select 1:1. Note: other limited options are available.

2. For "Fitting", choose Global (Full). For "Group By" select Color (as on the graph). Select "Rmax Unlinked By Sensor" to allow independent fitting of Rmax (maximal signal response upon saturating binding of the partner to the immobilized protein). Note: we do this for most assays, as sensors vary slightly in the amount of protein immobilized (see **Figure 4.3**, Loading).

3. On the table shown, make sure all sensor traces to be analyzed have the same color, so they will be analyzed as a global set. If needed, select one or more sensor traces to omit

from global fitting: under the "Include" column, right-click on the desired sensor position and select "Exclude Wells".

4. Click "Fit Curves!" to start the nonlinear regression analysis. Examine the fitting results, which include (i) overlay of regression curves with sensor data traces (as in **Figure 4.4**), (ii) plots of fitting residuals, and (iii) a table with determined parameter values (rate constants, Rmax, K_D) and statistics (standard errors for parameters, Chi-squared, R^2).

5. Under "Data Export", save fitting results by clicking "Export Table to .csv File". For graphing or further analysis of data/fitted curves with other software, click "Export Fitting Results" to save each sensor's data and fitted curve in a text file.

4.6 Figures

Figure 4.2

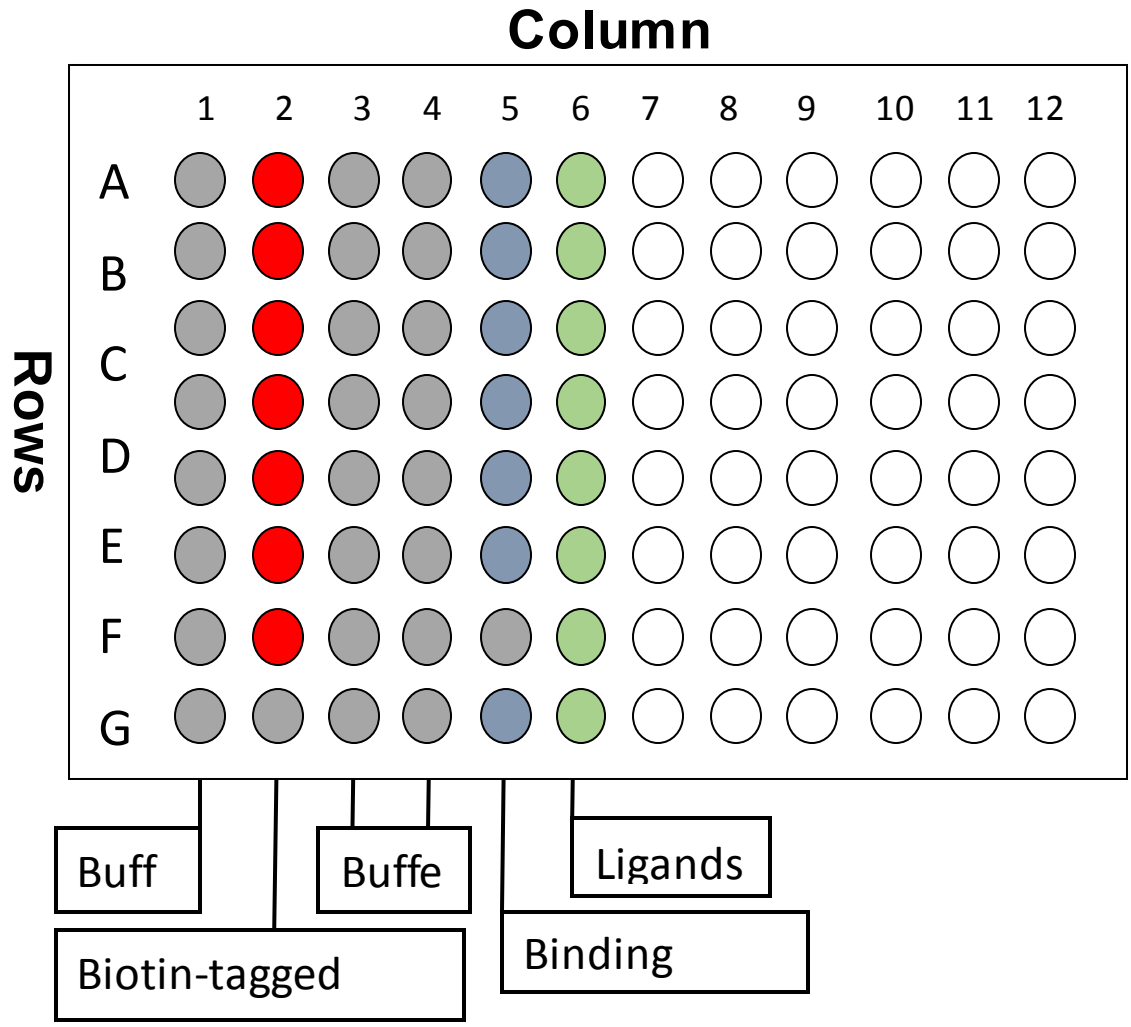

Figure 4.2. Schematic arrangement of samples in the 96-well sample plate. The sensors will be moved in parallel from column to column and can be moved either left or right as defined in a particular assay protocol. Wells with grey color represents assay buffer with and without ligands whereas red, blue and green represent immobilized protein, binding partner and ligands, respectively.

Figure 4.3

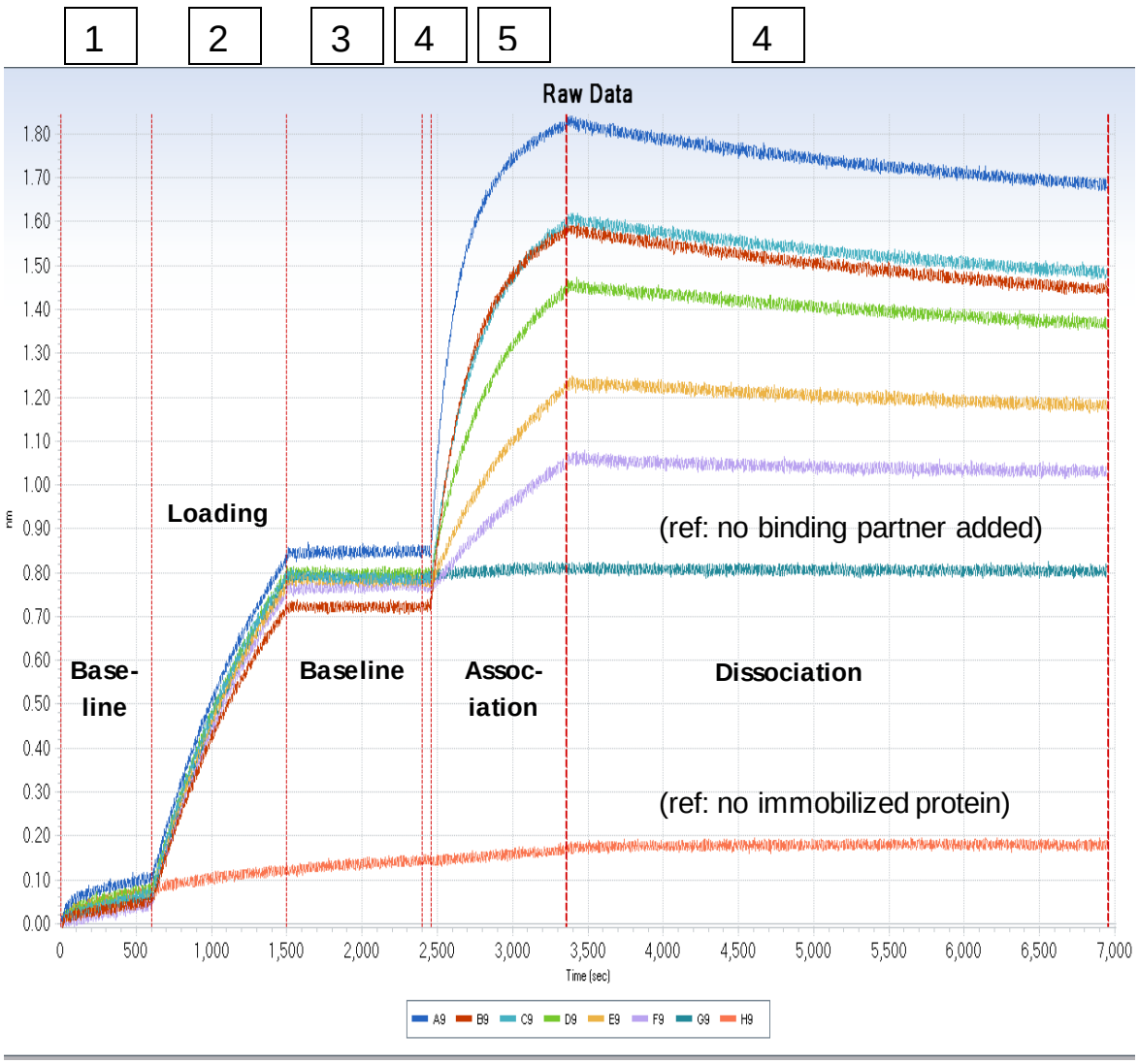
1
2
3
4
5
4
Raw Data
nm
1.80
1.70
1.60
1.50
1.40
1.30
1.20
1.10
1.00
0.90
0.80
0.70
0.60
0.50
0.40
0.30
0.20
0.10
0.00
Loading
(ref: no binding partner added)
Base-
line
Baseline
Assoc-
iation
Dissociation
(ref: no immobilized protein)
0
500
1,000
1,500
2,000
2,500
3,000
3,500
4,000
4,500
5,000
5,500
6,000
6,500
7,000
Time (sec)
A9
B9
C9
D9
E9
F9
G9
H9

Figure 4.3. Screen capture showing raw data from a BLI assay. Vertical red lines indicate movement of sensors between assay steps of the protocol. Step types are denoted on the image. Locations of buffer and samples are as shown in **Figure 4.2**. As noted by numbers along the top of the graph, streptavidin-coated sensors were moved between different columns of the sample plate in the following order: 123454. The legend below the graph indicates the color for each sensor's data trace. In the Loading step, each sensor except H was incubated with 50 nM biotinylated "ε" subunit. In the Association step, sensors were incubated with nM concentrations of "ε"-depleted F_1: 30 (A, H), 20 (B), 15 (C), 10 (D), 5 (E), 2.5 (F), 0 nM (G).

Figure 4.4

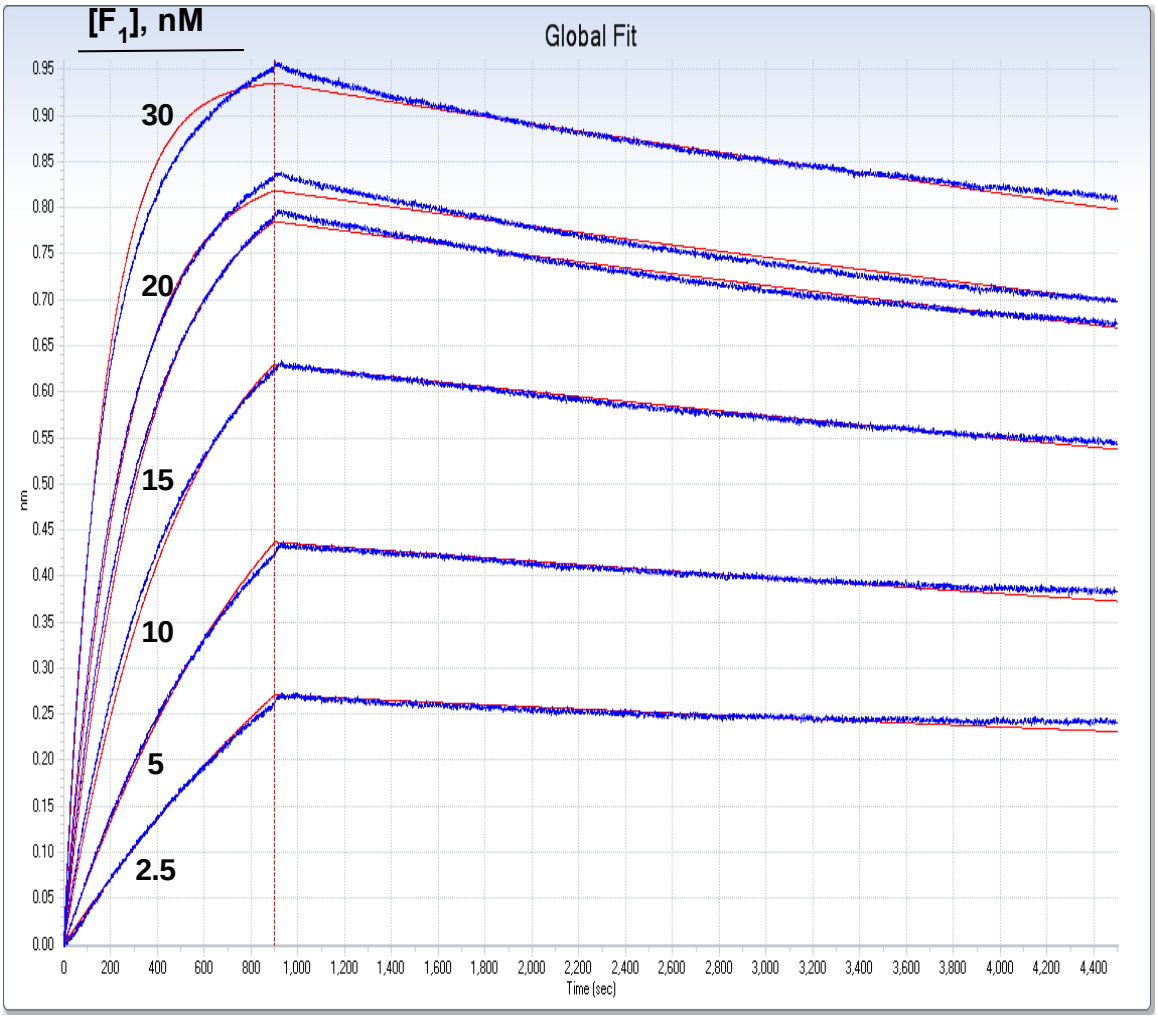

Figure 4.4. Screen capture of the analyzed data from the BLI assay of Figure 4.3. The data was processed and fitted as described in the text. Only Association and Dissociation steps are shown, divided by a vertical red line. The processed data curves are blue; the nonlinear regression fits from 1:1 global analysis are shown in red. Global fitting results[8]: ka = 2 x 105 m-1s-1 (±0.1%), kd = 4.8 x 10-5 s-1 ("±"0.1%), yielding KD = 0.24 nM. Goodness of fit: R2 = 0.999054. The maximal binding parameter (Rmax) was fit separately for each sensor, with mean value = 0.813 nm ("±"0.0803).

Figure 4.5

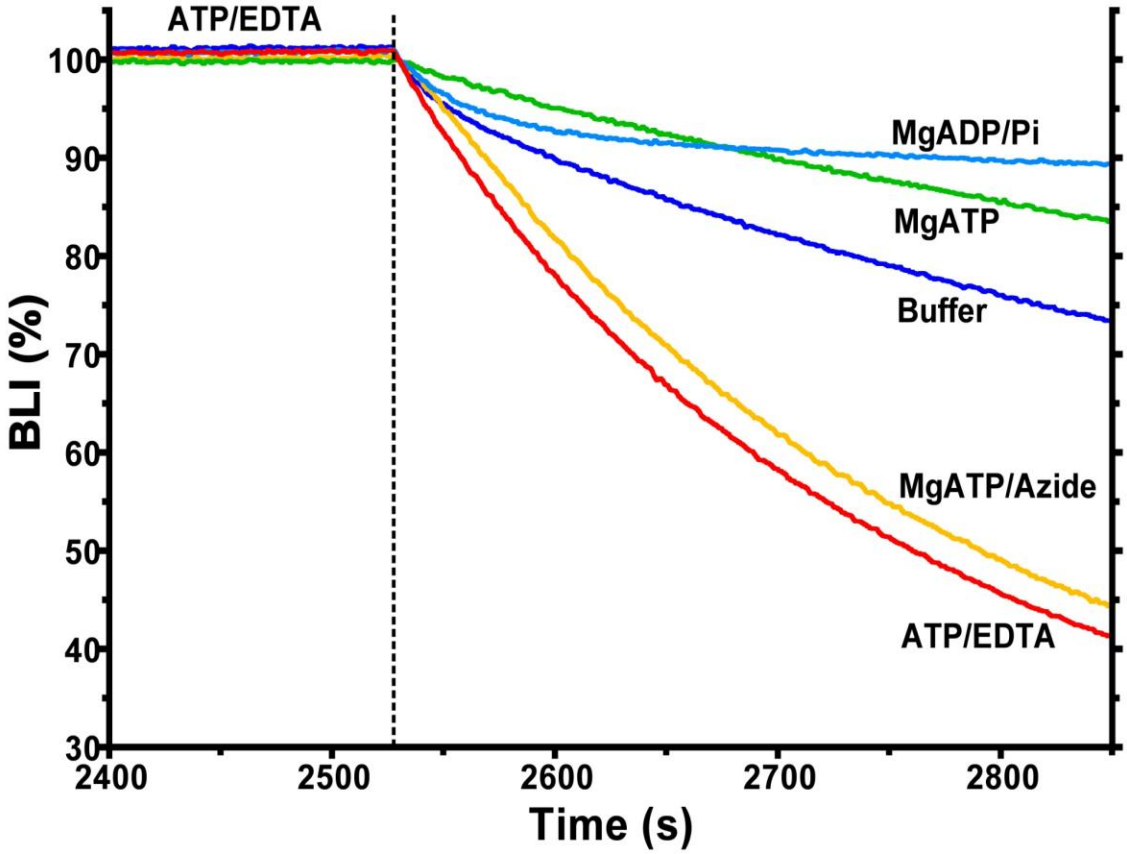
ATP/EDTA
MgADP/Pi
MgATP
Buffer
MgATP/Azide
ATP/EDTA
BLI (%)
100
90
80
70
60
50
40
30
2400
2500
2600
2700
2800
Time (s)

Figure 4.5. Results from a BLI assay showing allosteric effects of ligands on ε's conformation. F_1(-ε) was bound to sensor-immobilized ε in the presence of 1 mM ATP/EDTA. The end of the association phase and a portion of the dissociation phase are shown. During the dissociation step, distinct ligands for F_1 catalytic sites (listed for each trace) were included to observe their allosteric effects on dissociation of F_1 from sensorbound ε.

4.7 Acknowledgements

We thank FortéBio for providing graphics used in **Figure 4.1**. This work was supported by NIH grant GM083088 to T.M.D.

4.8 References

1. Nirschl, M., Reuter, F., Voros, Janos. Review of Transducer Principles for Label-Free Biomolecular Interaction Analysis. *Biosensors.* **1**, 70-92 (2011).
2. Homola, J. Present and future of surface plasmon resonance biosensors. *Anal. Bioanal. Chem*. **377**, 528-539 (2003).
3. Piehler, J., Brecht, A. & Gauglitz, G. Affinity Detection of Low Molecular Weight Analytes. *Anal. Chem*. **68**, 139-143, doi:10.1021/ac9504878 (1996).
4. Duncan, T. M. in *The Enzymes, vol. XXIII: Energy Coupling and Molecular Motors* Vol. 23 eds D.D. Hackney & F. Tamanoi. Elsevier Academic Press, 203-275 (2004).
5. Feniouk, B. A., Suzuki, T. & Yoshida, M. The role of subunit ε in the catalysis and regulation of F_OF_1-ATP synthase. *Biochim. Biophys. Acta*. **1757**, 326-338 (2006).
6. Cingolani, G. & Duncan, T. M. Structure of the ATP synthase catalytic complex (F_1) from *Escherichia coli* in an autoinhibited conformation. *Nat. Struc. Mol. Biol.* **18**, 701-707, doi:doi:10.1038/nsmb.2058 (2011).
7. Mirsaeidi, M. After 40 years, new medicine for combating TB. *Int. J. Mycobacteriol.* **2**, 1-2 (2013).
8. Shah, N. B., Hutcheon, M. L., Haarer, B. K. & Duncan, T. M. F_1-ATPase of Escherichia coli: The ϵ-inhibited state forms after ATP hydrolysis, is distinct from the ADP-inhibited state, and responds dynamically to catalytic site ligands. *J. Biol. Chem*. **288**, 9383-9395 (2013).

9. Burgess, T. L., Ross, S. L., Qian, Y.-x., Brankow, D. & Hu, S. Biosynthetic Processing of neu Differentiation Factor: glycosylation, trafficking, and regulated cleavage from the cell surface. *J. Biol. Chem*. **270**, 19188-19196 (1995).

10. Loo, T. W. & Clarke, D. M. Membrane Topology of a Cysteine-less Mutant of Human P-glycoprotein. *J. Biol. Chem*. **270**, 843-848 (1995).

11. Tsao, K.-L., DeBarbieri, B., Michel, H., and Waugh, D. S. A versatile plasmid expression vector for the production of biotinylated proteins by site-specific, enzymatic modification in *Escherichia coli*. *Gene*. **169**, 59-64 (1996).

12. Dayne, D. BioLayer Interferometry (BLI) – How Does it Work? FortéBio newsletter: *In Interactions*. **5**, 8-9 (2012).

13. Wartchow, C. *et al*. Biosensor-based small molecule fragment screening with biolayer interferometry. *J. Comput. Aided Mol. Des*. **25**, 669-676, doi:10.1007/s10822-011-9439-8 (2011).

14. Abdiche, Y., Malashock, D., Pinkerton, A. & Pons, J. Determining kinetics and affinities of protein interactions using a parallel real-time labelfree biosensor, the Octet. *Anal. Biochem*. **377**, 209-217, doi:http://dx.doi.org/10.1016/j.ab.2008.03.035 (2008).

Chapter Five

Targeting ε inhibition in *Mycobacterium tuberculosis* ATP synthase

5.1 Introduction

Mycobacterium tuberculosis (Mtb) is a pathogenic bacterium that has targeted humans from ancient times [1]. Even now, it infects 9 million people and kills between 1-2 million of them per year [2]. The pathogen is an obligate aerobe that primarily targets the lungs, causing pulmonary tuberculosis [3]. As the infection is mounted, the body responds via macrophages to counter the pathogen. Macrophages normally eliminate pathogens by engulfing and trapping them in an intracellular organelle called the phagosome. This phagosome then fuses with the lysosome and gives rise to a phagolysosome. The pathogen is killed by a combined effect of low pH and reactive oxygen species in the phagolysosome. Mtb is able to survive and even thrive within the macrophages as it prevents the fusion of phagosome with the lysosome [4, 5]. As the host senses this failure, the next step it takes is to limit the infection to a small area. As a result, hordes of different types of immune cells approach the infected macrophage and bind to it. Newer immune cells keep binding on top of the old ones and give rise to a nodule [6]. This is the characteristic nodule that is visible in chest X-rays and contains viable mycobacteria. Within the nodules, the pathogens experience scarcity of nutrition and thus undergo changes in the cellular composition and metabolism and become dormant [7]. At this stage, the infection gets limited and a balance is established between the pathogen and the immune system. If the immunity of the host weakens due to factors like stress or malnutrition, the bacteria become active and propagate. As a result, outside treatment is necessary to completely eliminate the pathogen from the body. At any given time, about 90% of infected individuals do not show any symptoms as the immune system is able to limit the infection [8]. However, in the remaining patients with active tuberculosis, the death rate is around 66% in the absence of

an effective treatment [9]. Development of antibiotics against Mtb allowed infections to be controlled and the number of deaths to be reduced steadily. The current regimen of treatment includes a cocktail of drugs given over a lengthy period of many months [10]. The long treatment duration is due to the fact that the current drugs can only target the active Mtb and are ineffective against the dormant pathogens. The pathogen cycles between dormant and active states. The patient has to maintain a lethal concentration of the drugs in the blood and play a waiting game with the pathogen, killing those that become active. This strategy is effective but is very time consuming as not all mycobacteria become active at the same time. This long treatment duration along with the indiscriminate use of antibiotics and the pathogen's own ways to counter the drugs are major factors that have led to emergence of multiple and in some cases, extreme drug resistance [11]. As a result, there is a dire need to develop new drugs that target the drug resistant strains.

For the past many years, researchers have focused on developing new classes of antibiotics that are potent against drug resistant Mtb. Recently, a new class of drugs, diarylquinolines, was discovered that can target the active and the dormant mycobacteria that are resistant to all the other treatments [12-14]. This drug was found to act by inhibiting proton transport by the **c**-ring of mycobacterial ATP synthase and it has been found to be active even against dormant mycobacteria [15, 16]. Its approval was fast-tracked by the US Food and Drug Administration (FDA) and the drug is commercially available (Bedaquiline; brand name Sirturo) [17]. Since Mtb is an obligate aerobe, the ATP synthase is essential for its viability [28]. The fact that the drug is able to kill dormant mycobacteria shows that, even in the dormant state, there is some basal amount of metabolism carried out by the bacteria and ATP synthase plays an important role in it. This is exciting news as

the drugs that target the enzyme do not have to wait for the dormant mycobacteria to become active in order to kill them. As a result, the treatment time can be shortened considerably.

The discovery and approval of Bedaquiline has provided the first novel class of drug against *M. tuberculosis* after forty years. While this has come as a respite for patients of drug resistant pulmonary tuberculosis, there is a caveat to using it for other diseases. As compared to the mitochondrial ATP synthase, the mycobacterial enzyme is >20,000-fold sensitive to Bedaquiline, but the drug's efficacy is limited to *M. tuberculosis* [18] and it is not potent against other bacterial pathogens [19]. To overcome this, others have tried modifying Bedaquiline to a form that successfully targets the ATP synthase of gram-positive pathogen *Staphylococcus aureus* [19]. However, the tradeoff of this modification has been the loss of selectivity of the drug for the mycobacterial enzyme (just over 10-fold higher than mitochondrial ATP synthase). Thus, while Bedaquiline can serve as a last resort drug against *M. tuberculosis*, against other pathogens, the potential for cross-reacting with mitochondrial ATP synthase is high. To reduce the potential for cross-reactivity, subunits that do not play the same role in bacterial and mammalian enzyme could be targeted.

As discussed in previous chapters, *in vivo* deletion of the entire C-terminal domain of *E. coli* ε subunit does not affect the function of enzyme with minimal effect on the growth. ATP synthase is dispensable in *E. coli* as it is a facultative anaerobe and can grow by fermentation. In contrast, *M. tuberculosis* is an obligate aerobe and grows only via respiration. As a result, ATP synthase is essential for viability. The mycobacterial ATP synthase has significant homology with the *E. coli* ATP synthase. The α and β subunits of mycobacterial ATP synthase contain >50% sequence homology with the *E. coli* enzyme.

In addition, functional sequence motifs such as the P-loop for binding of nucleotide, the acidic residue crucial for nucleophilic attack, and the DELSEED sequence are conserved in mycobacterial enzyme [7].

The enzyme may be inhibited by ADP as residues important for ADP inhibition and the release from inhibition are conserved [7]. Current data does not confirm whether the enzyme is also inhibited by the ε subunit. However, the N-terminal domain of ε in mycobacterial ATP synthase is conserved as compared to *E. coli* [7]. Moreover, the ε subunit of *M. tuberculosis* was found to block ATPase activity of F_1(-δε) of *Bacillus PS3* without binding ATP [20]. Thus, it is highly possible that the ε subunit is inhibitory in Mtb. A concern towards this assumption is that the ε subunit in Mtb is 17 amino acids shorter than the ε subunit of *E. coli* and based on modeling, most of the truncation is seen in the CTD. As the CTD is primarily responsible for inhibition, this poses a question against the efficacy of the Mtb ε to inhibit the enzyme. However, my data have shown that a shorter *E. coli* ε can inhibit the enzyme more strongly. So we cannot discard the possibility of strong ε-mediated inhibition in Mtb enzyme.

Studies have indicated that a tight regulation of the mycobacterial ATP synthase in ATP hydrolysis direction may exist [21]. It appears that the primary role of the enzyme is synthesis of ATP and hydrolysis is blocked. The apparent tight regulation is understandable considering the fact that, when *M. tuberculosis* resides in the nodules within human lungs or within the macrophages, the availability of nutrients is scarce. As a result, the bacterium should minimize ATP hydrolysis by the ATP synthase to ensure enough intracellular ATP is available to carry out physiological process vital for viability. In such conditions, interfering with ε's normal interactions within the enzyme could disrupt its inhibitory role

and reduce viability of the pathogen. Disruption of normal ε interactions may either lead to stronger inhibition of ATP synthesis activity, similar to what was observed in *E. coli*, or lead to reduced inhibition of ATP hydrolysis, with both scenarios leading to lower intracellular ATP. This could be fatal for the pathogen, especially in the dormant state.

Targeting ε inhibition of ATP synthase in Mtb can involve multiple strategies. The idea would be to either increase ATP hydrolysis or decrease ATP synthesis - both resulting in low availability of ATP. To increase ATP hydrolysis, small-molecule compounds that could bind to εCTD and prevent it from adopting the extended conformation could be developed. The small-molecule compounds may stabilize the interaction of εCTD with εNTD or they may act as a bulky moiety that blocks the entry of εCTD into the central cavity. Either way, the ATP hydrolysis activity may get activated, quickly depleting intracellular ATP pools. Reduction of ATP synthesis may be a more difficult approach as it would involve stabilizing the extended conformation of εCTD. This can be effected by a compound that can bind tightly with εCTD and the γ, α or β subunits. Such a compound may be generated by a Fragment-based approach [22]. Here, the enzyme may either remain inhibited for longer durations or become permanently inhibited. As a result, ATP synthesis activity may be reduced, affecting viability.

5.2 Current *M. tuberculosis* project

In order to develop an effective drug that carries out the above mentioned function(s), it is important to confirm that εCTD can inhibit the enzyme and that disruption of εCTD's interaction with Mtb enzyme leads to a growth defect. While working in the Duncan lab, I had the opportunity to start working in this direction. I hypothesized that deletion of the entire CTD of ε in mycobacterial ATP synthase would lead to increased hydrolysis of intracellular ATP and diminish growth. To test that, two plasmids encoding sequences of epitope-tagged ε subunit (FLAG tag, DYKDDDDK) [23] of *M. tuberculosis* ATP synthase were designed (by Tom Duncan) and obtained commercially (Genscript). Plasmids either encoded the entire *M. tuberculosis* H37Rv ε subunit (pUC57+atpC2) or its N-terminal domain (pUC57+atpC89s, residues 1-88). An integration-proficient vector, pMBC1260, which contains mycobacteriophage L5 integration sequences and allows integration into the mycobacterial chromosome [24], was provided by our collaborator, Dr. Kathleen McDonough from Wadsworth center, Albany. I transformed the ε-encoding plasmids and pMBC1260 into DH5α *E. coli* cells, and prepared plasmid DNA. Restriction digestion was used to remove the *atpC2* and *atpC89s* genes from pUC57 plasmid. They were inserted into pMBC1260 to obtain pMBC1260+atpC2 or pMBC1260+atpC89s, followed by transformation into DH5α cells. These constructs place the atpC gene after a strong constitutive Mtb promoter Rv1485. Thus, it is expected that the Flag-tagged ε (+/- CTD) will be expressed well and assemble into mycobacterial F_OF_1, hopefully in excess of the native ε that is still expressed from the chromosome. In Dr. McDonough's lab, I assisted in transforming pMBC1260, pMBC1260+atpC2, or pMBC1260+atpC89s into *M. bovis* BCG, *M. smegmatis* and a *M. tuberculosis* H37Rv auxotroph (attenuated) and

transformants were isolated in which chromosomal integration of each plasmid was confirmed. *M. smegmatis* is a non-pathogenic, fast growing relative of *M. tuberculosis* that can be grown in biosafety level 1 setting [25, 26]. Proper expression and assimilation of epitope-tagged ε in ATP synthase will initially be confirmed in *M. smegmatis* by immunoblotting, immunoprecipitation and SDS PAGE by the Duncan lab. Later, expression and assimilation will also be confirmed in *M. bovis* BCG and *M. tuberculosis* H37Rv auxotroph.

Dr. McDonough's lab has begun investigating the possible effects of the εCTD truncation on the growth of *M. bovis* BCG and *M. tuberculosis* H37Rv under various conditions. These growth conditions mimic the environmental factors that mycobacteria encounter within host cells/tissue, such as (1) low oxygen concentration, (2) low oxygen concentration with high carbon dioxide, or (3) increased nitric oxide. Preliminary results from these growth tests were mixed. Thus far, the εCTD truncation showed no significant effects on growth under several low oxygen conditions. However, the growth of *M. bovis* BCG expressing ε89S was reduced by the presence of the detergent, sodium dodecyl sulfate, which is thought to reflect a weakened cell wall [29]. This last initial effect is a promising indication of some metabolic defect caused by the εCTD truncation. However, the lack of effect on low-oxygen growth suggests that there is insufficient expression and/or incorporation of the Flag-ε89s into mycobacterial ATP synthases to cause a more significant growth defect; immunoblotting and immunoprecipitation tests will be needed to confirm this. It is possible that alternate molecular biology approaches will be needed to achieve predominant assembly of the Flag-ε (+/– CTD truncation) into mycobacterial ATP synthase. If this can be achieved, and more significant growth defects are observed in the

phenotypic assay, then other biochemical assays could be carried out to determine the effect of the truncation on ATP synthase function. For this, biochemical assays can be carried out using inverted membrane vesicles of *M. bovis* BCG and *M. tuberculosis* H37Rv auxotroph. Rates of ATP synthesis, ATP hydrolysis as well as proton translocation could be measured. The F_1 domain could be isolated from the mycobacterial membranes and further characterized for inhibition by ε [27]. Provided that a definite defect is seen with mutant ε, the next step would be to repeat the same experiments in pathogenic *M. tuberculosis,* and extend phenotypic assays to test for effects of the εCTD truncation on infection and survival of Mtb in a mouse macrophage system.

5.3 References

1. Zink AR, Sola C, Reischl U, Grabner W, Rastogi N, Wolf H, Nerlich AG: Characterization of Mycobacterium tuberculosis Complex DNAs from Egyptian Mummies by Spoligotyping. *Journal of Clinical Microbiology* 2003, 41(1):359-367.
2. CDC: Reported Tuberculosis in the United States. US Department of Health and Human Services, 2013.
3. Mandell G, L., Douglas, R,. Bennett, J, E.: Mandell, Douglas, and Bennett's principles and practice of infectious diseases, 7 edn. USA: Churchill Livingstone/Elsevier; 2010.
4. Houben ENG, Nguyen L, Pieters J: Interaction of pathogenic mycobacteria with the host immune system. *Current Opinion in Microbiology* 2006, 9(1):76-85.
5. Sundaramurthy V, Pieters J: Interactions of pathogenic mycobacteria with host macrophages. *Microbes and Infection* 2007, 9(14–15):1671-1679.
6. Grosset J: Mycobacterium tuberculosis in the Extracellular Compartment: an Underestimated Adversary. *Antimicrobial Agents and Chemotherapy* 2003, 47(3):833-836.
7. Lu P, Lill H, Bald D: ATP synthase in mycobacteria: Special features and implications for a function as drug target. *Biochimica et Biophysica Acta (BBA) - Bioenergetics* 2014, 1837(7):1208-1218.
8. Skolnik R: Global Health 101 2edn. USA: Jones & Bartlett Learning; 2011.
9. Organization WH: Tuberculosis Fact sheet N°104. World Health Organization, 2010.

10. CDC: Core Curriculum on Tuberculosis: What the Clinician Should Know. In, 5 edition. Center for disease control and prevention, USA, 2011.

11. O'Brien RJ, Nunn PP: The Need for New Drugs against Tuberculosis. *American Journal of Respiratory and Critical Care Medicine* 2001, 163(5):1055-1058.

12. Andries K, Verhasselt P, Guillemont J, Gohlmann HW, Neefs JM, Winkler H, Van Gestel J, Timmerman P, Zhu M, Lee E *et al*: A diarylquinoline drug active on the ATP synthase of *Mycobacterium tuberculosis*. *Science* 2005, 307(5707):223-227.

13. Diacon AH, Pym A, Grobusch M, Patientia R, Rustomjee R, Page-Shipp L, Pistorius C, Krause R, Bogoshi M, Churchyard G *et al*: The diarylquinoline TMC207 for multidrug-resistant tuberculosis. *New England Journal of Medicine* 2009, 360(23):2397-2405.

14. Koul A, Vranckx L, Dendouga N, Balemans W, Van den Wyngaert I, Vergauwen K, Gohlmann HWH, Willebrords R, Poncelet A, Guillemont J *et al*: Diarylquinolines are bactericidal for dormant mycobacteria as a result of disturbed ATP homeostasis. *Journal of Biological Chemistry* 2008, 283(37):25273-25280.

15. Koul A, Dendouga N, Vergauwen K, Molenberghs B, Vranckx L, Willebrords R, Ristic Z, Lill H, Dorange I, Guillemont J *et al*: Diarylquinolines target subunit c of mycobacterial ATP synthase. *Nat Chem Biol* 2007, 3(6):323-324.

16. Matteelli A, Carvalho ACC, Dooley KE, Kritski A: TMC207: the first compound of a new class of potent anti-tuberculosis drugs. *Future Microbiology* 2010, 5(6):849-858.

17. Mahajan R: Bedaquiline: First FDA-approved tuberculosis drug in 40 years. *International Journal of Applied and Basic Medical Research* 2013, 3(1):1-2.

18. Haagsma AC, Abdillahi-Ibrahim R, Wagner MJ, Krab K, Vergauwen K, Guillemont J, Andries K, Lill H, Koul A, Bald D: Selectivity of TMC207 towards mycobacterial ATP synthase compared with that towards the eukaryotic homologue. *Antimicrob Agents Chemother* 2009, 53(3):1290-1292.

19. Balemans W, Vranckx L, Lounis N, Pop O, Guillemont J, Vergauwen K, Mol S, Gilissen R, Motte M, Lançois D *et al*: Novel Antibiotics Targeting Respiratory ATP Synthesis in Gram-Positive Pathogenic Bacteria. *Antimicrobial Agents and Chemotherapy* 2012, 56(8):4131-4139.

20. Biuković G, Basak S, Manimekalai MSS, Rishikesan S, Roessle M, Dick T, Rao SPS, Hunke C, Grüber G: Variations of Subunit ε of the Mycobacterium tuberculosis F_1F_O ATP Synthase and a Novel Model for Mechanism of Action of the Tuberculosis Drug TMC207. *Antimicrobial Agents and Chemotherapy* 2013, 57(1):168-176.

21. Haagsma AC, Driessen NN, Hahn MM, Lill H, Bald D: ATP synthase in slow- and fast-growing mycobacteria is active in ATP synthesis and blocked in ATP hydrolysis direction. *FEMS Microbiol Lett* 2010, 313(1):68-74.

22. de Graaf C, Vischer HF, de Kloe GE, Kooistra AJ, Nijmeijer S, Kuijer M, Verheij MHP, England PJ, van Muijlwijk-Koezen JE, Leurs R *et al*: Small and colorful stones make beautiful mosaics: fragment-based chemogenomics. *Drug Discovery Today* 2013, 18(7–8):323-330.

23. Munro S, Pelham HR: Use of peptide tagging to detect proteins expressed from cloned genes: deletion mapping functional domains of Drosophila hsp 70. *The EMBO Journal* 1984, 3(13):3087-3093.

24. Lee MH, Pascopella L, Jacobs WR, Hatfull GF: Site-specific integration of mycobacteriophage L5: integration-proficient vectors for Mycobacterium smegmatis, Mycobacterium tuberculosis, and bacille Calmette-Guérin. *Proceedings of the National Academy of Sciences of the United States of America* 1991, 88(8):3111-3115.

25. Gordon RE, Smith MM: RAPIDLY GROWING, ACID FAST BACTERIA: II. Species' Description of Mycobacterium fortuitum Cruz. *Journal of Bacteriology* 1955, 69(5):502-507.

26. Brown-Elliott BA, Wallace RJ: Clinical and Taxonomic Status of Pathogenic Nonpigmented or Late-Pigmenting Rapidly Growing Mycobacteria. *Clinical Microbiology Reviews* 2002, 15(4):716-746.

27. Higashi T, Kalra VK, Lee SH, Bogin E, Brodie AF: Energy-transducing membrane-bound coupling factor-ATPase from Mycobacterium phlei. I. Purification, homogeneity, and properties. *Journal of Biological Chemistry* 1975, 250(16):6541-6548.

28. Sassetti, C.M., Boyd, D. H., and Rubin, E.J. Genes required for mycobacterial growth defined by high density mutagenesis. Molec. Microbiol. 2003, 48(1): 77-84.

29. Wade WG, Addy M: Antibacterial Activity of Some Triclosan-Containing Toothpastes and Their Ingredients. *Journal of Periodontology* 1992, 63(4):280-282.

Chapter Six

Discussion and Future Directions

6.1 Discussion

The current thesis work has led to some important discoveries about the function of the ε subunit in bacterial ATP synthase. It has been known that in bacterial ATP synthases, ε has a regulatory role mediated primarily through the C-terminal domain. To inhibit the enzyme, the C-terminal domain adopts what is known as the extended conformation and inserts in the central cavity of the α-β hexamer. Here it establishes extensive contacts with five subunits and effectively jams the rotor complex. This is akin to ramming a rod in a bicycle wheel with spokes and stopping the rotation. The research work presented here confirms this regulatory role of εCTD by the use of two *E. coli* mutants. The first mutant had the entire ε C-terminal domain genetically deleted whereas the second mutant had one cysteine residue introduced in each of the two α-helices of the εCTD. These cysteine residues formed a disulfide bond when exposed to oxidizing conditions. Thus both mutants prevented the εCTD from adopting the extended conformation and inhibiting the enzyme. The results showed that both mutants had increased ATPase activity when εCTD was prevented from adopting the extended state. When the double cysteine mutant was reduced to allow the α-helices to move freely and adopt the extended state, the activity was reduced. It was known that the εCTD is required for inhibition of the enzyme. Our results extend this understanding by indicating that it is the interactions of the εCTD in the ε_X conformation with the enzyme that is important for inhibition of the enzyme. And perturbing these interactions may lead to a change in inhibition of the enzyme.

We used F_1.ε binding assays to examine the effects of various ligands on the conformation of εCTD. This was a novel approach in which the dissociation of $F_1(-\delta\varepsilon)$ was

dependent on the conformation of εCTD. As a result, we were able to correlate the changes in dissociation rates of F_1(-δε) upon exposure to different ligands to conformational changes in εCTD. We also discussed the events taking place when γ rotates a 120° rotation when hydrolyzing one ATP molecule. Prior studies have suggested that one 120° rotation of γ can be divided into two substeps: (1) 80° rotation and (2) 40° rotation [1]. Studies (reviewed in [2, 3]) had indicated that binding of MgATP to the catalytic site induces the first 80° rotation of the γ subunit. At this position, the enzyme pauses for a brief period of time which is called a catalytic dwell. The next 40° rotation is limited by rates of hydrolysis and dissociation of Pi. Our studies showed that both the ε and ADP inhibition come into effect after hydrolysis at this catalytic dwell. However, F_1 crystal structures that are ADP- or ε-inhibited have shown the γ subunit at angles that are different from the catalytic dwell step [4, 5], with the ADP-inhibited F_1 structure showing γ at 95° whereas the ε-inhibited F_1 structure had γ rotated to 123°. We believe that at the catalytic dwell position, post hydrolysis, the enzyme can transition towards ADP- or ε-inhibition. When the enzyme gets ε-inhibited, the εCTD inserts in the α-β hexameric cavity at the catalytic dwell and then effects a partial rotation of γ to ~120° to stabilize the inhibitory conformation. This rotary position prevents inhibition of the enzyme by ADP. On the other hand, the ADP inhibition causes γ to rotate to 95°, where εCTD cannot insert. It is possible that γ may rotate back to the 80° position where εCTD can insert and cause the rotation to 120° at which point ADP inhibition cannot take place. The SM study by Sekiya et al. showed that γ experiences longer pause times for ε inhibition (up to 3.5 s) than ADP inhibition (~1 s) [6]. On average, the enzyme would stay longer in the ε-inhibited state than the ADP-inhibited one. This suggests that ε-inhibition predominates over the ADP-inhibition. Overall, the results

described above and in chapter two add to our understanding of conformational changes in εCTD in response to different reactants interacting with it at various stages of catalysis.

When the C-terminal domain of ε was truncated (εΔ5) in *E. coli* ATP synthase, the ATP synthesis activity of the enzyme was selectively inhibited with a direct impact on aerobic growth. There was no increase in the ε-mediated inhibition of ATPase activity on membranes as compared to WT ε. The differential effect of truncation on ATP synthesis versus hydrolysis is consistent with the proposal that ε functions by a bi-directional ratchet mechanism. These results also point to εCTD's role in preventing uncoupled activity of the enzyme. In the larger scheme of things for bacteria, this is important as they encounter harsh conditions that may lead to collapse of PMF or low ATP levels. Under those conditions, ε may help prevent the cells from rapidly exhausting intracellular ATP stock to generate PMF or nutrient stocks to generate ATP; either stock may be needed for vital physiological processes that ensure the survival of the organism. Consistent with this, other preliminary data in the Duncan lab show that ε88stop grows much slower at low pH conditions. At the same time, this opens the possibility of exploiting the reliance of bacterial ATP synthase on its ε subunit. Any compound or treatment that would prevent the ε subunit from functioning normally within the bacterial cell has the potential of affecting the viability of the cell. Hence, the ε subunit of pathogenic bacteria can serve as a potent target for antimicrobials that interfere with ε and hamper the function of ATP synthase of the pathogen.

6.2 Immediate future plans

The work done as a part of this thesis adds to the understanding of the role of the ε subunit in bacterial ATP synthase. However, in order to completely elucidate ε's role, further work is needed. For example, εΔ5 subunit showed loss of inhibitory effect in isolated F_1 domain (~20% inhibition vs ~90% inhibition by WT ε), even though its affinity is still high. As discussed earlier, the inhibition of the bacterial ATP synthase by its endogenous ε subunit is effected by εCTD adopting the extended conformation and inserting in the α-β central cavity to block functional rotation. The reduced inhibition of ATPase meant that εΔ5 is interacting differently with the enzyme as compared to WT ε. When the loss of contact area for εΔ5 was looked at by protein analysis software, Chimera, it appeared that four contact residues are lost along with loss of buried surface area, when εΔ5 adopts the extended conformation. This again suggests that the interaction of ε with the enzyme changes with deletion of the terminal five amino acids. It is natural to assume that this would lead to a change in the affinity of εΔ5 for F_1. We observed that the dissociation rate of F_1/ε complexes was reduced more than six-fold in the case of εΔ5. At this point, it is unclear what causes this change in dissociation rate. The possibility of ε binding to an alternative site looks likely. However, further investigation regarding the site of binding of the truncated ε is required.

It is important to study εΔ5's interactions in further detail because the results show for the first time that ε can be targeted to reduce ATP synthesis and subsequently, the aerobic growth of bacteria. Forcing the WT ε to mimic the behavior of εΔ5 may lead to similar effects in WT cells. Future experiments could include FRET (Forster Resonance Energy Transfer) [7] studies of εΔ5. For example, experiments can involve attaching

fluorophores to a site on β subunits which is close to the region where WT ε's CTD interacts. It has been described in the introduction of this thesis that ε can be cross-linked with the DELSEED region of the β subunit. So a site near the DELSEED region can be used for attaching the fluorophore. Another fluorophore can be attached near the Rossmann fold of γ where the helix1 of εCTD binds when ε adopts the ε_X state. With the third fluorophore attached in εhelix2, FRET values can be obtained. If εΔ5 binds to a site that is drastically different from the site where WT ε binds, the difference in FRET values may give an indication of it. Care should be taken to ensure that this fluorophore itself does not interfere with ε's normal interactions. Also, the fluorophore should be attached to any one β subunit in order to maximize the sensitivity of the assay. This poses a technical challenge as to how to ensure selective labeling of only one β subunit out of the three in one ATP synthase. A simple method would be to incubate the enzyme with sub-stoichiometric concentration of the fluorophore. This may allow labeling of one β per ATP synthase but does not guarantee that a second β will not be labeled. Using single molecule FRET can help work around this challenge to an extent. However, since γ can rotate, the distance between the fluorophores on γ and β subunit could be too large in some molecules to give FRET values. A more direct approach would be to resolve the crystal structure of F_1-ATPase with εΔ5 in its extended conformation. If the binding site of the εΔ5 CTD is observed to be a distinct one, follow up studies can include mutating the residue(s) of that site and observing its effect on *in vivo* and *in vitro* ATP synthase function in cells containing ATP synthase with εΔ5. As discussed above, the crystal structures of F_1 showed γ at 95° and 120° while many SM studies also suggested that γ had long pauses at the 80° position in ADP and ε inhibited states [6, 8, 9]. These conflicting results could be due to

technical challenges in SM studies to resolve the rotation over 40° rotation after the pause or they could suggest a real event as the crystal structures are end point results and do not reveal dynamic rotations. The results from chapter three indicated that εCTD may have different binding sites. It could be possible that the crystal structure of F_1 with εΔ5 may provide information to resolve this conflict.

6.3 General future plans

During the course of my thesis work, I have shown that the ε subunit of *E. coli* can be targeted to inhibit growth. In many bacterial species, the ε subunit has been shown to play a regulatory role in isolated F_1 or F_OF_1 [10-12]. In contrast, in mitochondria, the δ subunit (homolog of the bacterial ε subunit) has no known regulatory role [13]. Drugs that target the ε subunit of bacterial ATP synthase are thus less likely to cross-react with the mitochondrial ATP synthase and impair its function. When the amino acid sequences of the ε subunit from different pathogenic bacteria are aligned, it can be seen that there is considerable homology [13] (Fig. 6.1). Future projects could involve working with pathogens like *S. enterica* that cause diseases in humans as well as animals resulting in massive number of deaths. As noted earlier, *S. enterica* loses pathogenicity when ATP synthase is not assembled. As shown in Fig. 6.1, *S. enterica* exhibits ~99% sequence homology in the ε subunit as compared to *E. coli*. With that amount of sequence homology (primary protein structure), it is highly possible that there is high amount of 3-dimentional structural similarity and probable functional similarity. Both the *Salmonella* and *Escherichia* genera belong to the same family of *Enterbacteriaceae* and are gram negative, facultative anaerobes. The role of the ε subunit in *Salmonella* genus is not yet known but, considering the sequence homology as well as the phylogenetic proximity with *E. coli,* it is likely that its role is similar to *E. coli* ε. Another attractive target can be *Shigella dysenteriae*, which is also a facultatively anaerobic, gram negative pathogen belonging to the family *Enterobacteriaceae* [14]. *S. dysenteriae* causes extremely severe dysentery due to the presence of Shiga toxin [15]. Sequence alignment of its ε subunit with *E. coli* also showed high homology (Fig. 6.1). Thus, perturbing εCTD's interactions with the enzyme

in *Salmonella* and *Shigella* ATP synthases may provide similar results to those obtained with *E. coli*. Thus, this presents a possibility that perturbing the interactions of ε subunit of many pathogenic bacteria may result in reduced growth. Overall, the results published in this thesis open a new avenue of research to target ATP synthases of different bacteria with the goal of obtaining specific inhibitory agents.

Figure 6.1

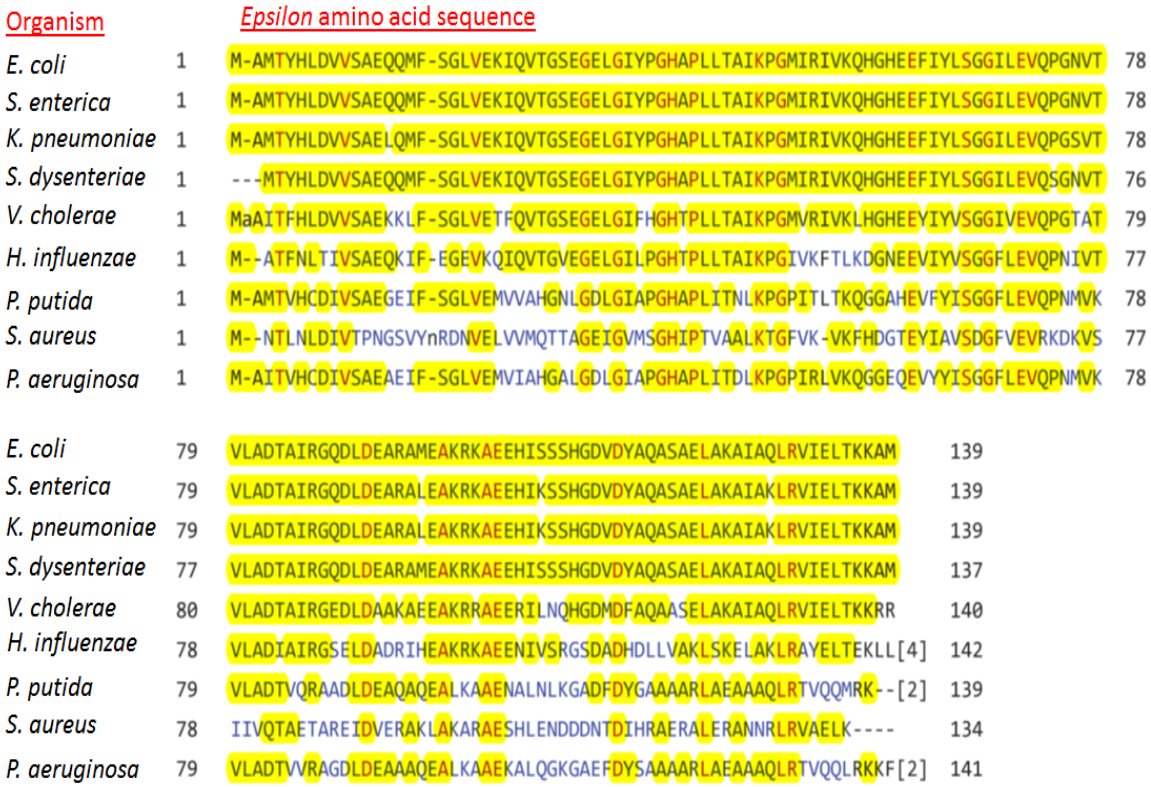
Organism
Epsilon amino acid sequence
E. coli 1 M-AMTYHLDVVSAEQQMF-SGLVEKIQVTGSEGELGIYPGHAPLLTAIKPGMIRIVKQHGHEEFIYLSGGILEVQPGNVT 78
S. enterica 1 M-AMTYHLDVVSAEQQMF-SGLVEKIQVTGSEGELGIYPGHAPLLTAIKPGMIRIVKQHGHEEFIYLSGGILEVQPGNVT 78
K. pneumoniae 1 M-AMTYHLDVVSAELQMF-SGLVEKIQVTGSEGELGIYPGHAPLLTAIKPGMIRIVKQHGHEEFIYLSGGILEVQPGSVT 78
S. dysenteriae 1 ---MTYHLDVVSAEQQMF-SGLVEKIQVTGSEGELGIYPGHAPLLTAIKPGMIRIVKQHGHEEFIYLSGGILEVQSGNVT 76
V. cholerae 1 MaAITFHLDVVSAEKKLF-SGLVETFQVTGSEGELGIFHGHTPLLTAIKPGMVRIVKLHGHEEYIYVSGGIVEVQPGTAT 79
H. influenzae 1 M--ATFNLTIVSAEQKIF-EGEVKQIQVTGVEGELGILPGHTPLLTAIKPGIVKFTLKDGNEEVIYVSGGFLEVQPNIVT 77
P. putida 1 M-AMTVHCDIVSAEGEIF-SGLVEMVVAHGNLGDLGIAPGHAPLITNLKPGPITLTKQGGAHEVFYISGGFLEVQPNMVK 78
S. aureus 1 M--NTLNLDIVTPNGSVYnRDNVELVVMQTTAGEIGVMSGHIPTVAALKTGFVK-VKFHDGTEYIAVSDGFVEVRKDKVS 77
P. aeruginosa 1 M-AITVHCDIVSAEAEIF-SGLVEMVIAHGALGDLGIAPGHAPLITDLKPGPIRLVKQGGEQEVYYISGGFLEVQPNMVK 78
E. coli 79 VLADTAIRGQDLDEARAMEAKRKAEEHISSSHGDVDYAQASAELAKAIAQLRVIELTKKAM 139
S. enterica 79 VLADTAIRGQDLDEARALEAKRKAEEHIKSSHGDVDYAQASAELAKAIAKLRVIELTKKAM 139
K. pneumoniae 79 VLADTAIRGQDLDEARALEAKRKAEEHIKSSHGDVDYAQASAELAKAIAKLRVIELTKKAM 139
S. dysenteriae 77 VLADTAIRGQDLDEARAMEAKRKAEEHISSSHGDVDYAQASAELAKAIAQLRVIELTKKAM 137
V. cholerae 80 VLADTAIRGEDLDAAKAEEAKRRAEERILNQHGDMDFAQAASELAKAIAQLRVIELTKKRR 140
H. influenzae 78 VLADIAIRGSELDADRIHEAKRKAEENIVSRGSDADHDLLVAKLSKELAKLRAYELTEKLL[4] 142
P. putida 79 VLADTVQRAADLDEAQAQEALKAAENALNLKGADFDYGAAAARLAEAAAQLRTVQQMRK--[2] 139
S. aureus 78 IIVQTAETAREIDVERAKLAKARAESHLENDDDNTDIHRAERALERANNRLRVAELK---- 134
P. aeruginosa 79 VLADTVVRAGDLDEAAAQEALKAAEKALQGKGAEFDYSAAAARLAEAAAQLRTVQQLRKKF[2] 141

Figure 6.1. Sequence alignment of ATP synthase ε subunit from different bacterial species. Amino acid sequences of nine known pathogenic or opportunistic pathogenic bacteria were aligned. The sequence files were obtained from Uniprot databank and aligned in Cobalt, a Constraint-based Multiple Protein Alignment Tool [16]. Colored regions demonstrate identity with *E. coli* ε subunit. Uniprot codes: P0A6E6 (*E. coli*), B5XZM5 (*K. pneumoniae*), Q9KNH6 (*V. cholerae* serotype 1), A5UGY8 (*H. influenzae*), Q88BX5 (*P. putida*), Q2FF25 (*S. aureus*), Q02DF5 (*P. aeruginosa*). NCBI accession codes: WP_001251962.1 (*S. enterica*), EFW49757.1 (*S. dysenteriae*).

6.4 References

1. Nishizaka T, Oiwa K, Noji H, Kimura S, Muneyuki E, Yoshida M, Kinosita K, Jr.: Chemomechanical coupling in F_1-ATPase revealed by simultaneous observation of nucleotide kinetics and rotation. *Nat Struct Mol Biol* 2004, 11(2):142-148.
2. Noji H, Okuno D, Ikeda T: Mechanochemistry of F_1 motor protein. *Chemical Science* 2011, 2(11):2086-2093.
3. Kinosita K, Jr.: F_1-ATPase: A Prototypical Rotary Molecular Motor. In: *Viral Molecular Machines*. *Volume 726*
4. Cingolani G, Duncan TM: Structure of the ATP synthase catalytic complex ($F(_1)$) from Escherichia coli in an autoinhibited conformation. *Nat Struct Mol Biol* 2011, 18(6):701-707.
5. Bowler MW, Montgomery MG, Leslie AG, Walker JE: How azide inhibits ATP hydrolysis by the F-ATPases. *Proc Natl Acad Sci USA* 2006, 103(23):8646-8649.
6. Sekiya M, Hosokawa H, Nakanishi-Matsui M, Al-Shawi MK, Nakamoto RK, Futai M: Single molecule behavior of inhibited and active states of Escherichia coli ATP synthase F_1 rotation. *J Biol Chem* 2010, 285(53):42058-42067.
7. Ha T: Single-molecule fluorescence resonance energy transfer. *Methods* 2001, 25(1):78-86.
8. Hirono-Hara Y, Noji H, Nishiura M, Muneyuki E, Hara KY, Yasuda R, Kinosita K, Jr., Yoshida M: Pause and rotation of $F(_1)$-ATPase during catalysis. *Proc Natl Acad Sci USA* 2001, 98(24):13649-13654.
9. Konno H, Murakami-Fuse T, Fujii F, Koyama F, Ueoka-Nakanishi H, Pack CG, Kinjo M, Hisabori T: The regulator of the F_1 motor: inhibition of rotation of

cyanobacterial F_1-ATPase by the epsilon subunit. *EMBO J* 2006, 25(19):4596-4604.

10. Smith JB, Sternweis PC: Purification of membrane attachment and inhibitory subunits of the proton translocating adenosine triphosphatase from Escherichia coli. *Biochemistry* 1977, 16:306-311.

11. Keis S, Stocker A, Dimroth P, Cook GM: Inhibition of ATP hydrolysis by thermoalkaliphilic F_1F_O-ATP synthase is controlled by the C terminus of the ε subunit. *J Bacteriol* 2006, 188(11):3796-3804.

12. Kato Y, Matsui T, Tanaka N, Muneyuki E, Hisabori T, Yoshida M: Thermophilic F_1-ATPase is activated without dissociation of an endogenous inhibitor, □ subunit. *J Biol Chem* 1997, 272(40):24906-24912.

13. Feniouk BA, Suzuki T, Yoshida M: The role of subunit ε in the catalysis and regulation of F_OF_1-ATP synthase. *Biochim Biophys Acta* 2006, 1757(5-6):326-338.

14. Hale TL, Keusch, G. T.: Shigella: Structure, Classification, and Antigenic Types. In: *Medical Microbiology*, 4 edition.

15. Zaidi MB, Estrada-García T: Shigella: A Highly Virulent and Elusive Pathogen. *Current tropical medicine reports* 2014, 1(2):81-87.

16. Papadopoulos JS, Agarwala R: COBALT: constraint-based alignment tool for multiple protein sequences. *Bioinformatics* 2007, 23(9):1073-1079.